Chemical and Biological Oceanographic Conditions in the Estuary and Gulf of St. Lawrence During 2023

Marjolaine Blais, Peter S. Galbraith, Martine Lizotte, Stephanie A. Clay, and Michel Starr

Regional Sciences Branch
Québec Region
Pelagic and Ecosystemic Sciences Division
Fisheries and Oceans Canada
Maurice Lamontagne Institute
850, Route de la Mer
Mont-Joli, QC
G5H 3Z4

2024

Canadian Technical Report of
Hydrography and Ocean Sciences 385

Fisheries and Oceans Canada | Pêches et Océans Canada

Canada

Canadian Technical Report of Hydrography and Ocean Sciences

Technical reports contain scientific and technical information of a type that represents a contribution to existing knowledge but which is not normally found in the primary literature. The subject matter is generally related to programs and interests of the Oceans and Science sectors of Fisheries and Oceans Canada.

Technical reports may be cited as full publications. The correct citation appears above the abstract of each report. Each report is abstracted in the data base *Aquatic Sciences and Fisheries Abstracts.*

Technical reports are produced regionally but are numbered nationally. Requests for individual reports will be filled by the issuing establishment listed on the front cover and title page.

Regional and headquarters establishments of Ocean Science and Surveys ceased publication of their various report series as of December 1981. A complete listing of these publications and the last number issued under each title are published in the *Canadian Journal of Fisheries and Aquatic Sciences*, Volume 38: Index to Publications 1981. The current series began with Report Number 1 in January 1982.

Rapport technique canadien sur l'hydrographie et les sciences océaniques

Les rapports techniques contiennent des renseignements scientifiques et techniques qui constituent une contribution aux connaissances actuelles mais que l'on ne trouve pas normalement dans les revues scientifiques. Le sujet est généralement rattaché aux programmes et intérêts des secteurs des Océans et des Sciences de Pêches et Océans Canada.

Les rapports techniques peuvent être cités comme des publications à part entière. Le titre exact figure au-dessus du résumé de chaque rapport. Les rapports techniques sont résumés dans la base de données *Résumés des sciences aquatiques et halieutiques*.

Les rapports techniques sont produits à l'échelon régional, mais numérotés à l'échelon national. Les demandes de rapports seront satisfaites par l'établissement auteur dont le nom figure sur la couverture et la page de titre.

Les établissements de l’ancien secteur des Sciences et Levés océaniques dans les régions et à l'administration centrale ont cessé de publier leurs diverses séries de rapports en décembre 1981. Vous trouverez dans l'index des publications du volume 38 du *Journal canadien des sciences halieutiques et aquatiques*, la liste de ces publications ainsi que le dernier numéro paru dans chaque catégorie. La nouvelle série a commencé avec la publication du rapport numéro 1 en janvier 1982.

Canadian Technical Report
of Hydrography and Ocean Sciences 385

2024

Chemical and Biological Oceanographic Conditions in the Estuary and Gulf of St. Lawrence During 2023

Marjolaine Blais, Peter S. Galbraith, Martine Lizotte, Stephanie A. Clay and Michel Starr

Regional Sciences Branch
Québec Region
Pelagic and Ecosystemic Sciences Division
Fisheries and Oceans Canada
Maurice Lamontagne Institute
850, Route de la Mer
Mont-Joli, QC
G5H 3Z4

Cat. No. Fs97-18/385E-PDF ISBN 978-0-660-73375-3 ISSN 1488-5417

Correct citation for this publication:

Blais, M., Galbraith, P.S., Lizotte, M., Clay, S.A. and Starr, M. 2024. Chemical and Biological Oceanographic Conditions in the Estuary and Gulf of St. Lawrence During 2023. Can. Tech. Rep. Hydrogr. Ocean Sci. 385: v + 84 p.

TABLE OF CONTENTS

ABSTRACT

Blais, M., Galbraith, P.S., Lizotte, M., Clay, S.A. and Starr, M. 2024. Chemical and Biological Oceanographic Conditions in the Estuary and Gulf of St. Lawrence During 2023. Can. Tech. Rep. Hydrogr. Ocean Sci. 385: v + 84 p.

An overview of the chemical and biological oceanographic conditions in the Estuary and Gulf of St. Lawrence in 2023 is presented as part of the Atlantic Zone Monitoring Program (AZMP). AZMP and regional program data are presented in relation to long-term means. Oxygen levels in deep waters reached record-low saturation levels in the northwest and central Gulf but remained near-normal in the Estuary. Acidification proxies reached record levels at station Rimouski, with pH decreasing to its lowest recorded point. Annual nutrient inventories were generally below normal in the surface layer and the mid-layer, and above normal in the deep layer. Annual inventories of vertically integrated chlorophyll a were either near normal or slightly below normal, except in the Estuary and northwest Gulf region. Annual surface chlorophyll a concentrations estimated from remote sensing were above normal due to large fall blooms that occurred across the Gulf. The spring and fall bloom timings were mostly near normal. Negative anomalies of zooplankton biomass were generally observed in the Gulf, including record lows in central Gulf and Cabot Strait, due to very low abundances of *Calanus hyperboreus.* Small calanoids, non-copepods and warm-water copepods generally exhibited below- or near-normal abundances. The phenology of the large *Calanus* spp. was early.

RÉSUMÉ

Blais, M., Galbraith, P.S., Lizotte, M., Clay, S.A. and Starr, M. 2024. Chemical and Biological Oceanographic Conditions in the Estuary and Gulf of St. Lawrence During 2023. Can. Tech. Rep. Hydrogr. Ocean Sci. 385: v + 84 p.

Un aperçu des conditions océanographiques chimiques et biologiques dans l'estuaire et le golfe du Saint-Laurent en 2023 est présenté dans le cadre du Programme de Monitorage de la Zone Atlantique (PMZA). Les données du PMZA et celles de programmes de monitorage régionaux sont présentées par rapport aux moyennes à long terme. Les niveaux d'oxygène dans les eaux profondes ont atteint des minimums records dans le nord-ouest et le centre du golfe, mais sont restés stables dans l'estuaire. Les indicateurs d'acidification ont atteint des niveaux records à la station Rimouski, avec le pH le plus faible jamais enregistré. Les inventaires annuels d'éléments nutritifs étaient généralement sous la normale dans la couche de surface et la couche intermédiaire, et au-dessus de la normale dans la couche profonde. Les inventaires annuels de chlorophylle a intégrée verticalement étaient soit près de la normale ou légèrement inférieurs, sauf dans l'estuaire et le nord-ouest du golfe. Les inventaires de chlorophylle a à la surface estimés par la télédétection étaient au-dessus de la normale en raison des fortes floraisons automnales partout dans le golfe. Le moment des floraisons printanières et automnales était généralement près de la normale. Des anomalies négatives de la biomasse de zooplancton ont généralement été observées dans le golfe, incluant des minimums records dans la région du centre du golfe et du détroit de Cabot, fortement influencées par les très faibles abondances de *Calanus hyperboreus*. Les abondances de petits calanoïdes, de non-copépodes et de copépodes d'eaux chaudes étaient généralement sous ou près de la normale. La phénologie des grands *Calanus* spp. était hâtive.

1. INTRODUCTION

The Atlantic Zone Monitoring Program (AZMP) was implemented in 1998 (Therriault et al. 1998) with the aim of 1) increasing Fisheries and Oceans Canada's (DFO) capacity to understand, describe, and forecast the state of the marine ecosystem, and 2) quantifying the changes in the ocean's physical, chemical, and biological properties and the predator–prey relationships of marine resources. AZMP provides data to support the sound development of ocean activities. A critical element of the AZMP observational program is the annual assessment of the distribution and variability of physical, chemical and biological properties of the water column. This report focuses on oxygen, acidification parameters, nutrients, and plankton communities.

A description of the spatiotemporal distribution of dissolved oxygen, acidification parameters (pH_T, aragonite and calcite saturation states [Ω]), nutrients (nitrate, silicate, and phosphate), and chlorophyll *a* (chl *a*) concentrations provides important information on biogeochemical cycling, water-mass movements and on the location, timing, and magnitude of biological production cycles. A description of the phytoplankton and zooplankton communities, distributions and phenologies provides important information on the organisms forming the base of marine food webs. Biogeochemical and plankton production cycles play a pivotal role in supporting healthy marine ecosystems, and their understanding is crucial for an ecosystem approach to fisheries management.

The AZMP derives its information on the state of the marine ecosystem from a combination of satellite remote sensing and *in situ* data collected at a network of sampling locations (high-frequency monitoring stations, cross-shelf sections) in each DFO region (Québec, Gulf, Maritimes, Newfoundland and Labrador; see Figure 1 for section locations in the St. Lawrence Gulf and Estuary) visited at a frequency of weekly to once annually (Galbraith et al. 2024a). The sampling design of the zonal AZMP provides valuable information on the natural variability in physical, chemical, and biological properties of the Northwest Atlantic continental shelf. Cross-shelf sections and ecosystem trawl surveys provide a broad scale overview of the conditions but are limited in their seasonal coverage. Strategically located high-frequency monitoring stations complement the seasonal sampling by providing more detailed information on seasonal-scale changes in ecosystem properties. In recent years, automated oceanographic buoys have also complemented the core observations with high temporal resolution data.

In this document, we review the chemical and biological (lower trophic levels) oceanographic conditions in the Estuary and Gulf of St. Lawrence in 2023. For conciseness purpose, the term Gulf is used to refer to the entire St. Lawrence Estuary and Gulf bioregion thereafter in the document. Changes in the physical pelagic environment influence both plankton community composition and annual biological production cycles, with implications for the energy transfer to higher trophic levels. Readers should refer to Galbraith et al. (2024b) for a complete description of the physical conditions that prevailed in the Gulf in 2023.

2. METHODS

2.1 SAMPLING

All sample collection and processing steps meet the standards of AZMP protocols (Mitchell et al. 2002). Field measurements included in this report were collected during dedicated AZMP surveys carried out in winter, early summer and fall (generally in March, June, and October) of each year and at two high-frequency monitoring stations (Figure 1). Oceanographic measurements made during multidisciplinary surveys (August and September; hereafter referred to as late summer surveys) and during the mackerel egg survey (June) were included for all years (2006–2023) for which these data are available. In this document, stations were grouped into four main regions for which biochemical indices are presented (Figure 1):

(1) Estuary/northwest Gulf: this region is generally deep (>200 m) and cold in summer. It is strongly influenced by freshwater runoff from the St. Lawrence River at the surface, and by dense waters flowing along the Laurentian Channel in deeper waters;

(2) Northeast Gulf: this region, with deep channels and a relatively wide shelf (shallower than 100 m), is characterized by high surface salinity;

(3) Central Gulf/Cabot Strait: this region is generally deep (>200 m) and is directly influenced by deep waters that mix at the continental slope (warm North Atlantic Central Water that has a Gulf Stream signature and cold Labrador Current water) and enter the Gulf through Cabot Strait;

(4) Magdalen Shallows: this region is shallow (<100 m) and warm at the surface in summer. It is largely influenced by the Gaspé Current.

These regions match those used in the Gulf for the DFO Ecosystem Approach to Fisheries Management. Since there are few biogeochemical data collected in Mécatina and Northumberland (Figure 1), indices will not be reported for those regions.

Table 1 provides details about the 2023 sampling surveys and Figure 2 and Figure 3 summarize the sampling effort during the seasonal surveys and at the high-frequency monitoring stations, respectively. Rimouski station (depth 320 m) has been sampled since 1991—about weekly throughout the summer, once or twice a month in early spring and late fall, and rarely in winter (except during the March survey) due to the presence of sea ice. It is representative of conditions in the Estuary/northwestern Gulf. In 2023, Rimouski station was visited on 23 occasions. Shediac Valley station (depth 84 m) is representative of conditions on the Magdalen Shallows and of the Estuary outflow. Shediac Valley station is at best sampled once monthly between May and November with nearly absent coverage from December through April, except during the March survey. Shediac Valley station was occupied on seven occasions in 2023, with four of those occupations occurring in spring. In addition to the occupations at the high-frequency monitoring stations, automated oceanographic buoys equipped with temperature, salinity, and fluorescence surface profilers (data collected every 30 minutes) have been deployed at the high-frequency stations since 2002 and 2004 at Rimouski and Shediac Valley stations, respectively. Deployment of these buoys typically occurs in late April or early May and recovery occurs in late October or early November.

Sampling along the oceanographic sections and at the high-frequency monitoring stations includes a Conductivity-Temperature-Depth profile (CTD; temperature, salinity, fluorescence, dissolved oxygen) as well as water sampling using Niskin bottles (surface, 10 m, 15 m, 25 m, 50 m, 100 m, 200 m, 300 m, 400 m, bottom). Water from the Niskin bottles is collected for the analysis of dissolved oxygen (Winkler method), seawater pH on the total scale (pH_T; spectrophotometry and dye perturbation calculation methods), aragonite and calcite saturation

states (Ω; calculated based on measurements of total alkalinity and pH_T via the CO2SYS program, see Gibb et al. 2023 for further details), nutrients (Seal Analytical AutoAnalyzer 3 or Alpkem AutoAnalyzer), chl *a* concentration (fluorometer), and phytoplankton enumeration (inverted microscopy) (Mitchell et al. 2002). Finally, mesozooplankton (<1 cm, hereafter referred to as zooplankton) is collected with bottom-to-surface vertical ring net tows (75 cm diameter, 200 µm mesh) for most surveys. Taxonomists are responsible for the identification, enumeration, and bulk biomass (dry weight) measurements of zooplankton samples collected during regular AZMP surveys (early summer and fall surveys) and September southern Gulf multidisciplinary survey, whereas samples collected during the August multidisciplinary survey and during the mackerel egg survey are analyzed using a semi-automated procedure developed with the ZooImage 5.5.2 software package (Grosjean et al. 2018; https://CRAN.R-project.org/package=zooimage) following the methodology described in Plourde et al. (2019) and Blais et al. (2023b). Since methods are different, and considering the larger mesh size of nets deployed during the mackerel egg survey (333 µm mesh), large calanoid taxa indices developed with the ZooImage analysis only include copepodite stages CIV–CVI, and these data are not included in the annual abundance estimates. Zooplankton data collected during September multidisciplinary survey are also presented separately and not included in the annual indices since they only cover the Magdalen Shallows and the stations' locations and total number change each year.

2.2 IN SITU METRICS

2.2.1 Oxygen

Oxygen concentration profiles are used to monitor hypoxic conditions in the Gulf. Oxygen concentration was measured using an oxygen probe (Sea-Bird SBE43) mounted on the CTD; the probe was calibrated against collected seawater samples from every cast which were analyzed by Winkler titration (for the calibration procedure, see Sea-Bird application notes 61-1, -2, -3). Annual average time series are based on gridded (2 km^2) inverse-distance-weighted interpolation, spatially averaged over every region and season.

2.2.2 Acidification parameters

While historical data on acidification parameters exist in the Estuary (*e.g.*, Mucci et al. 2011), systematic measurements of acidification parameters have been conducted in this region since 2014 (Gibb et al. 2023). These data are used to monitor the spatiotemporal variability in carbonate parameters in the Estuary, the region most affected by acidification across the Atlantic Zone (Galbraith et al. 2024a). Waters with saturation states below a threshold of 1 (<1) are considered undersaturated with respect to either aragonite or calcite, the two most common forms of calcium carbonate. These undersaturations promote the dissolution of exposed and unprotected calcium carbonate structures secreted by marine organisms, including shells, scales and exoskeletons (see Sulpis et al. 2021 and references therein). Monthly and annual averages were calculated from all samples collected in the top 15 m (surface layer) and in the bottom 50 m (bottom layer) of the water column.

2.2.3 Nutrients and phytoplankton

Nutrient and chl *a* concentrations (a proxy for phytoplankton biomass) collected along the AZMP sections and at the high-frequency monitoring stations were integrated over various depth intervals (i.e., 0–100 m for chl *a*; 0–50 m, 50–150 m, and 150 m–bottom for nutrients) using trapezoidal numerical integration. In 2016 and 2017, winter vertical profiles of nutrients all over the Gulf revealed that nutrient concentrations were relatively homogeneous in the upper 50 m of the water column. Thus, for typical years when vertical nutrient profiles are not available, including 2023, integrated nutrient values for the winter survey were calculated using surface

concentrations, assuming homogeneity of nutrient concentrations in the winter mixed layer. At the time of writing this report, nutrient samples from 2023 late summer and fall surveys had not been analyzed. Thus, the 2023 annual mean only includes winter and early summer nutrient samples and will be updated in next year's report. Spring nutrient drawdown was estimated using the difference between the March and June nitrate inventories (0–50 m) and is used as a proxy for phytoplankton spring production since the early summer sampling occurs after the spring bloom. Phytoplankton taxonomic identification is performed for the high-frequency monitoring stations since the beginning of the program, and since 2014 across the Gulf of St Lawrence.

2.2.4 Zooplankton

Since zooplankton samples are generally collected over the entire water column (0–50 m during the mackerel egg survey), zooplankton indices included in this report represent depth-integrated metrics. Only samples collected during regular AZMP surveys (early summer and fall) and analyzed by taxonomists were included in the calculation of regional zooplankton annual anomalies. A detailed list of species included in each copepod index is presented in Appendix 1. Since 2018, the results of a genetic study based on prosome length have been used to identify *Calanus finmarchicus* and *Calanus glacialis* (Parent et al. 2011).

We use the time series at Rimouski station to describe *C. finmarchicus* phenology and its evolution as adequate sampling and stage identification started almost 30 years ago at that station. However, sampling methodology has changed over time: from 1994 to 2004, prior to the use of AZMP standard nets (i.e., 75 cm diameter, 200 µm mesh bottom-to-surface ring net tows; Mitchell et al. 2002), *C. finmarchicus* copepodite stage abundance was determined using samples collected with 333 µm (CIV–CVI) and 73 µm (CI–III) mesh nets, towed from bottom to surface and from 50 m to surface, respectively. The 73 µm mesh nets were analyzed for only six years (1994, 1996–2000) of the time series (see Plourde et al. 2009 for details). In years prior to 2004 for which 73 µm samples were not analyzed, the abundance of CI–III in the 333 µm samples was adjusted based on a comparison performed with a 158 µm mesh net (S. Plourde, DFO, Mont-Joli, QC; unpublished data). The phenology of *C. finmarchicus* was characterized using the following steps: (1) stage-relative abundances were normalized (proportion of a copepodite stage/maximum proportion for the stage) within each year for CI–III, CIV, CV, and CVI (male and female) and (2) stage proportions were smoothed using a LOESS function (locally estimated scatterplot smoothing).

2.3 SATELLITE REMOTE SENSING OF OCEAN COLOR AND BLOOM METRICS

Satellite ocean colour data provide large-scale images of surface phytoplankton biomass (as indexed by chl a concentration). Daily satellite composite images within four ocean colour polygons (northwest Gulf, northeast Gulf, Magdalen Shallows, and Cabot Strait; Figure 4) supplement our ship-based observations, especially regarding the spring bloom phenology, and provide seasonal coverage and a large-scale context for interpreting our survey data. However, since ocean colour imagery provides information only on the surface of the oceans (i.e., a few tens of meters at best), it should be used as complementary information to the field data.

In this report, data collected from 2003 to 2023 by the Moderate Resolution Imaging Spectroradiometer (MODIS) "Aqua" sensor launched by NASA in July 2002 (4 km spatial resolution) are used to construct a continuous time series of surface chl a concentration for the four ocean colour polygons (Figure 4). The continued calibration and data reprocessing done by NASA ensure data quality over the whole MODIS time series (Xiong et al. 2020). Composite satellite images of remote sensing reflectance sourced from NASA's Goddard Space Flight

Center (https://oceancolor.gsfc.nasa.gov) were converted to chl *a* concentration using an algorithm based on empirical orthogonal function (EOF) analysis (Laliberté et al. 2018). Daily chl *a* concentrations were averaged over each ocean colour polygon and were extracted using the PhytoFit application v1.0.0 (Clay et al. 2021). Availability of ocean colour data is typically reduced during January, February, and December due to clouds, sea-ice cover, and low sun angles.

The timing of the spring phytoplankton bloom was derived by applying a LOESS function to the daily averages of log-10 transformed chl *a* concentration (weighted by percent coverage within the polygon, down to a minimum of 20%) and then by fitting a shifted Gaussian to the smoothed curve (Zhai et al. 2011). The start of the spring bloom corresponds to the day when chl *a* concentration reaches 20% of the maximum spring bloom amplitude and the peak timing is the day at which fitted chl *a* concentration reaches its maximum. Previous reports used the start index to characterize spring bloom timing (Blais et al. 2023a). However, since data are scarce at the winter/spring transition and may prevent an accurate determination of the spring bloom start in some cases, the peak timing appears as a more robust index to describe the timing of the spring bloom. Anomaly patterns are expected to remain similar considering the strong relationship between start and peak timings within each of the ocean colour polygons in the Gulf ($R^2 > 0.6$, $p < 0.001$). Parameters used to fit the Gaussian curves are described in Appendix 2.

Over the past few years, the intensity of fall blooms increased, particularly in the Estuary and northwest Gulf (Blais et al. 2023a). Information on the timing of these fall blooms is included in the current report. At high latitudes, the low incidence angle of sunlight in late fall affects the retrieval of ocean colour data. This results in truncated time series of daily chl *a* concentration that potentially miss the days with highest mean chl *a* concentration. Consequently, initiation of the fall bloom was calculated by applying the threshold method described in Layton et al. (2022) on the LOESS-smoothed daily averages of the log-10 transformed chl *a* concentration. Fall bloom start corresponds to the day when chl *a* concentration rises above the threshold of 5% over the annual median and remains above it for at least 14 consecutive days.

To characterize spring and fall bloom intensities but also phytoplankton production occurring in other seasons, seasonal chl *a* averages are reported. The season boundaries, which are considered unique to each polygon, are defined by the timing (start and end) of the spring and fall bloom over the climatology. Winter starts on the day of year 1 until spring bloom starts, and summer starts at the end of the spring bloom and ends at the start of the fall bloom. Fall ends on the day of year 365. Gaussian magnitude has previously been used to report on the intensity of the spring bloom (Blais et al. 2023a). Spring average anomaly time series should remain similar to previously published magnitude anomaly time series since both spring bloom magnitude and average spring chl *a* concentration are strongly correlated in the Gulf ($r = 0.86$, $p < 0.01$).

All ocean-colour polygons are located outside of the St. Lawrence River plume because satellite-based chl *a* concentration estimates in such areas are unreliable due to contamination by river inputs loaded with coloured matter of terrestrial origin. For the same reason, polygons are not directly adjacent to the coast. This also explains why spring bloom metrics in the Estuary cannot be derived from ocean colour data. Moreover, the significance of the spring bloom for the Estuary's food web remains unclear. In the Estuary, primary production is generally sustained throughout the summer and early fall due to frequent mixing episodes. This is in contrast to other regions where the spring bloom represents the main food pulse for zooplankton. For these reasons, we do not provide estimates of spring bloom metrics for the Estuary. However, high-temporal-resolution information on the phytoplankton dynamics at the surface of the Estuary is available from the surface fluorescence sensor on the oceanographic buoy located at Rimouski station and presented in this document. To increase the accuracy of

daily chl *a* concentration estimates, data from the buoy sensor were examined to remove daily outliers (± 3 SD) and were then calibrated against chl *a* concentrations measured in the water samples collected weekly at Rimouski station using a linear regression ($R^2 = 0.26$, $p < 0.001$).

2.4 ANNUAL ANOMALY SCORECARDS

Normalized anomalies for the chemical and biological indices presented in scorecards were computed for the high-frequency monitoring station and oceanographic regions. These anomalies are calculated as the difference between the variable's average for the season or for the complete year and the variable's climatological mean (usually 1999–2020 for *in situ* metrics and 2003-2020 for remote sensing metrics); this number is then divided by the standard deviation over the climatological period.

Anomalies are presented as scorecards with positive anomalies depicted as shades of red, negatives as blues, and anomalies within ± 0.5 SD as white (considered as normal conditions, *i.e.*, similar to the climatology). A standard set of indices representing anomalies of nitrate inventories in the mid-layer (50–150 m), phytoplankton biomass and bloom dynamics, mesozooplankton biomass, and the abundance of dominant mesozooplankton species and groups (*C. finmarchicus, Pseudocalanus* spp., total copepods, and total non-copepods) are produced for each AZMP region (Casault et al. 2024; Maillet et al. 2022). To visualize Northwest Atlantic shelf-scale patterns of environmental variation, a zonal scorecard including observations from all AZMP regions is presented in Galbraith (2024a).

Annual nutrient, phytoplankton, and zooplankton index anomalies are based on the mean annual concentration (mmol m^{-2} for nutrients, mg chl *a* m^{-2} for phytoplankton biomass) or density (cells L^{-1} for phytoplankton abundance, individuals m^{-2} for zooplankton abundance and g m^{-2} for zooplankton biomass) estimated at both high-frequency monitoring stations and in all Gulf regions of Figure 1. These annual estimates are derived from general linear models (GLM) of the form:

$\text{Log}_{10}(y) = \alpha + \beta_{\text{YEAR}} + \delta_{\text{MONTH}} + \varepsilon$ for the high-frequency monitoring stations and
$\text{Log}_{10}(y) = \alpha + \beta_{\text{YEAR}} + \delta_{\text{STATION}} + \gamma_{\text{SEASON}} + \varepsilon$ for the regions,

Where *y* is the response variable, either expressed as concentration or density, α is the intercept, and ε is the error. The GLM is applied to each region separately. For the high-frequency monitoring stations, β and δ are the categorical effects for year and month, respectively. For the regions, β, δ, and γ are the categorical effects of year, station, and season, respectively. We log-10 transformed concentrations and density values before computing anomalies to compensate for the skewed distribution of observations. We added one unit to *Density* terms for the abundance indices (phytoplankton and zooplankton counts) to include observations with values of zero. An estimate of the least-square means based on type III sums of squares is used as an estimate of the annual average. Results of the GLM (significance of each factor and adjusted R squared of the regression) are presented in Appendices 3 to 7. Four seasons (winter, early summer, late summer, and fall) are included in the GLM to estimate the annual average of surface nutrient inventories; three seasons are used to estimate the annual average of deeper nutrient inventories and phytoplankton indices (no data collection during winter); and two seasons (early summer and fall) are used to calculate annual estimates of zooplankton indices (zooplankton data collected during mackerel egg survey or late summer surveys are presented separately and their time series are based on seasonal arithmetic means).

3. OBSERVATIONS

3.1 PHYSICAL ENVIRONMENT

Stratification is one of the key physical parameters controlling primary production. For this reason, we present the upper water column stratification, calculated as the density difference between 50 m and the surface. In 2023, the timing of the spring freshet was near normal but runoff of the St. Lawrence River at Québec City was generally higher than normal from April until the end of the year (Galbraith et al. 2024b). This led to stronger-than-normal stratification for most months at Rimouski and Shediac Valley stations, especially during late summer/early fall (Figure 5). Similarly, in the Gulf, stratification was mostly above normal in August and October, as well as during March in the northernmost regions of the Gulf (Figure 6). In May and June, however, almost all locations exhibited weaker-than-normal stratification (Figures 5, 6). At the same time, the freshwater flow of rivers (other than St. Lawrence) flowing into the Estuary was also below normal (see Figure 7 in Galbraith et al. 2024b).

3.2 DEEP OXYGEN

Hypoxic waters (< 30% saturation levels) were found near 150 m deep in April 2023 at Rimouski station and most of the waters deeper than 200 m were considered to be severely hypoxic (<20 % saturation levels; Figure 7) in 2023. In the climatology, hypoxic waters were typically constrained below 200 m while severely hypoxic waters were only present below 250 m (Figure 7). In the Gulf, the lowest levels of dissolved oxygen (below 15% saturation at 300 m in recent years) were found in the deep waters at the head of the Laurentian Channel in the Estuary (Figure 8). In the deep channels, hypoxic waters extended from the Estuary to the centre or the western end of Anticosti Island, depending on the depth (Figure 8). Hypoxic waters were also found at the bottom of Anticosti and Esquiman channels in 2023. In comparison, the climatology shows oxygen levels to be above the hypoxia threshold everywhere in the Gulf at 200 m, as well as at the bottom of the northeast Gulf deep channels. In the Estuary in 2023, concentrations of dissolved oxygen remained relatively stable, or were slightly higher than last year's record lows, at 200, 250, 300 m and bottom depth (Figure 9). However, several record lows were measured at depths greater than 200 m in the other regions, especially in the northwest Gulf. The annual average dissolved oxygen saturation levels in the Estuary were 12 % (37 µM) at 300 m, and 25% (82 µM) in bottom waters (>100 m) in 2023 (Figure 9).

3.3 ACIDIFICATION PARAMETERS

In 2023, seasonal patterns of acidification parameters in the surface layer at Rimouski station closely mirrored the climatology. The highest pH_T values were observed during summer, coinciding with the activity of photosynthetic phytoplankton communities and warmer surface waters, both of which contribute to the reduction of CO_2 content (Figure 10). The annual anomalies of aragonite and calcite saturation states were positive, with annual averages exceeding the saturation horizon ($\Omega = 1$) in the surface layer. In the bottom layer, the seasonal pattern observed in 2023 deviated from the climatological norm. Both pH_T and Ω decreased to their minimum values during early summer in 2023, while these seasonal lows are typically reached during fall (Figure 10). These minimum values, measured in June, represented the lowest levels in the time series to date and resulted in the strongest annual negative anomalies observed across acidification parameters. Deep waters at Rimouski station have been undersaturated with respect to aragonite and calcite over the past decade (Figure 10).

3.4 NUTRIENTS

Distributions of dissolved inorganic nutrients (nitrate, silicate, phosphate) strongly co-vary in space and time (Brickman and Petrie 2003). For this reason and because nitrogen availability controls phytoplankton growth in coastal waters of the Gulf, emphasis in this document is given to the variability in nitrate concentrations and inventories, even though the distributions of other nutrients are also briefly discussed. In this document, we use the term “nitrate” to refer to the sum of nitrate and nitrite (NO_3^-+NO_2^-).

3.4.1 High-frequency monitoring stations

The two high-frequency monitoring stations typically exhibit a biologically mediated reduction in surface nitrate inventories in spring/summer, a minimum during summer, and a subsequent increase during fall/winter once water column mixing intensifies due to cooling processes and wind forcing (Figure 11). Seasonal stratification and mixing processes inversely influence the mid-layer nitrate inventories since the mid-layer nutrient pool supply the surface one (Figure 11). Surface and mid-layer nitrate inventories are typically two to three times higher and about three to four times higher, respectively, at Rimouski station than at Shediac Valley station (Figure 11). In 2023, surface nitrate inventories were mostly below normal during summer and near normal during the other seasons at Rimouski station. At Shediac Valley, they were either below or near normal during spring and early summer (no nutrient data available later in the year; Figure 11). The mid-layer nitrate inventory was either normal or below normal at Rimouski station, with particularly strong negative anomalies in late June/early July, and it was mostly near-normal at Shediac Valley (Figure 11). Complete vertical nitrate profiles reveal that June was associated with very low nitrate concentrations throughout the water column at Rimouski station, and the strongest negative anomalies were observed near the bottom year-round (Figure 12). At Shediac Valley, March was associated with the strongest negative anomalies in the surface layer (Figure 13).

3.4.2 Gulf regions

The spatial distribution of nitrate in the surface layer during winter 2023 was similar to the climatology with maximal concentrations in the Estuary and around the Gaspé Peninsula. However, the nitrate inventories were below normal across the Gulf, except for a small region within the lower Estuary where they were near normal (Figure 14). The estimated nitrate drawdown during spring was generally lower than normal, which could suggest low phytoplankton spring bloom intensity, except for the lower Estuary and the northeast coast (Figure 14). Surface layer nitrate inventories stayed below normal during early summer in the western Gulf and northeast coast of the Gulf, and were generally near normal in the southeastern Gulf (Figure 15). The mid-layer anomalies were somewhat similar to the surface ones, but the Magdalen Shallows and northeastern Gulf were associated with positive anomalies instead. They were particularly strong on the Magdalen Shallows. The deep waters showed mostly positive anomalies during early summer, except in the Estuary/northwest Gulf where indices were mostly near normal (Figure 15).

3.4.3 Scorecards

Annual averages of all nutrients were mostly negative in the surface layer across the Gulf (Figure 16). Surface phosphate inventories were at record low in the three southernmost locations (Figure 16). Linear regression of the surface layer nitrate annual averages suggests a significant (p <0.001) decrease of ca. 20% in the Gulf over the past 25 years. In the mid-layer, nitrate and silicate inventories were also below normal in the northern Gulf, but near normal elsewhere. Phosphate inventories showed negative anomalies across the Gulf, with strong minimum on record at Shediac Valley (Figure 17). In the deep layer, nutrient annual inventories

showed mostly strong positive anomalies throughout the Gulf, except for nitrates at Rimouski station (record low) and in the Estuary/northwest Gulf region (Figure 18). Positive anomalies of deep-water nitrate inventories have regularly been observed in central Gulf/Cabot Strait since 2012, and since 2019 in the other regions. Record-high inventories of deep nitrates and silicates were observed in the central Gulf/Cabot Strait region in 2023. However, the negative anomaly of 2023 in the Estuary/northwest Gulf region ends a series of three consecutive years of positive anomalies in nitrates. At Rimouski station, the trend of mostly negative anomalies, which started in 2016, continues (Figure 18).

The Redfield-Brzezinski C:Si:N:P ratio, which presumes equilibrium between phytoplankton composition and the deep-ocean nutrient inventory, is 106:15:16:1 (Redfield 1958; Brzezinski 1985). In the deep waters of the Gulf, the N:P ratio is lower than the target of 16, with climatology averages ranging from 11.2 to 12.4 while the Si:N ratios tend to be higher than the target of 0.94, ranging between 1.2 and 2.0 (Figure 18). The climatology N:P (Si:N) ratio is highest (lowest) at the entrance of the Laurentian Chanel and decreases (increases) as water progresses up the deep channel from Cabot Strait to the Estuary. In 2023, the deep layer N:P ratios were below normal in all regions while Si:N ratios were above normal, including record low and record high for a second consecutive year in the Estuary/northwest Gulf region and at Rimouski station. Interestingly, these patterns of lower-than-normal N:P and higher-than-normal Si:N have been consistent over the last seven years in most of the Gulf (Figure 18).

3.5 PHYTOPLANKTON

3.5.1 High-frequency monitoring stations

Seasonal water-column integrated chl *a* concentration patterns at each high-frequency monitoring station are distinct. Maximum chl *a* is typically reached during early summer and stays at relatively high levels until late summer/early fall at Rimouski station. At Shediac Valley station, the maximum is reached in early spring (no data in March) before diminishing rapidly and staying low for the remainder of the year (Figure 19). Following the spring bloom, chl *a* inventories are typically two to three times higher at Rimouski station than at Shediac Valley station (Figure 19). In 2023, chl *a* inventories generally remained below normal at Rimouski station, except during the spring bloom in June, which was on time with the climatology, and during a relatively small late summer bloom in August (Figure 19). Vertical profiles show that phytoplankton biomass was generally constrained within the top 10 m of the water column at Rimouski station (Figure 20). At Shediac Valley, chl *a* inventories mirrored the climatology (Figure 19). There was a subsurface chlorophyll *a* maximum in late April, suggesting the spring bloom was already in its late stage at that time (Figure 21).

Phytoplankton abundance at Rimouski station was highly variable in 2023, being either largely below or above normal, and rarely near normal (Figure 22). Both spring and late summer bloom periods were numerically dominated by flagellates, although these periods were also associated with an increase in the proportion of diatoms (Figure 22). At Rimouski station in 2023, the relative abundance of diatoms was approximately half the typical climatological levels throughout the year. Conversely, the proportion of dinoflagellates was about three times higher than the climatological norm and reached a relative abundance peak of 12% in November (Figure 22). Similar to phytoplankton biomasses, total phytoplankton abundances closely followed the climatological averages at Shediac Valley station (Figure 23). However, in June, September and October, the proportion of diatoms was notably lower than normal. This decrease was compensated by an increase in flagellates and dinoflagellates whose relative proportions were nearly three times higher than usual (Figure 23).

3.5.2 Gulf regions

Chlorophyll *a* inventories are typically highest in the Estuary and around the Gaspé Peninsula during early and late summer. This region becomes less of a phytoplankton hotspot during fall as chl *a* maxima typically expand into the central Gulf and northern Magdalen Shallows (Figure 24). In early and late summer 2023, chl *a* inventories (0–100 m) were mostly below normal across the Gulf (Figure 24), with the exception of the Estuary/northwest Gulf in June. There, the strong positive anomaly suggests that a spring bloom occurred at that time, similar to what was observed at Rimouski station. During fall, chl *a* inventories were near normal in most of the Gulf but were above normal along the northern shore of the Gulf (Figure 24).

In 2023, the highest phytoplankton abundance was observed during winter, in Northumberland Sound (Figure 25). Maxima of diatom relative abundances were recorded in June on the western side of Cabot Strait and in the Estuary/northwest Gulf region, coinciding with the strong positive anomaly of chl *a* inventories in the latter (Figure 25). As observed at the high-frequency monitoring stations, flagellate relative abundances were generally much higher than that of diatoms, especially during winter and fall (Figure 25).

3.5.3 Scorecards

Overall, annual averages of chl *a* inventories were near or slightly below normal, except for the Estuary/northwest Gulf region where the timing of the spring bloom coincided with AZMP early summer survey (Figure 26). Chl *a* inventories during fall were also higher than normal in the northern Gulf regions. For the sixth consecutive year, a fall bloom larger than usual has been observed in the Estuary/northwest Gulf (Figure 26). Positive anomalies of fall chl *a* inventories have been regularly observed over the past decade across the Gulf (Figure 26), representing an increase of roughly 30% of phytoplankton biomass during fall over the time series.

Since 2016, total phytoplankton abundances have regularly shown positive anomalies, driven by the higher-than-normal abundances of flagellates in most regions. During the same period, the Estuary/northwest Gulf region (and Rimouski station) has been the only one to experience regular diatom positive anomalies (Figure 27). However, both Rimouski station and the Estuary/northwest Gulf region exhibited negative anomalies in diatom abundances in 2023, with the lowest diatom abundance at Rimouski station over the time series. Diatom anomalies were mostly normal elsewhere in the Gulf in 2023 (Figure 27). In contrast, flagellate and dinoflagellate abundances were generally above normal throughout the Gulf in 2023, including a record-high abundance of dinoflagellates in the Estuary/northwest Gulf region (Figure 27).

3.5.4 Satellite remote sensing and oceanographic buoy data

Observations from the oceanographic buoy at Rimouski station are reported within this section as they compare well with satellite remote sensing data in terms of temporal and vertical (thin surface layer) resolution, providing similar indices of phytoplankton biomass. Surface chl *a* concentration estimated from the oceanographic buoy in 2023 suggests a phenology similar to what was observed from water samples collected at Rimouski station (Figure 19), with peaks of concentration in early June and in August. Chlorophyll *a* concentrations from the buoy were below normal in May until late summer when they were mostly near normal (Figure 28). In the remote sensing ocean colour polygons, phytoplankton biomass maxima reached during spring bloom were highly variable, ranging from 3 mg chl *a* m^{-3} to 18 mg chl *a* m^{-3}. Phytoplankton biomass reached its highest level of the time series in the northeast Gulf (Figure 28), where a widespread spring bloom occurred in April (Figure 29). Meanwhile biomass was slightly below normal on the Magdalen Shallows and slightly above normal in the two other polygons (Figure 28). All polygons showed markedly higher-than-normal phytoplankton biomass during fall (Figure 28). The fall bloom seems to have started in early September in the Estuary and

around the Gaspé Peninsula and then expanded to the Magdalen Shallows and the northern shore of the Gulf in October (Figure 30).

The spring bloom timing was generally normal, with only a slight delay on the Magdalen Shallows (Figure 31). The fall bloom was earlier than normal in the northeast Gulf, slightly delayed in Cabot Strait and near normal elsewhere. Bloom fits for 2023 are available in Appendix 2. Overall, annual averages suggest that phytoplankton biomass at the surface was above normal everywhere except at Rimouski station (Figure 31). Such widespread and strong positive anomalies have never been witnessed over the time series and are mostly due to the strong fall bloom that occurred across the Gulf. In the northeast Gulf, both spring and fall chl a averages in 2023 represent record highs of the time series (Figure 31). Both *in situ* and remote sensing data suggest that the fall bloom was mostly located in freshwater-influenced areas and along the northern shore of the Gulf (Figures 24, 30).

3.6 ZOOPLANKTON

3.6.1 High-frequency monitoring stations

In 2023, zooplankton biomasses were consistently below the climatology throughout the year at Rimouski station and mostly near-normal at Shediac Valley (Figure 32). Copepod abundances, however, were generally near normal at Rimouski station, with a few instances of higher-than-normal levels between June and September (Figure 33). The copepod community composition was relatively similar to the climatology, although the relative contribution of *C. hyperboreus* was largely reduced in 2023 (Figure 33). The abundances of non-copepods at Rimouski station were generally slightly below normal, except on two occasions in June (Figure 34). *Bryozoa* and *Chaetognatha,* typically absent from the dominant taxa in the non-copepod community according to climatology, were present in 2023. In contrast, *Mollusca* and *Polychaeta* was nearly absent during the entire year (Figure 34). At Shediac Valley, the abundance of copepods was variable throughout the year (Figure 35). In late May and June, the higher-than-normal abundances recorded were accompanied by a large contribution of *C. finmarchicus* (Figure 35). The abundances of non-copepods were also variable throughout the year, with higher-than-normal levels recorded in May (Figure 36). At Shediac Valley station as well, *Bryozoa* and *Chaetognatha* occupied a larger proportion of the community than normal at different times of the year, while both *Mollusca* and *Echinoderma* were absent from the dominant taxa in 2023 (Figure 36).

Despite a large peak of early copepodite stages (CI—CIII) in June, the abundances of *C. finmarchicus* were generally near normal at Rimouski station until late summer when they became above normal for the rest of the year (Figure 37). These high abundances followed a second pulse of CI-CIII copepodite stages in August (Figure 37). At Shediac Valley station, the highest and above normal *C. finmarchicus* abundances were observed in late May/early June instead, in association with the peak of early copepodite stages (Figure 37). In October, the slightly above average abundance corresponded to a proportion of CV stage that was much higher than normal (Figure 37).

The abundances of *C. hyperboreus* were strongly below normal at both high-frequency monitoring stations in 2023 (Figure 38). Early copepodite stages were nearly absent in May at Rimouski station. From that point onward, the proportion of CV stage was almost twice the climatological average while the CIV copepodite stage accounted for less than 10% of the population (Figure 38). Similarly, at Shediac Valley, no CI copepodite stage individuals were observed in April. By June, the population consisted solely of CV stage individuals, nearly 10 times the typical proportion observed at that time of the year (Figure 38).

The abundances of *Pseudocalanus* spp. were near normal during most of the year at Rimouski station (Figure 39). Abundances were above normal in spring and near normal afterwards at Shediac Valley (Figure 39). The phenology of *Pseudocalanus* spp. at Rimouski station was similar to that of *C. finmarchicus*, with the main pulse of early copepodite stages occurring in June, and a later pulse occurring in late summer. The June CI-CIII peak was about a month later than normally observed (Figure 39).

Changes in the timing of zooplankton development are further described using the detailed seasonal pattern of the relative abundance of *C. finmarchicus* copepodite stages at Rimouski station from 1994 to 2023 (Figure 40). A scorecard showing the anomaly of the first day when the normalized proportion of CIV was higher than 0.35 and the day of the maximal normalized proportion of CIV (visually defining the end of early-stage peaks of CI–CIII) was also added to provide an objective tool to describe *C. finmarchicus* phenology. Overall, there is a trend towards an earlier population development, with anomalies for both indices being nearly always negative since 2013. This trend was reinforced by the consecutive record lows of the first day index in 2021 and 2022. The phenology indices in 2023 also suggest a very early phenology for *C. finmarchicus*; the anomalies were only slightly higher than the last two years of record lows (Figure 40). From 2010 to 2014, there was a second distinct pulse of early stages in late summer and a similar pattern has also been clearly seen since 2021 (Figure 40).

3.6.2 Gulf regions

Zooplankton biomass is usually concentrated in the deep channels of the Gulf, where the large copepod *C. hyperboreus* is more abundant. As a result, zooplankton biomass tends to be lower on the coastal portions of sampling sections and on the Magdalen Shallows. Although this general pattern persisted in 2023, there were some deviations: higher-than-normal zooplankton biomass was observed on the Magdalen Shallows during fall, while lower-than-normal biomasses were observed in the northeast Gulf in early summer and in central Gulf/Cabot Strait during both seasons (Figure 41). In central Gulf/Cabot Strait, the early summer zooplankton biomass was at record low (Figure 41). Similarly, for a second consecutive year, *C. hyperboreus* abundances were at record lows in the Estuary/northwest Gulf during early summer, and in central Gulf/ Cabot Strait during both seasons (Figure 42). The highest abundances of *C. hyperboreus* in 2023 were observed near Cape Breton Island during early summer (Figure 42).

During early summer 2023, the abundances of *C. finmarchicus* were highest on the northern edge of the sections located in the Estuary/northwest Gulf region, and on the Magdalen Shallows (Figure 43). In fall, they were highest near Cape Breton Island. The Estuary/northwest Gulf and Magdalen Shallows regions exhibited higher-than-normal *C. finmarchicus* abundances during both seasons, including a time series record high in the Magdalen Shallows in fall. In the other regions, *C. finmarchicus* abundances were near normal during both seasons (Figure 43).

The abundance distribution patterns of *Pseudocalanus* spp. were somewhat similar to that of *C. finmarchicus* (Figure 44). In the Estuary/northwest Gulf region, highest abundances were observed on the northern edge of the sections. During fall, the highest abundances were sampled on the eastern side of the Magdalen Shallows section and near Cape Breton Island. During early summer, *Pseudocalanus* spp. abundances were mostly close to normal, except on the Magdalen Shallows where they were among the highest of the time series (Figure 44). During fall, however, the abundances were strongly below normal in most regions, setting new record lows in the northeast Gulf and in central Gulf/Cabot Strait (Figure 44).

The 2023 seasonal averages for zooplankton indices from the mackerel egg survey on the Magdalen Shallows and from the northern Gulf late-summer survey (ZooImage) generally agree with the AZMP time series (Figure 45). The abundance of *C. finmarchicus* was much higher

than normal on the Magdalen Shallows during early summer while the other indices were either slightly below (*C. hyperboreus*) or near normal. In the northern Gulf during late summer, only *C. finmarchicus* abundances showed above-normal levels; the other indices were largely below normal, even setting a record low for *C. hyperboreus* abundance for a second consecutive year (Figure 45). In agreement with previous observations, September zooplankton biomass was slightly below normal on Magdalen Shallows, with *C. hyperboreus* abundances being at record lows (Figure 46).

3.6.3 Scorecards

The time series of annual zooplankton biomass anomalies highlight recent major changes in the community, with mostly near-normal to negative anomalies across the Gulf since 2009 (Figure 47). Over the time series, there is a significant decrease of zooplankton biomass (p <0.05) in the Estuary/northwest Gulf region, and in the central Gulf/Cabot Strait region, representing a biomass loss of about 15% in the Estuary/northwest Gulf, and about 35% in the central Gulf/Cabot Strait. In 2023, annual zooplankton biomass anomalies were mostly below normal to near normal, and set a new record low in central Gulf/Cabot Strait region. Only Magdalen Shallows showed a zooplankton biomass positive anomaly, similar to the previous year (Figure 47).

Zooplankton biomass is strongly influenced by the abundance of large *Calanus* spp. The annual abundances of *C. finmarchicus* ranged from near normal to above normal in all regions, and were at record highs on the Magdalen Shallows and at Shediac Valley (Figure 48). The observation of strong positive anomalies of *C. finmarchicus* in four out of six locations is a first over the past decade. *C. hyperboreus*, however, showed strong negative anomalies, including unprecedented low abundances at Rimouski station, in the Estuary/northwest Gulf and in central Gulf/Cabot Strait (Figure 49). This represents the third year of large and widespread negative anomalies for *C. hyperboreus*. Consequently, the large calanoid index also reached a record low in central Gulf/Cabot Strait, but its anomalies were positive in the Estuary/northwest Gulf and on the Magdalen Shallows. This index has shown mostly near normal to negative anomalies since 2010 (Figure 49).

The general decrease in zooplankton biomass over time is consistent with the increase in the abundance of *Pseudocalanus* spp., total copepods, non-copepods, small calanoids and cyclopoïds, for which positive anomalies have been regularly observed since around 2014 (Figures 48, 49: see Appendix 1 for a detailed list of species included in each of these indices). In 2023, many of these groups presented fewer positive anomalies than they did over the past decade or so. This is the case for the index of small calanoids, which had negative anomalies in most regions. The non-copepod index showed a positive anomaly only at Shediac Valley station, and the *Pseudocalanus* spp. and total copepod indices were at record low abundances in central Gulf/Cabot Strait (Figure 48).

The abundance of warm-water copepods has also increased since 2011 (Figure 49). However, in 2023, above-normal anomalies were only encountered at Rimouski station and in the Estuary/northwest Gulf region. At these locations, *Metridia lucens* was responsible for these high abundances (result not shown). Cold-water copepods have also regularly shown positive anomalies in most regions since 2016, including 2023 (Figure 49). It is mostly *M. longa* abundance, that accounts for these positive anomalies (not shown). For the first time since the early 2000s, all non-copepod taxa showed either near-normal or lower-than-normal mean annual abundances in all locations, except for *Crustacea* in the Estuary/northwest Gulf region (Figure 50).

In general, annual anomalies were coherent among the high-frequency monitoring stations and their associated Gulf region (Figures 47–49). This suggests a high reliability of our annual

estimates throughout the Gulf even though data collection is limited to early summer and fall surveys for zooplankton indices.

4. DISCUSSION

4.1 ENVIRONMENTAL CONDITIONS

The timing of water column stratification onset and its strength play a role in defining spring bloom phenology, phytoplankton production, species succession, and trophic interactions throughout the growth season (Levasseur et al. 1984). In 2023, the absence of data collection in April at Rimouski station prevented the observation of the spring stratification pattern. However, the very strong St. Lawrence River freshet in April and early May (Galbraith et al. 2024b) suggests that the onset of stratification at Rimouski station was probably slightly earlier than or near normal. The marine heatwave in late summer/early fall (Galbraith et al. 2024b) only explains one third of the very strong stratification observed at that time. In addition to the effect of water column stratification on phytoplankton dynamics, thermal properties of the surface, cold intermediate layer (CIL; correspond to the winter surface mixed layer that has been isolated from the atmosphere through seasonal warming of the surface layer), and deep-water masses play a role in defining zooplankton dynamics (Plourde et al. 2002). Galbraith et al. (2024b) reported on the physical conditions that prevailed in the Gulf during 2023, showing warmer-than-normal conditions for most indices and water column layers which likely had both direct and indirect effects on the chemical and biological conditions observed.

In the Gulf, a dissolved oxygen value of 100 µmol L^{-1} at 300 m corresponds to approximately 30% saturation. Water with oxygen levels below this threshold is considered hypoxic, which can hamper the survival of some species such as Atlantic cod (Plante et al. 1998). The combination of AZMP data with the time series published by Gilbert et al. (2005) indicates that the deep waters of the Estuary have consistently been hypoxic since 1984. Changes in dissolved oxygen of the deep waters entering the Gulf at the continental shelf are related to the varying proportions of Labrador Current water (LCW; colder/fresher, high dissolved oxygen levels) and North Atlantic Central Water (NACW; warmer/saltier, low dissolved oxygen levels), which together form the source of Gulf deep waters (McLellan 1957, Lauzier and Trites 1958, Gilbert et al. 2005). In recent years, the contribution of NACW to the deep Gulf waters has increased (Gilbert et al. 2005, Galbraith et al. 2024b) and could now be at nearly 100% (Jutras et al. 2023). These deep waters take approximately three to four years to travel from the mouth of the Laurentian Channel to the Estuary (Gilbert 2004). During this time, the dissolved oxygen content decreases due to *in situ* respiration and oxidation of organic material by microbes as the water progresses to the channel heads. Thus, the record low saturation levels measured in 2022 in the deep waters of Cabot Strait and now in the central and northwest Gulf in 2023 suggest that the hypoxic conditions of the Estuary could worsen in a near future.

Given the inherent properties of the Gulf source waters (NACW vs. LCW; Gilbert et al. 2005), changes in their mixing ratio at Cabot Strait imply that a decrease of 1.46 µmol L^{-1} of oxygen might be expected for each 0.1°C temperature increase. However, today's deep oxygen concentrations at Cabot Strait represent a decline of ca. 70 µmol L^{-1} compared with their concentrations in the early 1970s (ca. 190 µmol L^{-1} at 300 m; Gilbert et al. 2005), for a nearly 2.0°C increase in temperature over the same period (Fig. 49 in Galbraith et al. 2024b). Deep-water temperature in the Estuary has increased by 1.81°C at 300 m over the past 50 years (Fig. 49 in Galbraith et al. 2024b) while oxygen concentration has decreased from ca. 105 µmol L^{-1} (Gilbert et al. 2005) to 37.1 µmol L^{-1}. This is over twice as much as expected from the temperature changes according to the mixing ratio of source waters. Thus, warming of bottom water and reduced initial oxygen saturation levels through changes in the mixing ratio of

source waters are not the only factors contributing to the decrease in oxygen concentrations in the Gulf. Other factors that can cause variability in oxygen concentration of deep waters include interannual changes in the vertical flux of organic matter, modifications in microbial metabolic processes such as increased respiration in warmer waters, and a reduction of deep inflow transport and bottom water ventilation via increased stratification (Jutras et al. 2023).

Ocean acidification represents another oceanic stressor arising from anthropogenic activities and associated environmental changes (Pörtner et al. 2019). Ocean acidification is primarily driven by the absorption of atmospheric carbon dioxide (CO_2) by the oceans, leading to widespread alterations in oceanic chemistry, including declines in carbonate ion concentrations and pH, which may threaten marine organisms that produce calcium carbonate structures such as shells and skeletons. Acidification may be further exacerbated in nearshore and estuarine waters from shifts in hydrographic and biogeochemical processes (Cai et al. 2021; Doney 2010). In surface water layers, spatiotemporal variability in hydrodynamic conditions (e.g., sea ice dynamics, freshwater inputs, circulation), physical conditions (e.g., temperature, salinity, gas exchange), and biogeochemistry (nutrient supply, organic matter production and respiration) are important drivers of the seasonal fluctuations in acidification parameters. Overall interannual variability in these surface waters is also linked to increasing atmospheric CO_2 concentrations. Acidification processes in deep waters may be influenced by the seasonal cycle of phytoplankton production via the downward flux of organic matter and its concurrent microbial remineralization which consumes O_2 and produces CO_2. Microbial respiration can thus exacerbate ocean acidification and deoxygenation, a phenomenon frequently observed in deep waters (Klein et al. 2020 and references therein). The Gulf of St. Lawrence has experienced the fastest decrease in pH of the Atlantic Zone, at a rate of about 0.04 units per decade since 1934 (Bernier et al. 2023). This is particularly notable in the St. Lawrence Estuary, as evidenced at Rimouski station, where waters of the deep layer exhibited record low values of pH as well as undersaturation with respect to aragonite and calcite in 2023. Future increases in atmospheric CO_2, water column stratification and downward fluxes of organic material and their remineralization in deep waters are expected to lead to a spatial expansion of calcium carbonate undersaturation in bottom waters of the lower St. Lawrence Estuary during the next decades (Lavoie et al. 2020).

Winter mixing is a critical process for bringing nutrient-rich deep water to the surface. In the Gulf, winter convection is partly driven by buoyancy loss of surface waters attributable to cooling and reduced freshwater runoff, brine rejection associated with sea-ice formation, and wind-driven mixing prior to ice formation (Galbraith 2006). Warmer-than-normal surface waters throughout the winter, minimal sea-ice formation, and reduced volume of winter mixed-layer can be associated with low winter convection and may reduce the amount of nutrients available for spring primary production. Since 2010, various temperature and ice-cover indices have indicated significant warming of the Gulf (Galbraith et al. 2024b). These anomalies are tied with significant decreases in the nitrate content of the surface layer over the time series. In 2023, several indices were indicative of low winter convection. Large freshwater runoffs most of the year, and intense and numerous marine heatwaves further intensified stratification later in the year (Galbraith et al. 2024b). The freshwater inflow typically accounts for up to 35% of nutrient input to the Estuary (Lavoie et al. 2021). However, high freshwater inflow and resulting stratification, as observed in 2023, may reduce the strength of upwellings at the head of the Laurentian Chanel. Consequently, the negative anomalies observed in the mean annual surface nutrient inventories across most regions in 2023, were likely primarily driven by physical conditions rather than biological consumption. The strong spring bloom in the northeast Gulf could have further emphasized nutrient depletion in that area. The delay in sea ice formation (Galbraith et al. 2024b) could also have prolonged phytoplankton production. However, unlike

2022, remote sensing in 2023 showed no evidence of significant phytoplankton production during winter.

Since 2012, positive anomalies in deep-water nitrates have regularly been observed in the central Gulf and Cabot Strait in association with greater contribution of NACW to the water masses composition (Gilbert et al. 2005, Galbraith et al. 2024b, Jutras et al. 2023). Additionally, reduced exchanges between the upper layer and the CIL, associated with generally increased stratification, might further increase the deep nutrient pool. The year 2023 marks the seventh consecutive year of rather strong nutrient ratio anomalies in most of the Gulf deep waters (negative anomalies for N:P and positive anomalies for Si:N). At Rimouski station and in the Estuary/northwest Gulf, the nutrient ratio anomalies even reached record levels in 2023. Deep-water masses entering the Gulf through Cabot Strait have unique nutrient ratio signatures. However, as the water masses circulate through the Laurentian Chanel, the nutrient signatures are altered by microbial processes involved in nitrogen cycling such as nitrification and denitrification (typically occurring in hypoxic to anoxic conditions, see review by Hutchins and Capone 2022). As water progresses from Cabot Strait to the Estuary, changes in nutrient ratio associated with concomitant decreases in nitrate and oxygen concentrations suggest that denitrification is a major driver of nitrate levels in deep waters. A recent study highlighted the intensification of fixed-nitrogen removal processes over the past 15 years in the Estuary in association with the expansion of the hypoxic zone (Pascal et al. 2024).

4.2 PHYTOPLANKTON

Except at Rimouski station, where sampling regularly covers the spring bloom period, phytoplankton production during the spring bloom must be inferred either from indirect indices, such as the difference between the nutrient inventory of the surface mixed layer from winter to early summer (drawdown), or from satellite observations. The estimate of nutrient drawdown during spring suggests that bloom production in 2023 was generally below normal, except in the Estuary and in a small part of northeast Gulf, in relative agreement with the phytoplankton biomass distribution observed by remote sensing in April. The intensity of the spring bloom is largely controlled by the availability of nitrogen at the onset of stratification and by overwintering copepods (Sommer and Lengfellner 2008). Considering the low zooplankton biomass over the Gulf during the 2021-2023 period, and the below-normal abundances of *C. hyperboreus* that is a major consumer of spring bloom production (Plourde et al. 2003), low nitrate availability in March likely played a key role in limiting the intensity of the spring bloom in most locations.

No distinct trends in the timing of the spring bloom were identified over the time series in the Gulf. Under global warming scenarios, an earlier onset of stratification is expected to trigger an earlier spring bloom. However, the expected concomitant large freshet (due to an increase in precipitation) may prevent the accumulation of phytoplankton biomass in the water column in regions under the influence of freshwater, which may instead delay bloom start in these regions (Levasseur et al. 1984, Zakardjian et al. 2000). In 2023, a year of larger-than-normal spring freshet, the timing of the bloom was either near-normal (Rimouski and northwest Gulf) or delayed (Magdalen Shallows) in the regions under the influence of freshwater. Another foreseen outcome of the increased stratification under warmer conditions is the larger contribution of smaller sized cells, known to perform better in nutrient-poor and highly stratified waters, to the phytoplankton assemblage (Legendre and Rassoulzadegan 1995). The first glance at taxonomic composition over the Gulf provided in this report supports this hypothesis, with mostly positive anomalies of flagellates since 2016. Warmer conditions combined with increased freshwater input may also promote harmful algal blooms (HABs) of toxin-producing

dinoflagellates (Boivin-Rioux et al. 2021, Boivin-Rioux et al. 2022). The proportion of dinoflagellates was unusually high in 2023 at both high-frequency monitoring stations.

For all seasons except spring, ocean colour data retrieved from remote sensing are complemented with *in situ* observations. These two sources of data have regularly differed in their respective anomaly outputs in regards to seasonal phytoplankton biomasses. Divergences, when occurring, can be explained by several factors including the vertical structure of phytoplankton in the water column; computational discrepancies in seasonal anomalies (complete season in each ocean-colour polygon versus a few days in each Gulf region for *in situ* sampling — timing of sampling of each dedicated AZMP surveys is indicated in Figure 28); timing of *in situ* sampling with respect to phytoplankton phenology; difference in the volume of water sampled by each method, cloud cover, etc. During the 2018-2021 period, ocean colour data often shown below-normal chl a concentrations in the thin surface layer during fall while *in situ* data have regularly suggested positive phytoplankton biomass anomalies in recent years. However, in 2023, these two sources of observations both suggested that phytoplankton biomass was above normal in many regions during fall, with possible implications for higher trophic levels. An increased occurrence of fall storms, as frequently observed in recent years (Galbraith et al. 2023), and the associated input of nutrients to the surface layer promotes ideal growth conditions for phytoplankton, especially if combined with a reduction in grazing pressure. In fall 2023, however, no wind storm capable of explaining the strong surface blooms occurred. Both *in situ* (Figure 24) and ocean colour data (Figure 30) suggest that the fall blooms were mostly located in the freshwater-influenced areas and along the northern shore of the Gulf. Deposition of nitrogen-rich particles from wildfire plumes during the extensive and long-lasting forest fires occurring in northern Quebec during summer 2023 could have contributed to the nutrient enrichment of river flows and promoted the development of fall blooms, similarly to previous observations from other regions of the world (Liu et al. 2022, Seok et al. 2024).

4.3 ZOOPLANKTON

Zooplankton biomass has generally been below normal in recent years, with several record-low levels in 2016–2017 and again in 2021–2023. Lower biomass is typically associated with a decrease in the abundance of large zooplankton species. The mean weight of large calanoids (e.g., *C. hyperboreus*: 3.5 mg per adult female) is between one and two orders of magnitude greater than that of small calanoids (e.g., *Pseudocalanus* spp.: 0.02 mg per adult female) (Conover and Huntley 1991, Plourde et al. 2003). Thus, low abundance of large calanoids has a greater impact on zooplankton biomass than the high abundances of *Pseudocalanus* spp., which have been regularly observed over recent years. In these years, the increase in small calanoids seems to be coupled with an increase in non-copepod abundance, mostly larvae of benthic organisms. Suitability of environmental conditions, competition for food, the availability of large versus small phytoplankton cells, and/or differential predation pressure might favour the dominance of either one of these communities, *i.e.*, one dominated by large calanoids versus one dominated by a combination of small calanoids and non-copepods (Hall et al. 1976; Daewel et al. 2014), with potential implications for the pelagic food web and pelago–benthic coupling. In 2023, however, the community composition was similar to that of the 2000–2010 decade, *C. finmarchicus* was abundant and the small calanoids and non-copepod community was near or below average, despite low zooplankton biomass.

Life cycle strategies vary among large copepod species, and so do the environmental drivers influencing their phenology. For instance, interannual variations in the abundance of *C. hyperboreus* and its phenology is known to be mostly influenced by spring conditions, including timing of sea-ice retreat and temperature (Plourde et al. 2003, Lehoux et al. 2021), while late summer and early fall environmental conditions also influence the phenology of

C. finmarchicus since part of the population is still active during that period. Moreover, the timing of reproduction of each taxa relative to the freshet — considering its influence on water-mass circulation and transport in regions that are under the influence of freshwater (Runge et al. 1999) — can largely influence zooplankton spatial distribution and result in dissimilarities in the spatial pattern of different species (Brennan et al. 2021).

In 2023, the strong negative anomalies of zooplankton biomass and *C. hyperboreus* abundances in all regions but Magdalen Shallows likely resulted from environmental conditions. The early sea-ice retreat could explain the early phenology of *C. hyperboreus*, as suggested by its high CIV/CI-CIV ratio in May, at both high-frequency monitoring stations. The peak of *C. hyperboreus* early copepodite stages presumably occurred in April (no data in April) at Rimouski station, coinciding with the maximal spring freshet (Galbraith et al. 2024b) which likely promoted their export to the Magdalen Shallows. There, the high proportion of *C. hyperboreus* diapausing CV in early summer most probably favoured their retention in this region (Brennan et al. 2019). Also, the near absence of diapausing CIV stage at Rimouski station suggests that recruitment of *C. hyperboreus* was unusually low in the Estuary in 2023.

The peak timing (June) of *C. finmarchicus* early copepodite stages at Rimouski station was coupled with the timing of the spring bloom in this area and probably enhanced their survival rates, while their retention within the Estuary was maximized by calmer hydrodynamical conditions post-freshet. However, the marked asymmetry in *C. finmarchicus* abundances between the Estuary's northern and southern shores combined with their high abundances on the Magdalen Shallows in early summer suggests that transport still occurred between both regions, maybe prior to the main CI─CIII copepodite peak. Under favourable conditions, *C. finmarchicus* may produce a second cohort that typically develops in late summer, a phenomenon that has increased in occurrence since 2010. A second cohort of *C. finmarchicus* developed in August 2023 at Rimouski station, likely benefiting from the short late summer bloom and potentially explaining the absence of a fall bloom in the Estuary, contrary to elsewhere in the Gulf.

The northeast Gulf and the central Gulf/Cabot Strait regions are less influenced by freshwater; environmental conditions modifying the zooplankton community in these regions might instead include CIL conditions, the volume and temperature of cold and saline Labrador Shelf water that flows into northeast Gulf through the Strait of Belle Isle or the mixing ratio of source waters that enters the deep Laurentian Chanel through Cabot Strait. Differences in these environmental drivers might explain why these two regions often show distinct anomaly patterns for the zooplankton assemblage compared to observations elsewhere. In 2023, these two regions showed neutral or negative anomalies for almost all zooplankton indices. Such limited top-down control on phytoplankton growth might explain the strong blooms that were observed in the northeast Gulf, and might suggest higher export of organic matter to the bottom waters.

4.4 PERSPECTIVES

The unprecedented low pH levels in the St. Lawrence Estuary in 2023 as well as record-low oxygen saturation values in the northwestern and central Gulf highlight the need for continued studies on the impacts of deoxygenation and ocean acidification on the vulnerability of aquatic species and their associated biological and ecological processes. Moreover, the drivers of the observed changes in nutrient inventories, phytoplankton biomass, and zooplankton community composition and size structure, how they interact and how they are expected to evolve, still remain to be fully understood. While the roles of predation and changing predator stocks in the observed trends have yet to be determined, it is possible to get some insight into the effect of environmental variables on biological components using a simple correlation matrix (Figure 51). Among other things, this matrix shows that a cold CIL—which would imply higher winter

convection and a later onset of stratification—promotes a late bloom start and high surface nitrate inventories. Zooplankton biomass is strongly positively correlated to a community dominated by large copepods and inversely correlated with small calanoids and non-copepods as would be expected. Thermal properties of the water column and spring bloom dynamics—especially its timing—could be major drivers of zooplankton assemblage. Indeed, it seems that a cold CIL favours high zooplankton biomass (negative correlation) while a cold deep layer reduces the abundance of non-copepods (positive correlation). Phytoplankton community composition and changes in species succession may also be important drivers for the zooplankton assemblage, but they were not included in this correlation matrix since time series outside of the high-frequency monitoring stations are too short for statistical significance. It is possible that the highly stratified and nutrient-poor conditions along with reduced grazing of recent years promoted the increased abundance of flagellates (Cloern 2017, Cushing 1989, Ward et al. 2012) seen in the Gulf. In turn, these processes could favour the development of small calanoid/non-copepod assemblage, as in the traditional view of smaller grazer feeding on smaller phytoplankton cells (Kiørboe 1993, Legendre and Rassoulzadegan 1995). These environmental drivers may also trigger changes in the developmental timing of zooplankton taxa (not illustrated in Figure 51), such as the earlier development of large *Calanus*. Overall, these preliminary analyses highlight the importance of bottom-up controls in shaping zooplankton communities, although the relative importance of these processes is not yet well understood.

5. SUMMARY

This document reports on the chemical and biological (plankton) conditions in the Gulf of St. Lawrence observed in 2023 in the context of warmer-than-normal conditions prevailing since 2010.

- Deep dissolved oxygen concentrations remained relatively stable at Rimouski station and in the Estuary, near last year's record lows. New record lows were observed at 250 m, 300 m and in the bottom waters of the northwest Gulf, as well as at 250 m in the central Gulf. Average annual saturation levels were 12 % (37 $\mu mol\ L^{-1}$) at 300 m and 10% (34 $\mu mol\ L^{-1}$) in the bottom waters of the Estuary in 2023.
- Acidification parameters reached record levels in the bottom waters at Rimouski station, with pH_T and saturation states of carbonate calcium dropping to their lowest point in the time series.
- Nutrient inventories were strongly below normal in the surface layer of the Gulf, mostly below normal in the mid-layer, and above normal in the deep layer except for nitrates in the Estuary/northwest Gulf region and at Rimouski station (record low).
- Since 2017 and continuing through 2023, the positive anomalies of deep nutrient content are associated with negative anomalies of the N:P ratio and positive anomalies of the Si:N ratio.
- Annual averages of *in situ* chl a inventory were either below normal or near normal, except in the Estuary/northwest Gulf where both spring and fall blooms were captured by oceanographic surveys.
- Flagellate and dinoflagellate abundances were generally higher than normal in 2023, a recurrent pattern since 2016 and 2019, respectively. Diatom abundances were below normal at Rimouski station and in the Estuary/northwest Gulf region, a first since 2017.
- Ocean colour data revealed higher-than-normal annual surface chl a concentrations in most locations, primarily due to the strong fall bloom that occurred across the Gulf and led to

record-high fall phytoplankton biomass in most locations. Phytoplankton spring biomass production was extremely high in the northeast Gulf.

- Timings of spring and fall blooms were generally normal, spring bloom was delayed on the Magdalen Shallows and fall bloom was early in the northeast Gulf and delayed in Cabot Strait.
- Zooplankton biomass was generally below normal and reached the lowest level on record in the central Gulf/Cabot Strait region. Concomitantly, very low abundances of *C. hyperboreus* were observed everywhere in the Gulf, particularly at Rimouski station, in the Estuary/northwest Gulf and in the central Gulf/Cabot Strait where record-low abundances were observed.
- The abundances of *C. finmarchicus* reached record high levels on the Magdalen Shallows. Abundances of *C. finmarchicus* was also higher than normal in the Estuary/northwest Gulf region, and at the high-frequency monitoring stations.
- The phenology of large *Calanus* at Rimouski station was earlier than usual and among the earliest of the time series at this high frequency station for *C. finmarchicus*.
- The shift in the zooplankton community size structure toward a higher proportion of small copepods and non-copepods, observed over the past decade, was not seen in 2023. The community composition in 2023 was more similar to the pre-2010 communities, with several negative anomalies of small copepods, non-copepods and *Pseudocalanus* spp., and positive anomalies of *C. finmarchicus* in the regions under the influence of freshwater.

ACKNOWLEDGEMENTS

The data used in this report would not be available without the amazing work of the AZMP team (Félix St-Pierre, David Leblanc, Caroline Lafleur, Anthony Ouellet, Nicolas Coulombe, Sylvain Dubé, Guillaume Mercier, Myranda Blouin, Michel Rousseau, Véronique Desborbes, Marie-Noëlle Bourassa and Hélèna Talbot) in organizing and carrying out AZMP surveys, analyzing samples, and ensuring quality control of the data. We thank Jean-Yves Couture, Marie-France Beaulieu, Caroline Lebel and Christian Turcotte for preparation and standardization of the phytoplankton and zooplankton data; Claude Potvin and Aude Boivin-Rioux for preparation, analysis and calibration of the acidification data; Jeff Spry, Kevin Pauley, Jay Bugden and Lindsay Beazley for providing data from Shediac Valley station; and Emmanuel Devred for the large contribution and support in providing ocean colour data. We are grateful to Christiane Dufresne and Emmanuel Devred for their critical reviews.

REFERENCES

Bernier, R. Y., Jamieson, R. E., Kelly, N. E., Lafleur, C., Moore, A. M. 2023. State of the Atlantic Ocean Synthesis Report. Canadian Technical Report of Fisheries and Aquatic Sciences, 3544: v + 219 p.

Blais, M., Galbraith, P.S., Plourde, S. and Lehoux, C. 2023a. Chemical and Biological Oceanographic Conditions in the Estuary and Gulf of St. Lawrence during 2022. Can. Tech. Rep. Hydrogr. Ocean Sci. 357 : v + 70 p.

Blais, M., Galbraith, P.S., Plourde, S., Lehoux, C. and Devine, L. 2023b. Chemical and Biological Oceanographic Conditions in the Estuary and Gulf of St. Lawrence during 2021. DFO Can. Sci. Advis. Sec. Res. Doc. 2023/045. iv + 74 p.

Boivin-Rioux, A., Starr, M., Chassé, J., Scarratt, M., Perrie, W., and Long, Z. 2021. Predicting the effects of climate change on the occurrence of the toxic dinoflagellate *Alexandrium catenella* along Canada's east coast. Front. Mar. Sci. 7:608021. doi:10.3389/fmars.2020.608021

Boivin-Rioux, A., Starr, M., Chassé, J., Scarratt, M., Perrie, W., Long, Z., and Lavoie, D. 2022. Harmful algae and climate change on the Canadian East Coast: Exploring occurrence predictions of *Dinophysis acuminata*, *D. norvegica*, and *Pseudo-nitzschia seriata*. Harmful Algae 112: 102183. doi: 10.1016/j.hal.2022.102183

Brennan, C.E., Maps, F., Gentleman, W.C., Plourde, S., Lavoie, D., Chassé, J., Lehoux, C., Krumhansl, K.A., and Johnson, C.L. 2019. How transport shapes copepod distributions in relation to whale feeding habitat : Demonstration of a new modelling framework. Prog. Oceanogr. 171: 1–21. doi:10.1016/j.pocean.2018.12.005.

Brennan, C.E., Maps, F., Gentleman, W.C., Lavoie, D., Chassé, J., Plourde, S., and Johnson, C.L. 2021. Ocean circulation changes drive shifts in Calanus abundance in North Atlantic right whale foraging habitat: A model comparison of cool and warm year scenarios. Prog. Oceanogr. 197:102629. https://doi.org/10.1016/j.pocean.2021.102629

Brickman, D., and Petrie, B. 2003. Nitrate, silicate and phosphate atlas for the Gulf of St. Lawrence. Can. Tech. Rep. Hydrogr. Ocean Sci. 231: xi + 152 p.

Brzezinski, M. A. 1985. The Si:C:N ratio of marine diatoms: interspecific variability and the effect of some environmental variables. J. Phycol. 21: 347-357.

Cai, W.-J., Feely, R. A., Testa, J. M., Li, M., Evans, W., Alin, S. R., Xu, Y.-Y., Pelletier, G., Ahmed, A., Greeley, D. J., Newton, J. A., and Bednaršek, N. 2021. Natural and Anthropogenic Drivers of Acidification in Large Estuaries. Annual Review of Marine Science. 13:23–55. https://doi.org/10.1146/annurev-marine-010419-011004.

Casault, B., Beazley, L., Johnson, C., Devred, E., and Head, E. 2024. Chemical and Biological Oceanographic Conditions on the Scotian Shelf and in the Eastern Gulf of Maine during 2022. Can. Tech. Rep. Fish. Aquat. Sci. 3589 : vi + 72 p.

Clay, S., Layton, C., and Devred, E. 2021. BIO-RSG/PhytoFit: First release (Version v1.0.0). Zenodo. https://doi.org/10.5281/zenodo.4770754.

Cloern, J.E. 2017. Why large cells dominate estuarine phytoplankton. Limnol. Oceanogr. doi: 10.1002/lno.10749

Conover, R. J., and Huntley, M. 1991. Copepods in ice-covered seas - Distribution, adaptations to seasonally limited food, metabolism, growth patterns and life cycle strategies in polar seas. J. Mar. Syst. 2: 1–41.

Cushing, D.H. 1989. A difference in structure between ecosystems in strongly stratified waters and in those that are only weakly stratified. J. Plankton Res. 11(1): 1-13.

Daewel, U., Hjøllo, S.S., Huret, M., Ji, R., Maar, M., Niiranen, S., Travers-Trolet, M., Peck, M.A., and van de Wolfshaar, K. E. 2014. Predation control of zooplankton dynamics: a review of observations and models. ICES J. Mar. Sci. 71(2): 254–271.

Doney, S. C. 2010.The Growing Human Footprint on Coastal and Open-Ocean Biogeochemistry. Science, 328:1512-1516. https://doi.org/10.1126/science.1185198.

Galbraith, P. S. 2006. Winter water masses in the Gulf of St. Lawrence. J. Geophys. Res. 111, C06022, doi: 10.1029/2005JC003159.

Galbraith, P.S., Chassé, J., Shaw, J.-L., Dumas, J. Lefaivre, D. and Bourassa, M.-N. 2023. Physical Oceanographic Conditions in the Gulf of St. Lawrence during 2022. Can. Tech. Rep. Hydrogr. Ocean Sci. 354 : v + 88 p.

Galbraith, P.S., Blais, M., Lizotte, M., Cyr, F., Bélanger, D., Casault, B., Clay, S., Layton, C., Starr, M., Chassé, J., Azetsu-Scott, K., Coyne, J., Devred, E., Gabriel, C.-E.,Johnson, C.L., Maillet, G., Pepin, P., Plourde, S., Ringuette, M., Shaw, J.-L.. 2024a. Oceanographic conditions in the Atlantic zone in 2023. Can. Tech. Rep. Hydrogr. Ocean. Sci. 379 : v + 38 p.

Galbraith, P.S., Chassé, J., Shaw, J.-L., Dumas, J. and Bourassa, M.-N. 2024b. Physical Oceanographic Conditions in the Gulf of St. Lawrence during 2023. Can. Tech. Rep. Hydrogr. Ocean Sci. 378 : v + 91 p.

Gibb, O., Cyr, F., Azetsu-Scott, K., Chassé, J., Childs, D., Gabriel, C.-E., Galbraith, P. S., Maillet, G., Pepin, P., Punshon, S., and Starr, M. 2023. Spatiotemporal variability in pH and carbonate parameters on the Canadian Atlantic continental shelf between 2014 and 2022, Earth Syst. Sci. Data, 15, 4127–4162, https://doi.org/10.5194/essd-15-4127-2023.

Gilbert, D. 2004. Propagation of temperature signals from the northwest Atlantic continental shelf edge into the Laurentian Channel. ICES CM, 2004/N: 7, 12 pp.

Gilbert, D., Sundby, B., Gobeil, C., Mucci, A., and Tremblay, G.-H. 2005. A seventy-two-year record of diminishing deep-water oxygen in the St. Lawrence estuary: The Northwest Atlantic connection. Limnol. Oceanogr., 50(5): 1654–1666.

Grosjean, P., Denis K., and Wacquet G. 2018. ZooImage: Analysis of numerical plankton images. R package version 5.5.2. https://CRAN.R-project.org/package=zooimage

Hall, D.J., Threlkeld, S.T., Burns, C.W., and Crowley, P.H. 1976. The size-efficiency hypothesis and the size structure of zooplankton communities. Annu. Rev. Ecol. Evol. Syst. 7: 177–208.

Hutchins, D.A., and Capone, D.G. The marine nitrogen cycle: new developments and global change. 2022. Nat Rev Microbiol. 20: 401–414. https://doi.org/10.1038/s41579-022-00687-z

Jutras, M., Mucci, A., Chaillou, G., Nesbitt, W.A., and Wallace D.W.R. 2023. Temporal and spatial evolution of bottom-water hypoxia in the St. Lawrence estuarine system. Biogeosciences. 20: 839-849.

Kiørboe, T. 1993. Turbulence, phytoplankton cell-size, and the structure of pelagic food webs. Adv. Mar. Biol. 29: 1–72. doi:10.1016/S0065-2881(08)60129-7.

Klein S.G., Steckbauer A., and Duarte C.M. 2020. Defining CO_2 and O_2 syndromes of marine biomes in the Anthropocene. Glob Chang Biol. 26(2):355-363. doi:10.1111/gcb.14879.

Laliberté, J., Larouche, P., Devred, E., and Craig, S. 2018. Chlorophyll-a concentration retrieval in the optically complex waters of the St. Lawrence Estuary and Gulf using principal component analysis. Remote Sens. 10, 265, doi: 10.3390/rs10020265.

Lavoie, D., Lambert, N., Rousseau, S., Dumas, J., Chassé, J., Long, Z., Perrie, W., Starr, M., Brickman, D., Azetsu-Scott, K. 2020. Projections of future physical and biochemical conditions in the Gulf of St. Lawrence, on the Scotian Shelf and in the Gulf of Maine using a regional climate model. Can. Tech. Rep. Hydrogr. Ocean Sci. 334: xiii + 102 p.

Lavoie, D., Lambert, N., Starr, M., Chassé, J., Riche, O., Le Clainche, Y., Azetsu-Scott, K., Béjaoui, B., Christian, J.R., and Gilbert, D. 2021 The Gulf of St. Lawrence biogeochemical model: A modelling tool for Fisheries and Ocean management. Front. Mar. Sci. 8:732269, doi: 10.3389/fmars.2021.732269.

Lauzier, L.M., and Trites, R.W. 1958. The deep waters of the Laurentian Channel. J. Fish. Res. Board Can. 15: 1247–1257.

Layton, C., Devred, E., DeTracey B. 2022. A comparison of phytoplankton spring bloom fitting methods using MODIS satellite-derived chlorophyll-a concentration for the Maritimes region. Can. Tech. Rep. Hydrogr. Ocean Sci. 340: vii +22 p.

Legendre L., and Rassoulzadegan, F. 1995. Plankton and nutrient dynamics in marine waters. Ophelia. 41(1): 153-172. doi: 10.1080/00785236.1995.10422042.

Lehoux, C., Plourde, S., Chamberland, J.-M., and Benoît, H. 2021. Linking interannual variations of capelin abundance indices in the Gulf of St. Lawrence to environmental proxies of bottom-up regulation of cohort strength. DFO Can. Sci. Advis. Sec. Res. Doc. 2021/068. iv + 51 p.

Levasseur, M., Therriault, J.-C., and Legendre, L. 1984. Hierarchical control of phytoplankton succession by physical factors. Mar. Ecol. Prog. Ser. 19: 211–222.

Liu, D., Zhou, C., Keesing, J.K., Serano, O., Werner, A., Fang, Y., Chen, Y., Masque, P., Kinloch, J., Sadekov, A., and Du., Y. 2022. Wildfire enhances phytoplankton production in tropical oceans. Nat. Commun. 13: 1348. https://doi.org/10.1038/s41467-022-29013-0

Maillet, G., Bélanger, D., Doyle, G., Robar, A., Rastin, S., Ramsay, D., and Pepin, P. 2022. Optical, Chemical, and Biological Oceanographic Conditions on the Newfoundland and Labrador Shelf during 2018. DFO Can. Sci. Advis. Sec. Res. Doc. 2022/075.

McLellan, H.J. 1957. On the distinctness and origin of the slope water off the Scotian Shelf and its easterly flow south of the Grand Banks. J. Fish. Res. Board Can. 14: 213–239.

Mitchell, M. R., Harrison, G., Pauley, K., Gagné, A., Maillet, G., and Strain, P. 2002. Atlantic Zonal Monitoring Program sampling protocol. Can. Tech. Rep. Hydrogr. Ocean Sci. 223: iv + 23 p.

Mucci, A., Starr, M., Gilbert, D., and Sundby, B. 2011. Acidification of Lower St. Lawrence Estuary Bottom Waters. Atmosphere-Ocean, 49:3, 206-218, DOI: 10.1080/07055900.2011.59926

Pascal, L., Cloutier-Artiwat, F., Zanon, A., Wallace D.W.R., and Chaillou, G. 2024. Fixed-nitrogen loss in a deoxygenating coastal ocean: Insights from the Estuary and Gulf of St. Lawrence. ESS Open Archive. doi: 10.22541/essoar.171560871.19656696/v1

Parent, G.J., Plourde, S. and Turgeon, J. 2011. Overlapping size ranges of Calanus spp. off the Canadian Arctic and Atlantic coasts: impact on species' abundances. J. Plankton Res. 33:1654–1665.

Plante, S., Chabot, D., and Dutil, J.-D. 1998. Hypoxia tolerance in Atlantic cod. J. Fish Biol. 53: 1342–1356.

Plourde, S., Dodson, J. J., Runge, J. A., and Therriault, J.-C. 2002. Spatial and temporal variations in copepod community structure in the lower St. Lawrence Estuary, Canada. Mar. Ecol. Prog. Ser. 230: 221–224.

Plourde, S., Joly, P., Runge, J.A., Dodson, J., and Zakardjian B. 2003. Life cycle of *Calanus hyperboreus* in the lower St. Lawrence Estuary and its relationship to local environmental conditions. Mar. Ecol. Prog. Ser. 255: 219–233.

Plourde, S., Maps, F., and Joly, P. 2009. Mortality and survival in early stages control recruitment in *Calanus finmarchicus*. J. Plankton Res. 31(4): 371–388.

Plourde, S., Lehoux, C., Johnson, C. L., Perrin, G., and Lesage, V. 2019. North Atlantic right whale (*Eubalaena glacialis*) and its food: (I) a spatial climatology of *Calanus* biomass and potential foraging habitats in Canadian waters. J. Plankton Res. 41(5): 667–685.

Pörtner, H.-O., Roberts, D. C., Masson-Delmotte, V., Zhai, P., Tignor, M., Poloczanska, E., Mintenbeck, K., Nicolai, M., Okem, A., Petzold, J., et al. 2019. IPCC special report on the ocean and cryosphere in a changing climate. IPCC Intergovernmental Panel on Climate Change (IPCC).

Redfield A. C. 1958. The biological control of chemical factors in the environment. Am. Sci. 46, 205–221.

Runge, J. A., Castonguay, M., de Lafontaine, Y., Ringuette, M., and Beaulieu, J. L. 1999. Covariation of climate, zooplankton biomass and mackerel recruitment in the southern Gulf of St. Lawrence. Fish. Oceanogr. 8(2): 139–149.

Seok, M.W., Ho Ko, Y., Park, K.T., and Kim, T.W. 2024. Possible enhancement in ocean productivity associated with wildfire-derived nutrient and black carbon deposition in the Arctic Ocean in 2019-2021. Mar. Pollut. Bull. 201:116149. https://doi.org/10.1016/j.marpolbul.2024.116149

Sommer, U., and Lengfellner, K. 2008. Climate change and the timing, magnitude, and composition of the phytoplankton spring bloom. Global Change Biol. 14: 1199–1208.

Sulpis, Olivier; Jeansson, Emil; Dinauer, Ashley; Lauvset, Siv K.; Middelburg, and Jack J. 2021. Calcium carbonate dissolution patterns in the ocean. Nature Geoscience. 14(6): 423 - 428.

Therriault, J.-C., Petrie, B., Pépin, P., Gagnon, J., Gregory, D., Helbig, J., Herman, A., Lefaivre, D., Mitchell, M., Pelchat, B., Runge, J., and Sameoto, D. 1998. Proposal for a Northwest Atlantic zonal monitoring program. Can. Tech. Rep. Hydrogr. Ocean Sci. 194: vii + 57 p.

Ward, B. A., Dutkiewicz, S., Jahn, O., and Follows, M.J. 2012. A size-structured food-web model for the global ocean. Limnol. Oceanogr. 57: 1877–1891. doi:10.4319/lo.2012.57.6.1877.

Xiong, X., Angal, A., Chang, T., Chiang, K., Lei, N., Li, Y., Sun, J., Twedt, K., and Wu, A. 2020. MODIS and VIIRS calibration and characterization in support of producing long-term high-quality data products. Remote Sens. 12:3167; doi:10.3390/rs12193167.

Zakardjian, B.A., Gratton, Y., Vézina, A.F. 2000. Late spring phytoplankton bloom in the Lower St. Lawrence Estuary: the flushing hypothesis revisited. Mar. Ecol. Prog. Ser. 192: 31–48.

Zhai, L., Platt, T., Tang, C., Sathyendranath, S., and Hernández Walls, R. 2011. Phytoplankton phenology on the Scotian Shelf. ICES J. Mar. Sci. 68: 781–791.

TABLES

Table 1. List of oceanographic surveys with dates and sampling activities for each Gulf region/subregion. While numbers of CTD/bottle are indicated for each subregion, numbers of nets are only indicated for main regions (see region vs. subregion in Figure 1).

High Frequency monitoring stations

Dates (2023)	Vessel	Station	CTD/Bottle	Net
Mar. 7–Nov. 23	*Beluga II* (+ others)	Rimouski	23	20
Mar. 19–Oct. 27	Multiple	Shediac Valley	7	5

Surveys

Survey	Dates (2023)	Vessel	Region/subregion	CTD/Bottle	Net
Winter	Mar. 10–22	GC-945 Helicopter	Estuary	5	0
			Northwest Gulf	9	
			Northeast Gulf	22	0
			Central Gulf	9	0
			Cabot Strait	7	
			Magdalen Shallows	32	0
			Total	84	0
Early summer	Jun. 8– 26	Coriolis II	Estuary	14	18
			Northwest Gulf	14	
			Northeast Gulf	13	7
			Central Gulf	15	11
			Cabot Strait	5	
			Magdalen Shallows	39	64
			Total	100	100
Late summer	Aug. 17–29 Sep.	Teleost	Estuary	8	6
			Northwest Gulf	7	
			Northeast Gulf	8	6
			Central Gulf	18	11
			Cabot Strait	3	
			Magdalen Shallows	85	13
			Total	129	21
Fall	Oct. 17– 30	Coriolis II	Estuary	15	17
			Northwest Gulf	14	
			Northeast Gulf	22	7
			Central Gulf	9	9
			Cabot Strait	7	
			Magdalen Shallows	32	12
			Total	99	45

FIGURES

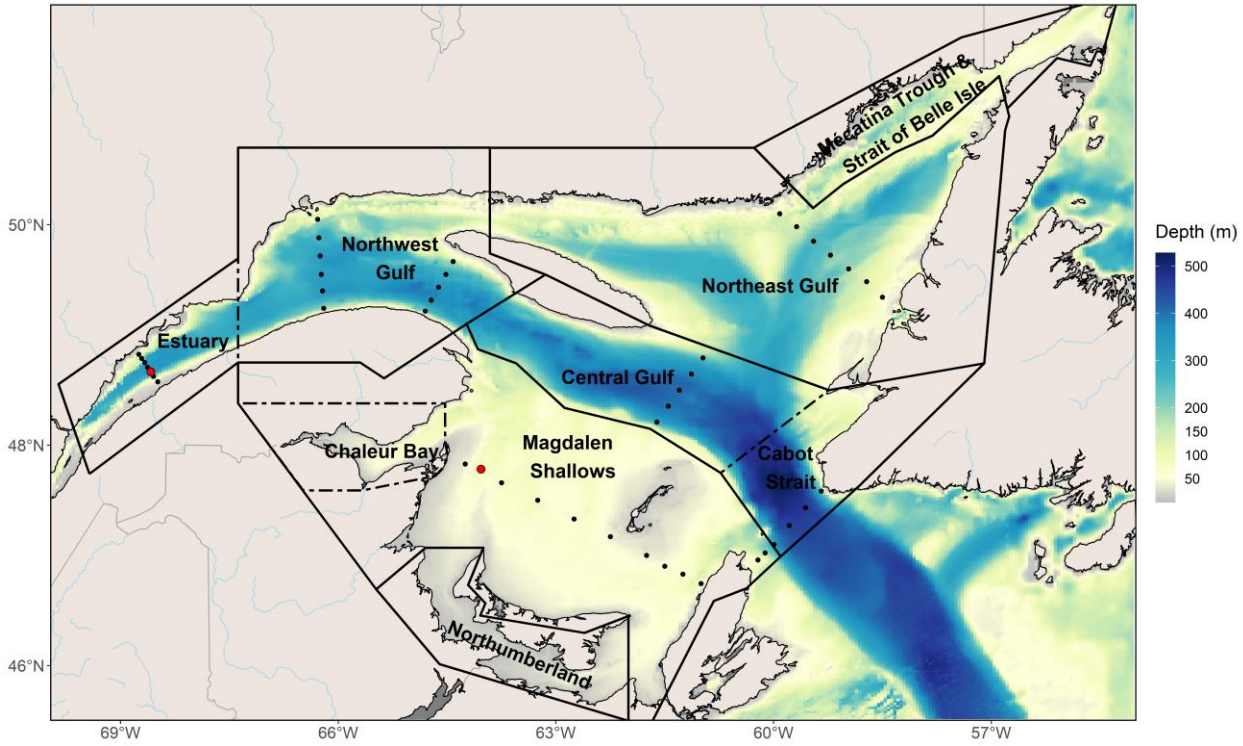

Figure 1. Bathymetric map of the Estuary and Gulf of St. Lawrence showing core AZMP sampling stations on the different sections (black circles) and high-frequency Rimouski and Shediac Valley stations (red circles). Dashed lines indicate region subdivisions.

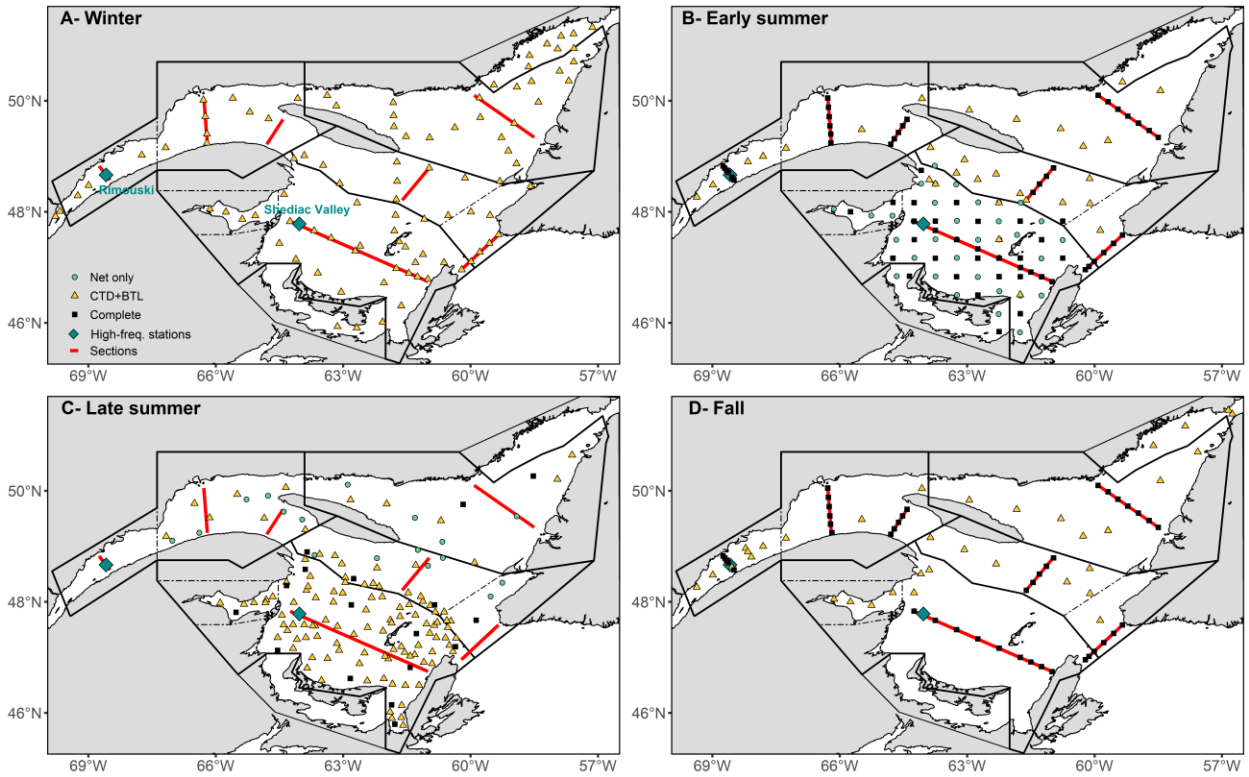

Figure 2. Locations of stations sampled during winter (A), early summer (B), late summer (C), and fall (D) 2023 (see Figure 1 caption for region and subregion descriptions). A complete station indicates that a CTD profile, water collection and zooplankton net tows were performed.

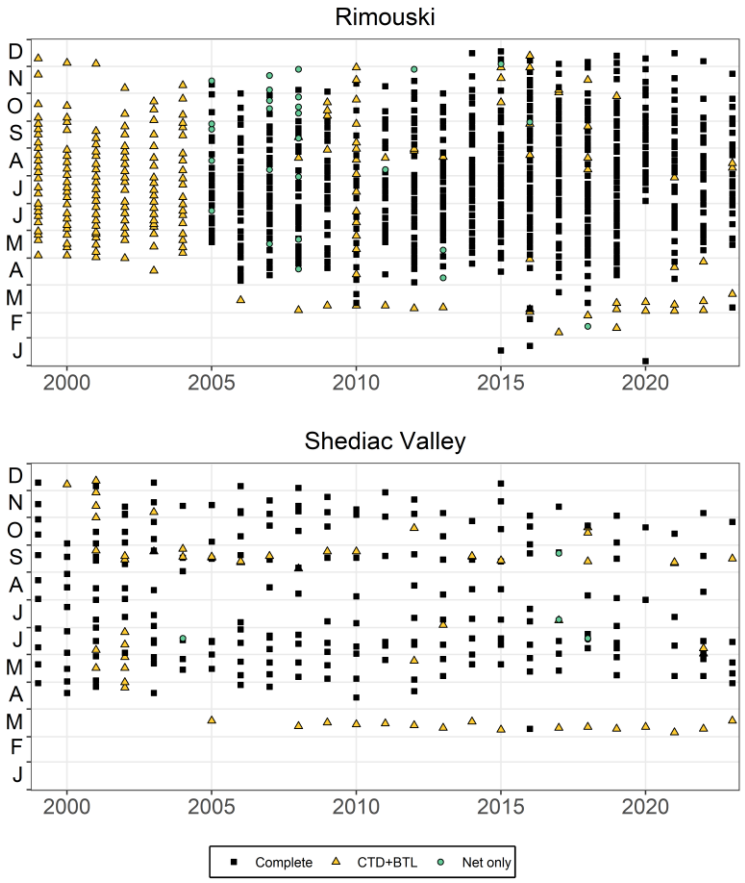

Figure 3. Sampling frequency at Rimouski and Shediac Valley stations from 1999 to 2023. Sampling included CTD/bottle as well as plankton net tows most of the time (weather permitting).

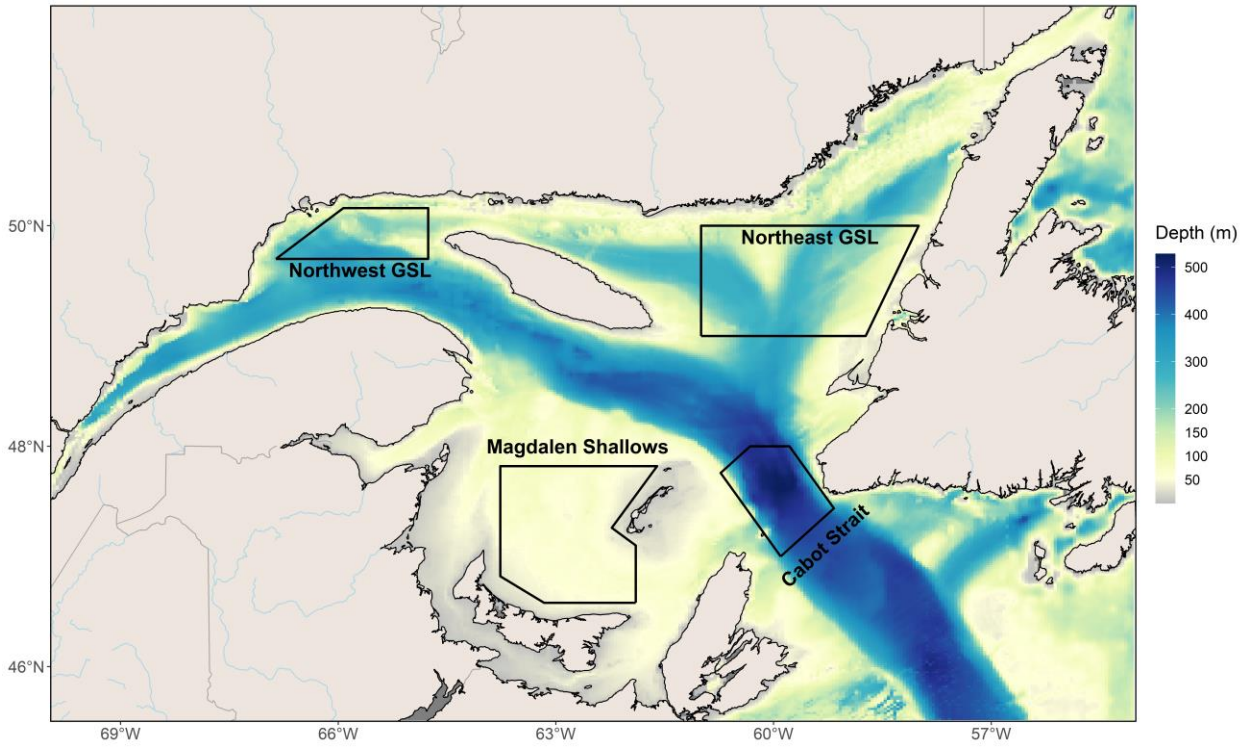

Figure 4. Ocean colour polygons used for the spatial/temporal analysis of satellite ocean colour data.

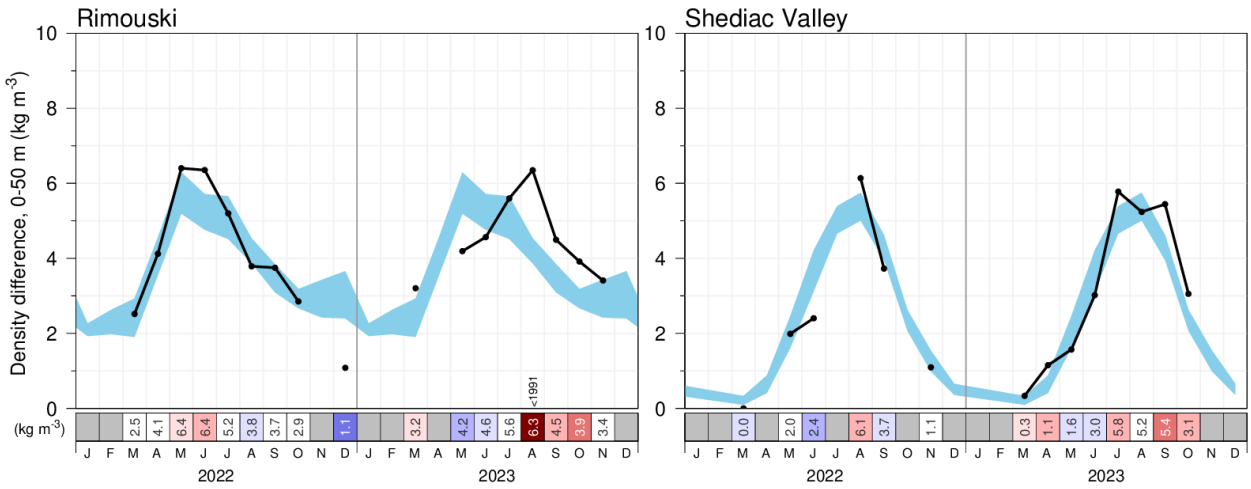

Figure 5. Seasonal stratification index during 2022 and 2023 at Rimouski and Shediac Valley stations. The blue area represents the climatological monthly mean ± 0.5 SD (1991–2020). Numbers in the scorecard are monthly density differences in kg m^{-3}. Blue colours indicate weaker-than-normal stratification (negative anomaly), reds are stronger-than-normal levels (positive anomaly), and white represents normal levels. For anomalies greater than 2 SD from normal, the prior year with a greater anomaly is indicated, with the less-than symbol (<) indicating a series record since that first year of observations.

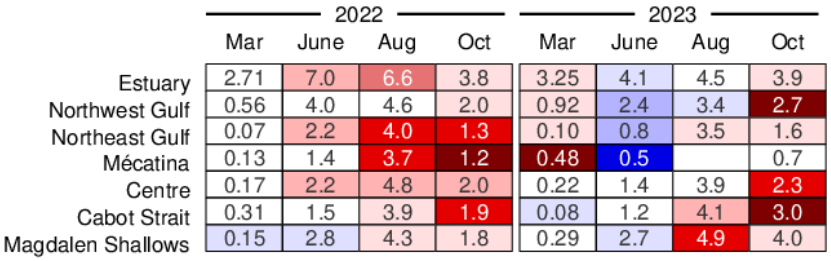

Figure 6. Monthly averaged stratification for the Gulf-wide oceanographic surveys in 2022 and 2023. Blue colours indicate weaker-than-normal stratification levels (negative anomalies), reds are stronger-than-normal levels (positive anomalies), and white represents normal levels (± 0.5 SD 1991-2020 climatology). This figure is adapted from Figure 57 of Galbraith et al. (2024b).

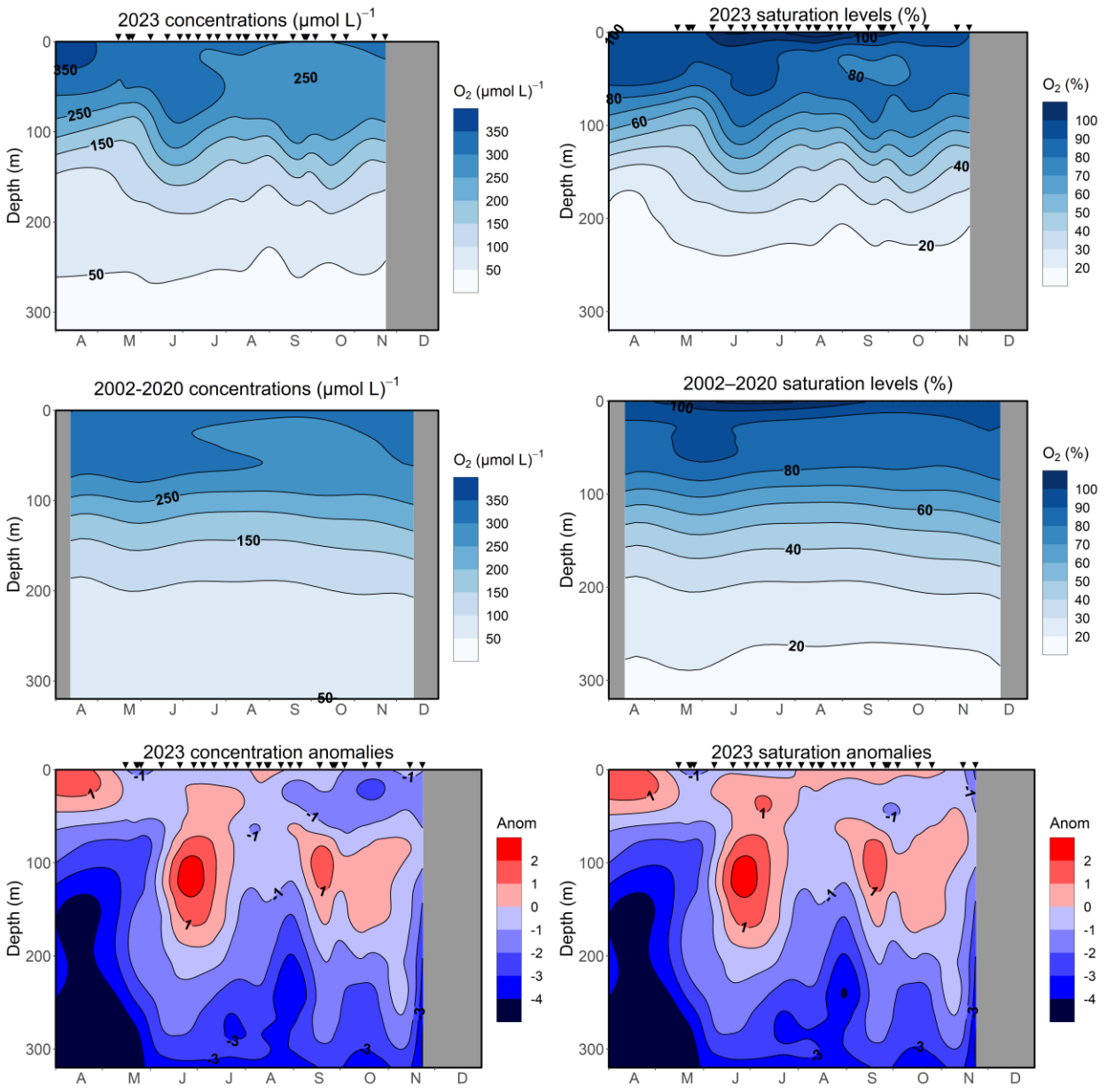

Figure 7. Vertical profiles of oxygen concentration (left panels) and saturation (right panels) at Rimouski station in 2023 (upper panels), climatology 1991-2020 (centre panels) and normalized anomalies (bottom panels). For anomalies, blue colours indicate below-normal levels (negative anomalies), reds are above-normal levels (positive anomalies), and white represents normal levels. Black triangles indicate the timing of the station occupation.

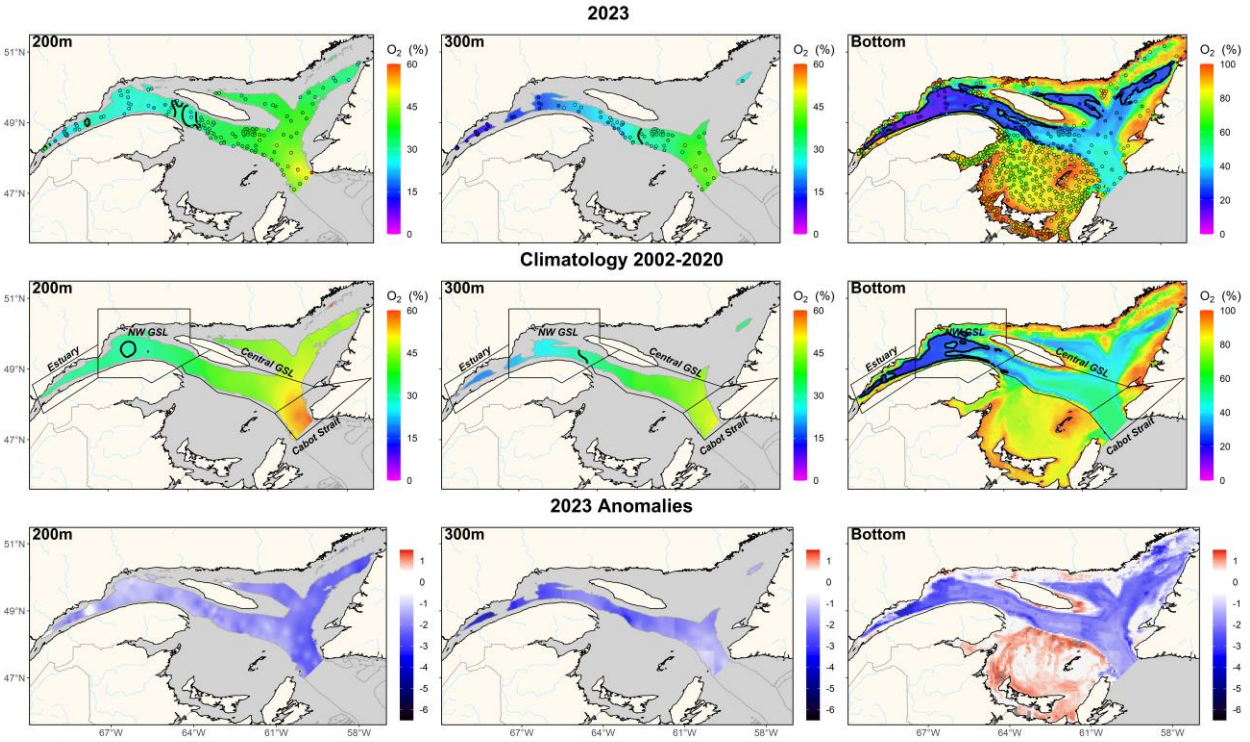

Figure 8. Annual averaged distribution of dissolved oxygen saturation at depths of 200 m, 300 m, and at the bottom in the Estuary and Gulf of St. Lawrence during 2023 (upper panel). The climatology (2002–2020; middle panel) and anomalies (lower panel) are also shown. The black contour line (30% saturation) identifies the area were waters are hypoxic. Blue colours indicate below-normal levels (negative anomalies), reds are above-normal levels (positive anomalies), and white represents normal levels. Open circles show station locations in 2023.

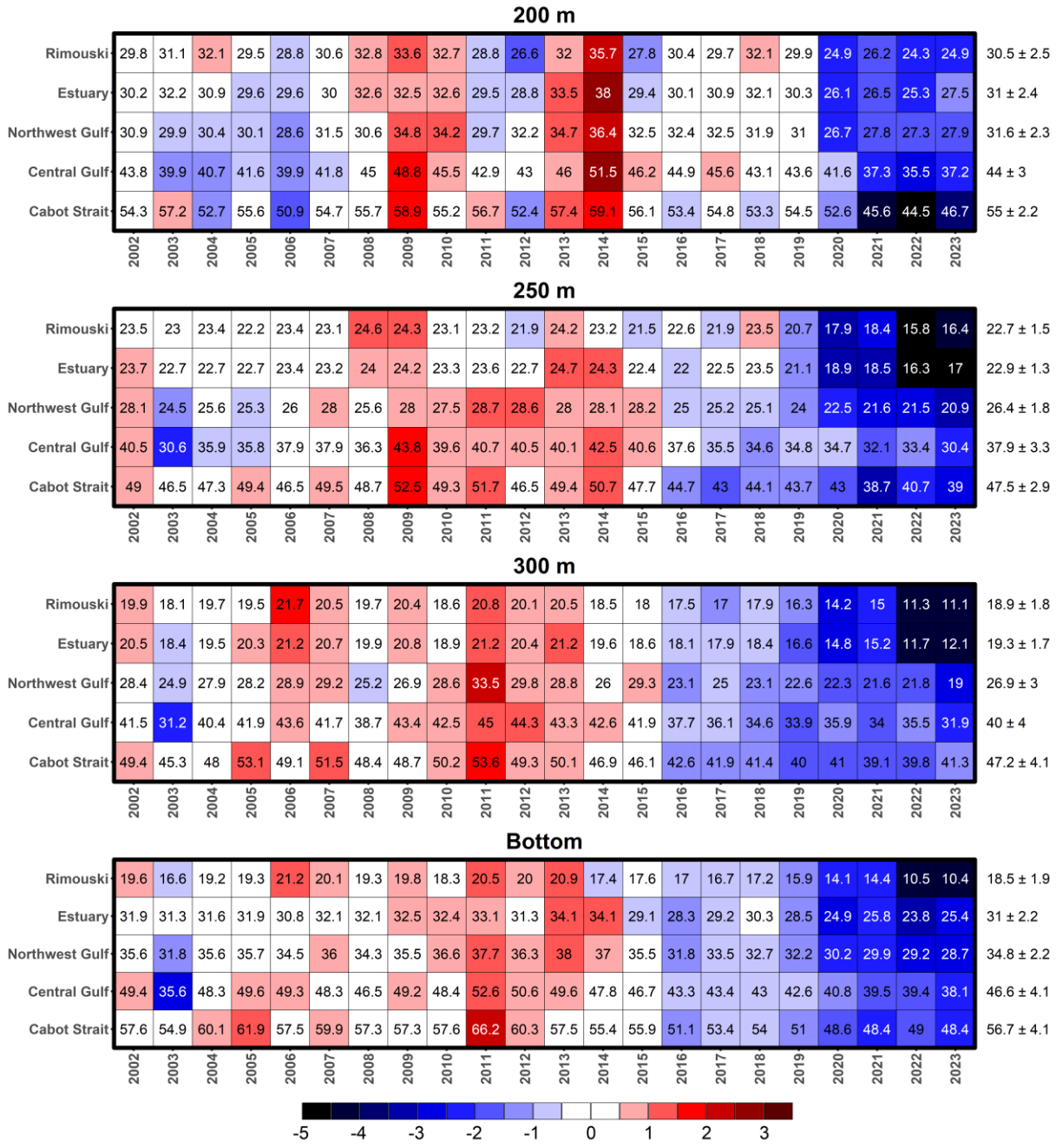

Figure 9. Annual averages of deep-layer dissolved oxygen saturation (%) at 200 m, 250 m, and 300 m and at the bottom (for locations deeper than 100 m). The numbers on the right are the 2002–2020 climatological means and standard deviations, and the numbers in the boxes are the oxygen saturation levels. Blue colours indicate below-normal levels (negative anomalies), reds are above-normal levels (positive anomalies), and white cells represent normal levels. White text is used for readability purposes when anomalies are higher (lower) than 2 SD (-2 SD) throughout this document.

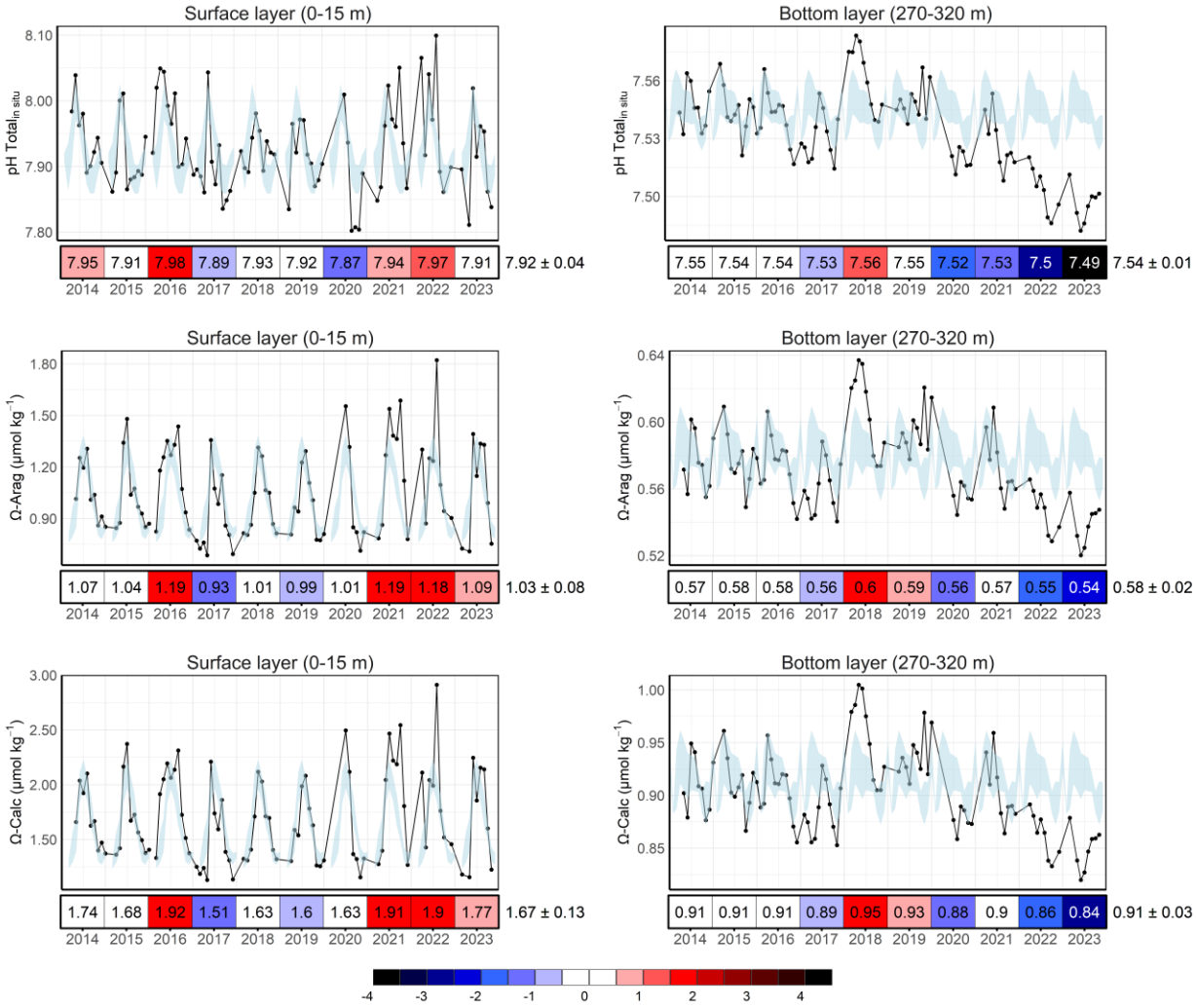

Figure 10. Time series of pH_T (upper panels), Ω-Aragonite (middle panels) and Ω-Calcite (bottom panels) monthly and annual averages at Rimouski station in the surface (left panels) and bottom layers (right panels). The monthly climatology (2014-2020) is represented by the blue shading. The numbers on the right of the scorecard are the 2014–2020 climatological means and standard deviations, and the numbers in the boxes are the annual averages. Blue colours indicate below-normal values (negative anomalies), reds are above-normal values (positive anomalies), and white represents normal values.

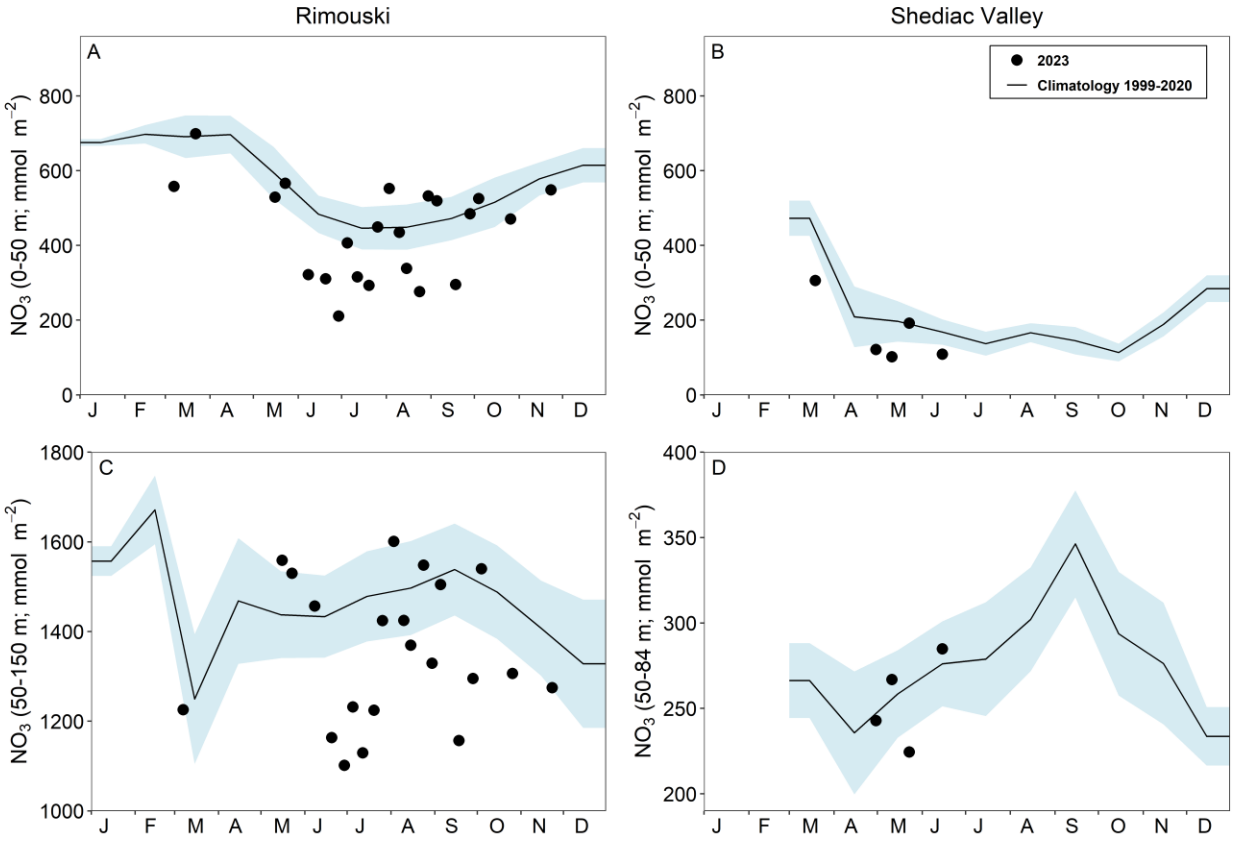

Figure 11. Surface nitrate inventories (0–50 m; top panels) and mid-layer nitrate inventories (50–150 m for Rimouski and 50–84 m for Shediac Valley; bottom panels) in 2023 (black circles) with monthly mean conditions (± 0.5 SD) for the 1999–2020 climatology (black line with blue shading) at Rimouski and Shediac Valley stations.

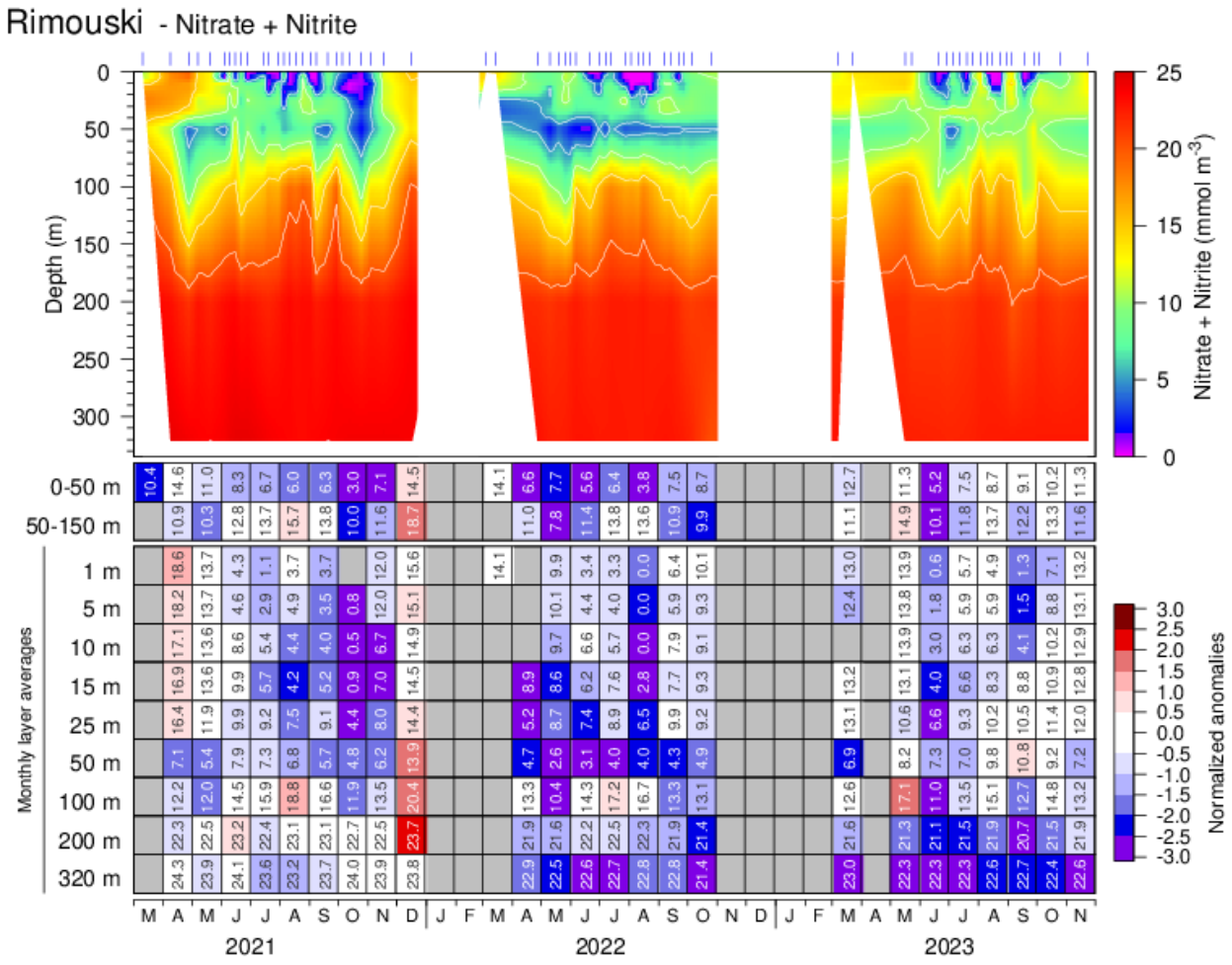

Figure 12. Nitrate concentrations at Rimouski station during the 2021 to 2023 sampling seasons. Contour (white lines) plots present smoothed data from individual sampling events while monthly depth layer averages are shown in the tables below the graphics (mmol m^{-3}). Tick marks above contour plots indicate timing of full-depth casts. Scorecard cell colours indicate normalized anomalies based on the 1999–2020 climatology. Blue colours indicate below-normal levels (negative anomalies), reds are above-normal levels (positive anomalies), and white represents normal levels.

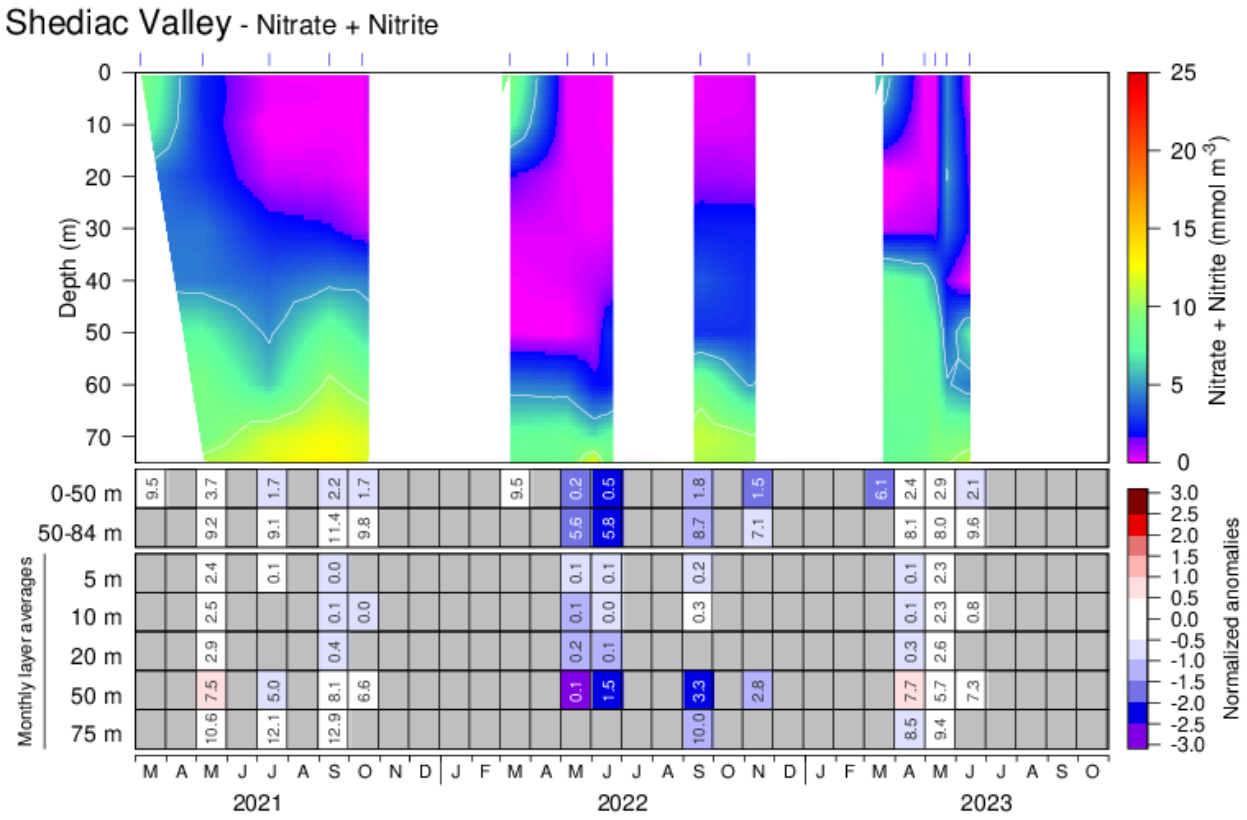

Figure 13. Nitrate concentrations at Shediac Valley station during the 2021 to 2023 sampling seasons. Contour (white lines) plots present smoothed data from individual sampling events while monthly depth layer averages are shown in the tables below the graphics (mmol m^{-3}). Tick marks above contour plots indicate timing of full-depth casts. Scorecard cell colours indicate normalized anomalies based on the 1999–2020 climatology. Blue colours indicate below-normal levels (negative anomalies), reds are above-normal levels (positive anomalies), and white represents normal levels.

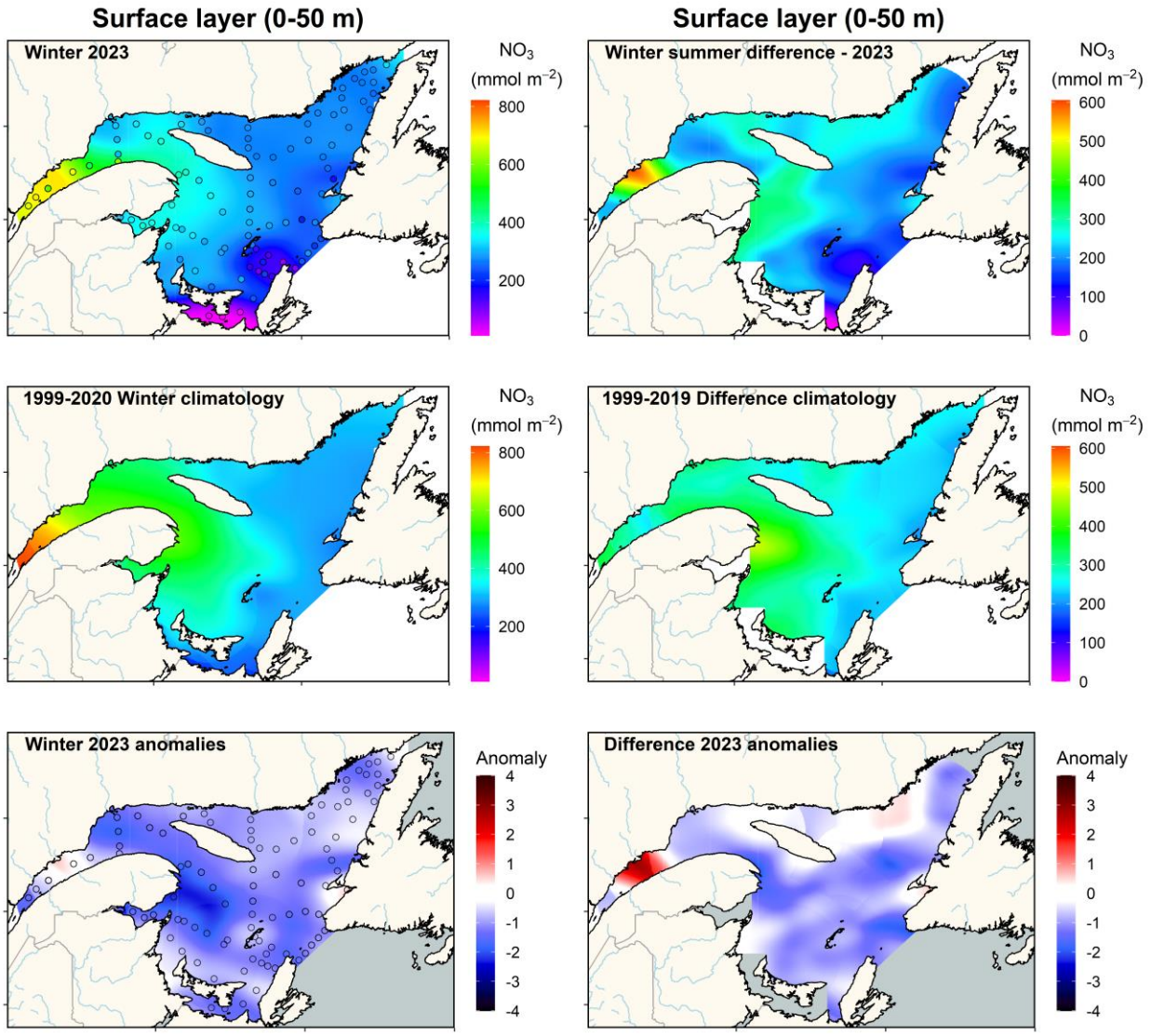

Figure 14. Nitrate inventories (mmol m^{-2}) in the surface layer (0–50 m) of the Estuary and Gulf of St. Lawrence during early March 2023 (upper left panel). Difference in nitrate inventories (mmol m^{-2}) in the surface layer of the Estuary and Gulf of St. Lawrence between winter and early summer (upper right panel). The climatology (1999–2020 for winter, 1999–2019 for difference; middle panels) and anomalies (lower panels) are shown. Blue colours indicate below-normal levels (negative anomalies), reds are above-normal levels (positive anomalies), and white represents normal levels.

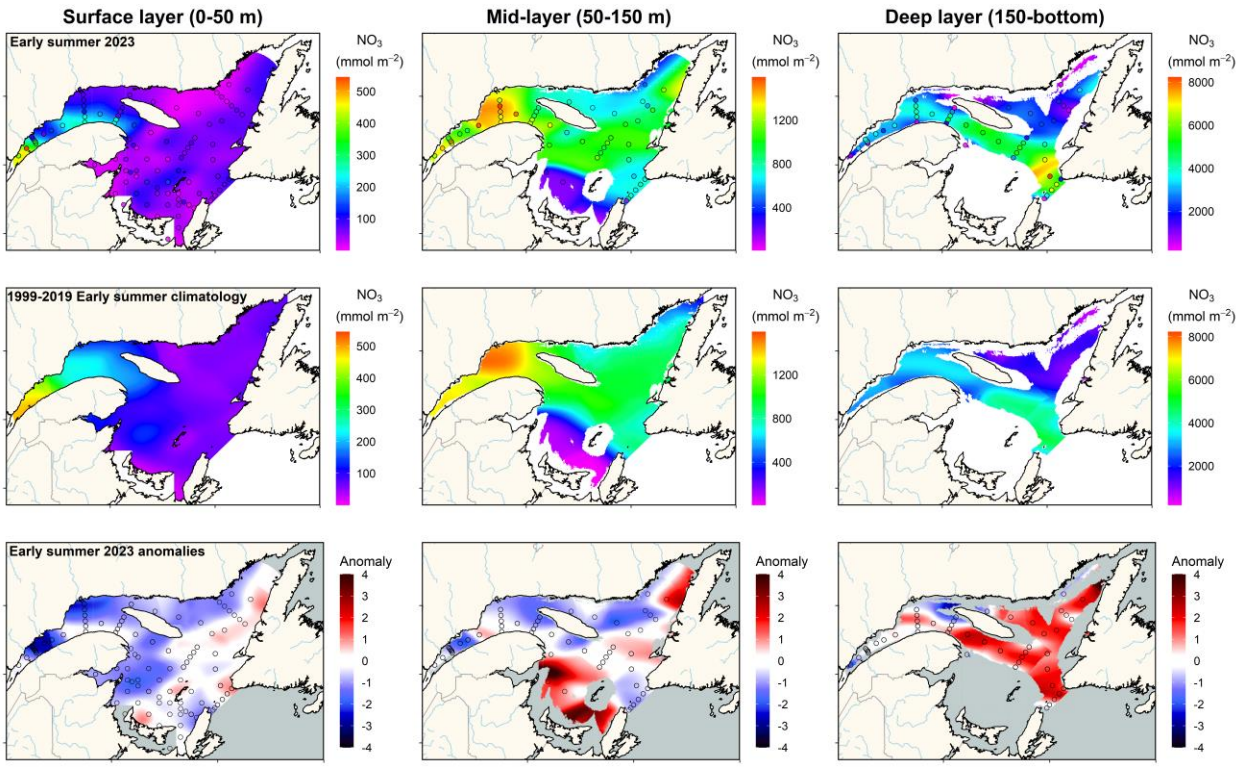

Figure 15. Nitrate inventories (mmol m^{-2}) in the surface (left panels), mid (middle panels), and deep (right panels) layers of the Estuary and Gulf of St. Lawrence during early summer 2023 (upper panels). The climatology (1999–2019; middle panels) and anomalies (lower panels) are shown for each layer. Blue colours indicate below-normal levels (negative anomalies), reds are above-normal levels (positive anomalies), and white represents normal levels.

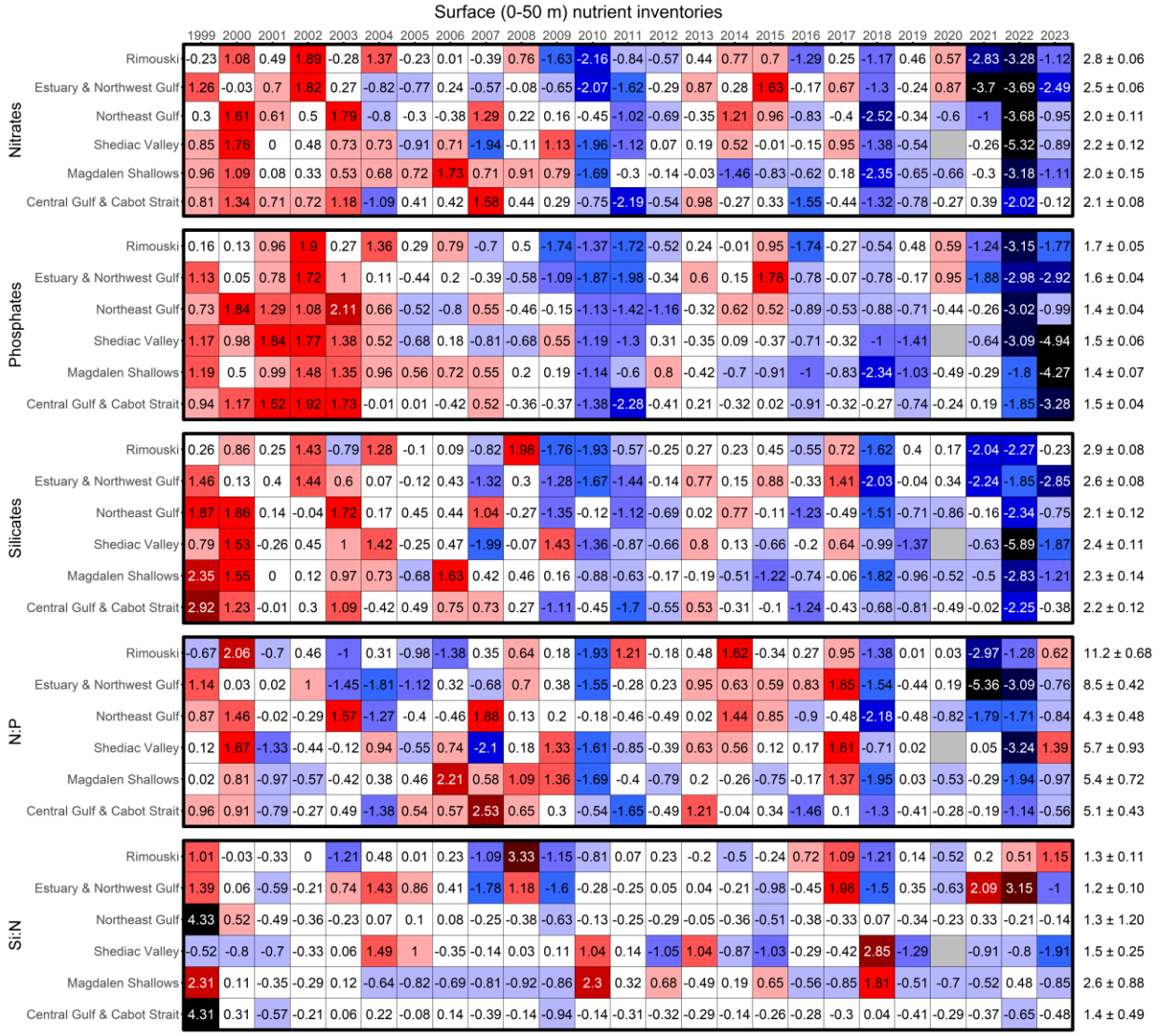

Figure 16. Time series of normalized annual anomalies for nutrient inventories and ratios in the surface layer (0–50 m) for high-frequency monitoring stations and Gulf regions. The numbers on the right are the 1999–2020 climatological means and standard deviations in units of $\log_{10}$(mmol m^{-2}) for nutrient inventories; nutrient ratios are dimensionless and have not been log-transformed. Blue colours indicate below-normal levels (negative anomalies), reds are above-normal levels (positive anomalies), and white represents normal levels.

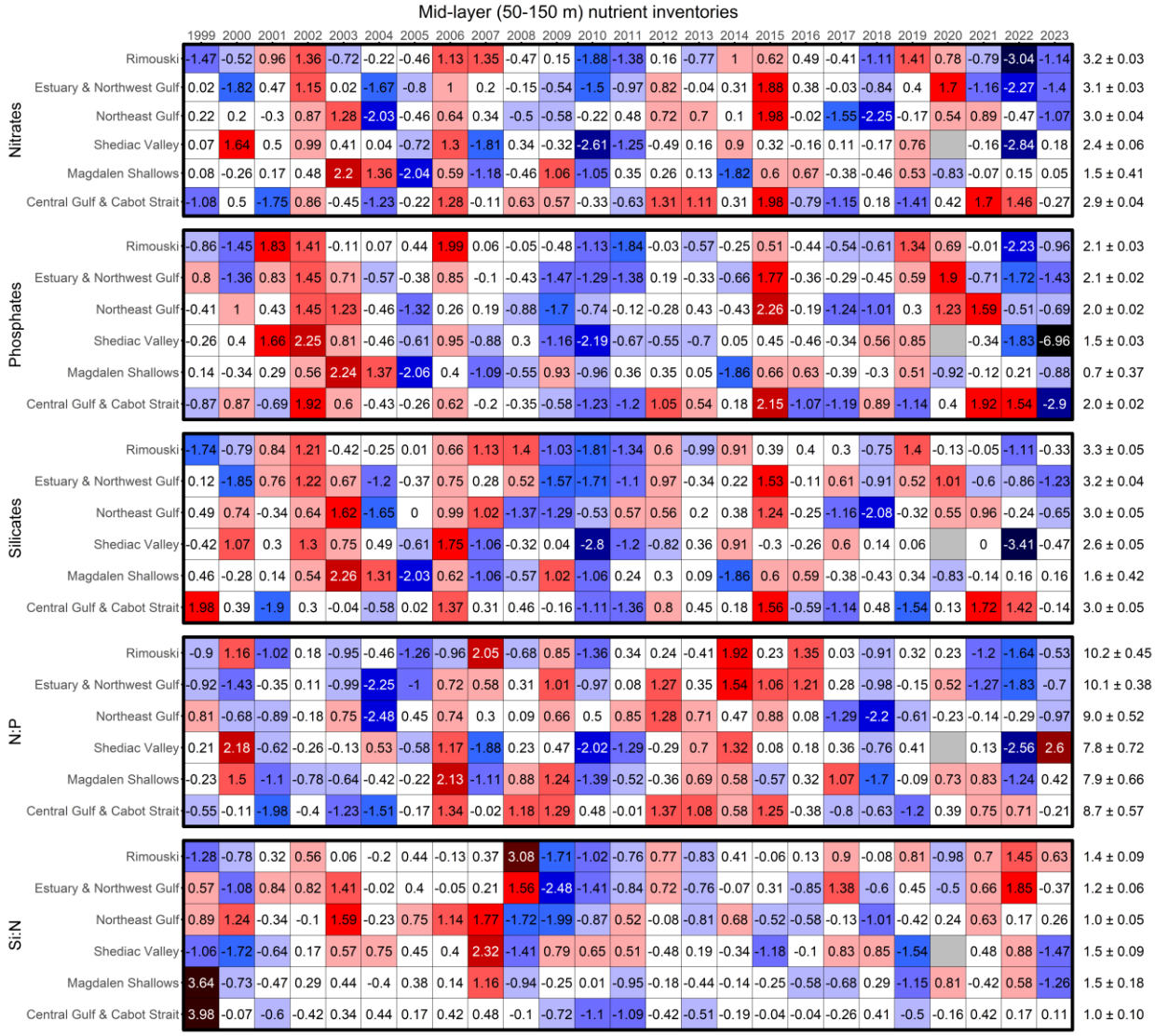

Figure 17. Time series of normalized annual anomalies for nutrient inventories and ratios in the mid-layer (50–150 m) for high-frequency monitoring stations and Gulf regions. The numbers on the right are the 1999–2020 climatological means and standard deviations in units of $\log_{10}$(mmol m^{-2}) for nutrient inventories; nutrient ratios are dimensionless and have not been log-transformed. Blue colours indicate below-normal levels (negative anomalies), reds are above-normal levels (positive anomalies), and white represents normal levels.

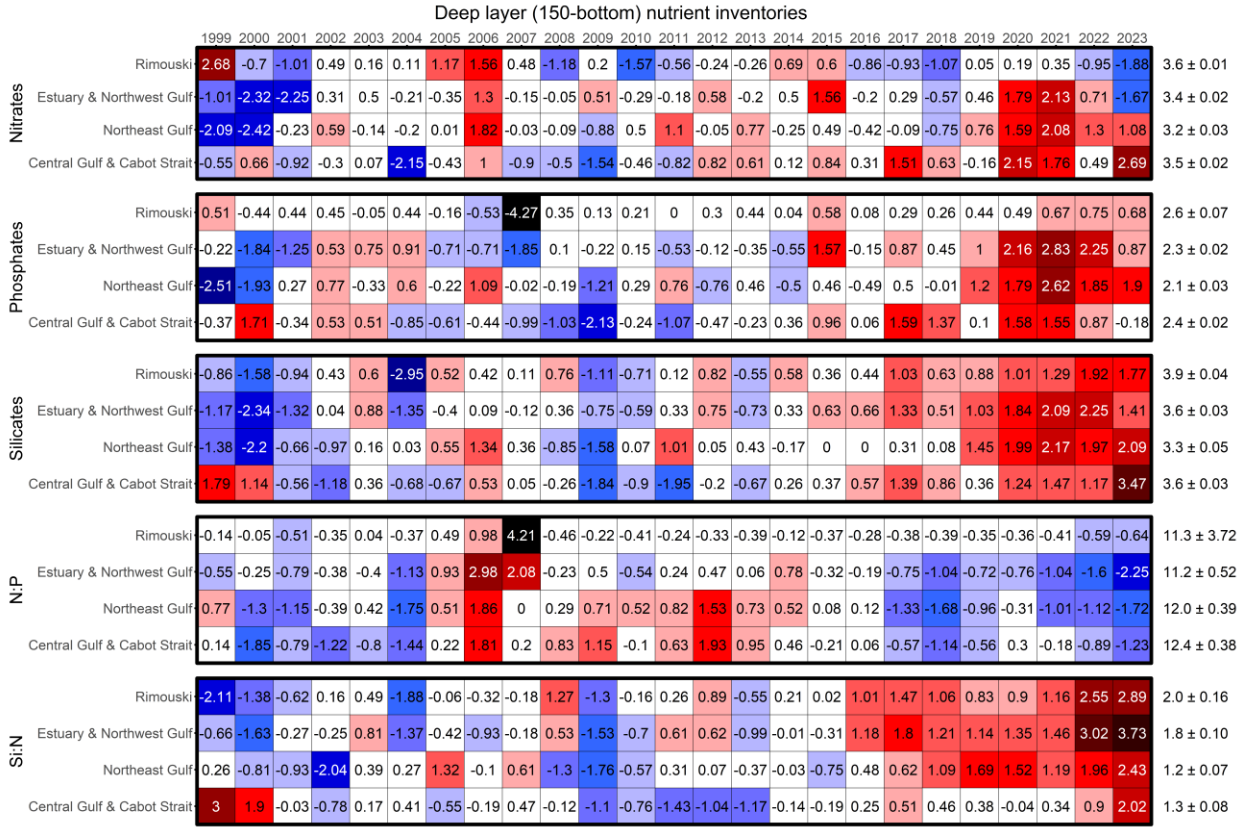

Figure 18. Time series of normalized annual anomalies for nutrient inventories and ratios in the deep layer (150–bottom) for high-frequency monitoring stations and Gulf regions. The numbers on the right are the 1999–2020 climatological means and standard deviations in units of $\log_{10}$(mmol m^{-2}) for nutrient inventories; nutrient ratios are dimensionless and have not been log-transformed. Blue colours indicate below-normal levels (negative anomalies), reds are above-normal levels (positive anomalies), and white represents normal levels.

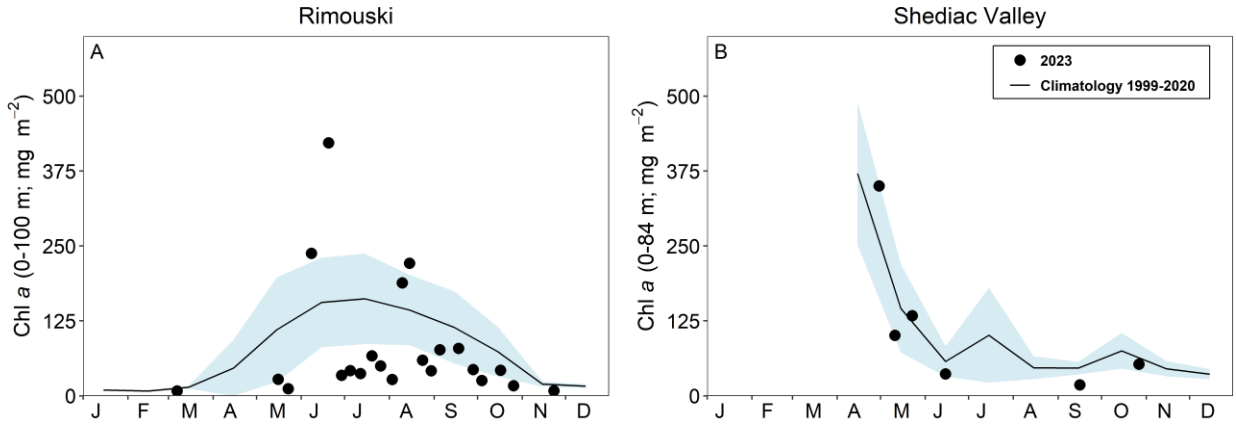

Figure 19. Chlorophyll a inventories (0–100 m for Rimouski and 0–84 m for Shediac Valley) in 2023 (black circles) with monthly mean conditions (± 0.5 SD) for the 1999–2020 climatology (black line with blue shading) at Rimouski and Shediac Valley stations.

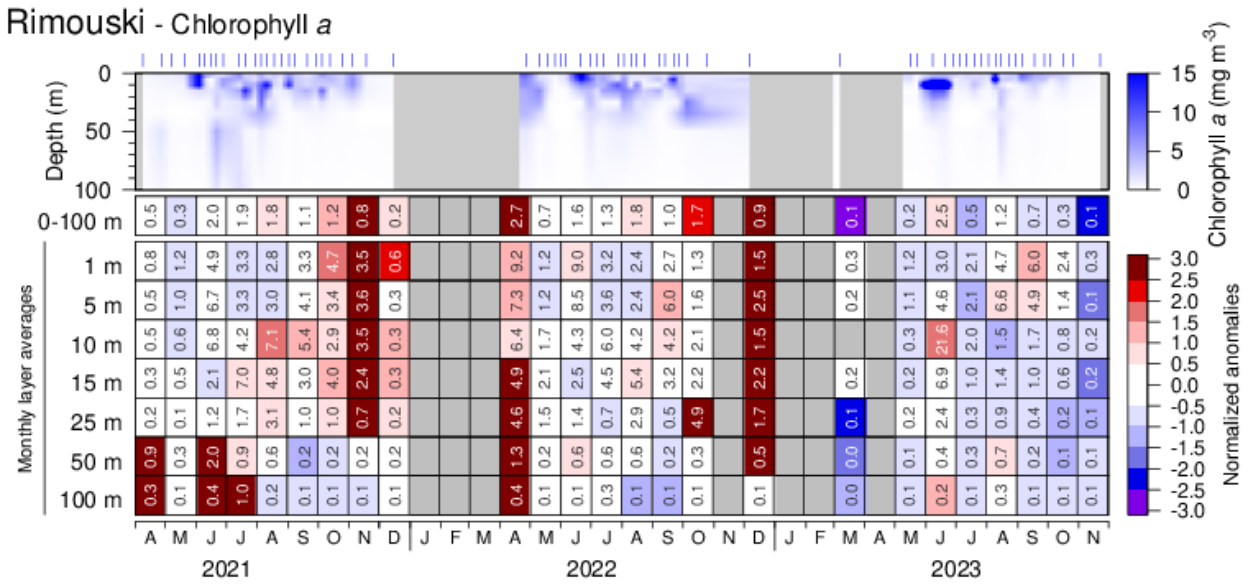

Figure 20. Chlorophyll a concentrations at Rimouski station during the 2021 to 2023 sampling seasons. Contour plots (white lines) present smoothed data from individual sampling events while monthly depth layer averages are shown in the tables below the graphics (mg m^{-3}). Scorecard cell colours indicate normalized anomalies based on the 1999–2020 climatology. Blue colours indicate below-normal levels (negative anomalies), reds are above-normal levels (positive anomalies), and white represents normal levels.

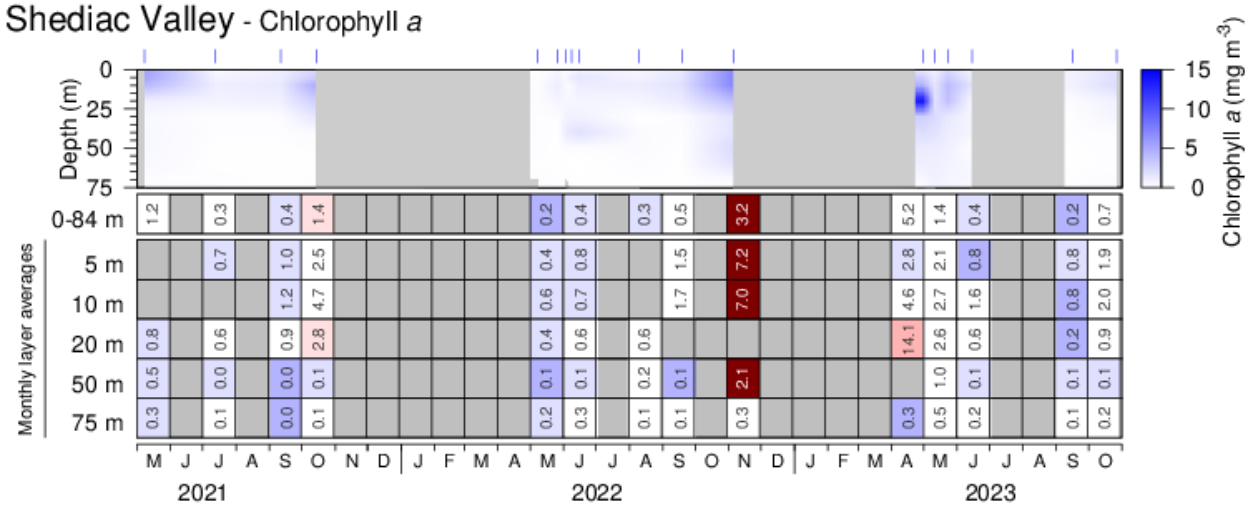

Figure 21. Chlorophyll a concentrations at Shediac Valley station during the 2021 to 2023 sampling seasons. Contour plots (white lines) present smoothed data from individual sampling events while monthly depth layer averages are shown in the tables below the graphics (mg m^{-3}). Scorecard cell colours indicate normalized anomalies based on the 1999–2020 climatology. Blue colours indicate below-normal levels (negative anomalies), reds are above-normal levels (positive anomalies), and white represents normal levels.

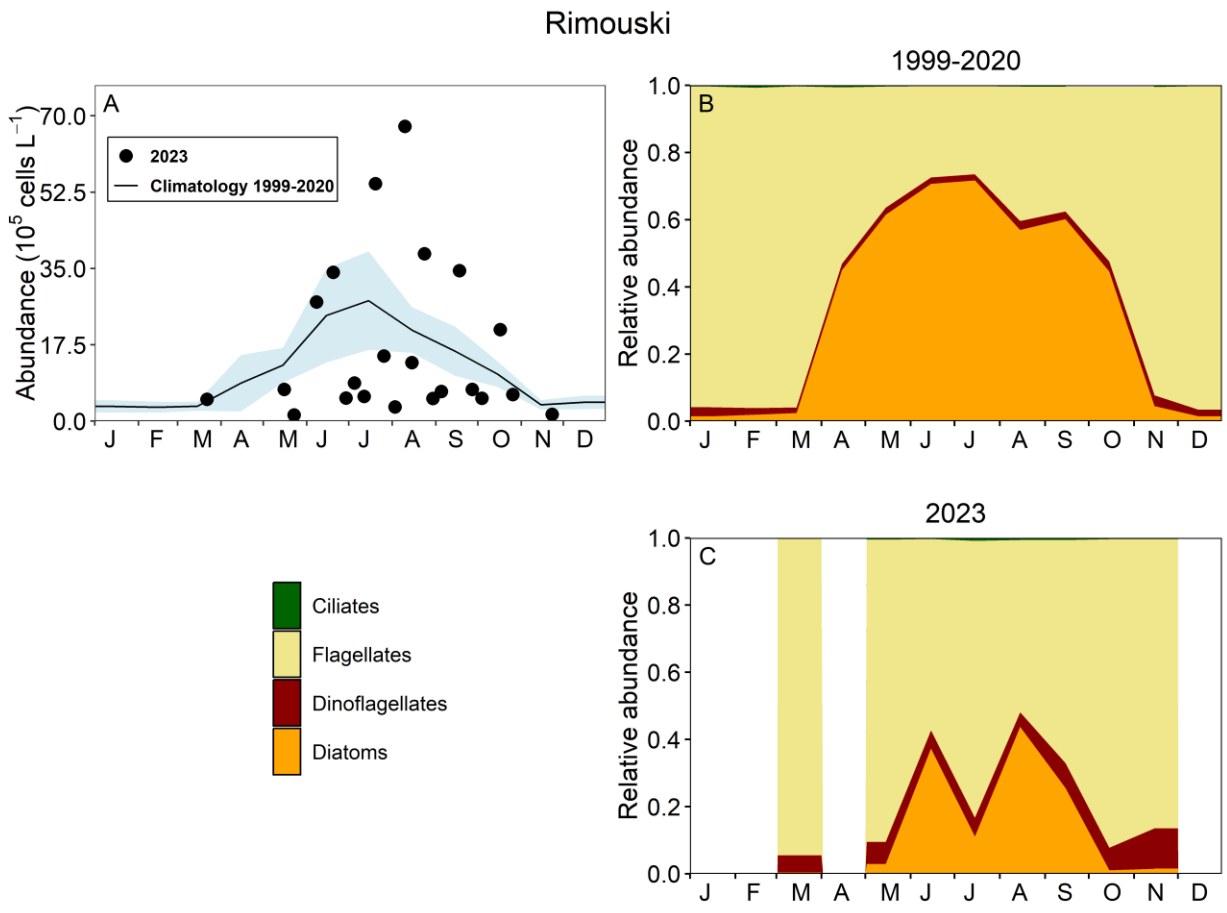

Figure 22. Phytoplankton abundance (A) and community composition at Rimouski station for the 1999–2020 climatology (B) and for 2023 (C). Blue shading on panel (A) represents ± 0.5 SD of the monthly mean phytoplankton abundance for the climatology. While ciliate abundances were included in the graphics, they are barely visible because they represent < 1% of phytoplankton cells each month for the climatology.

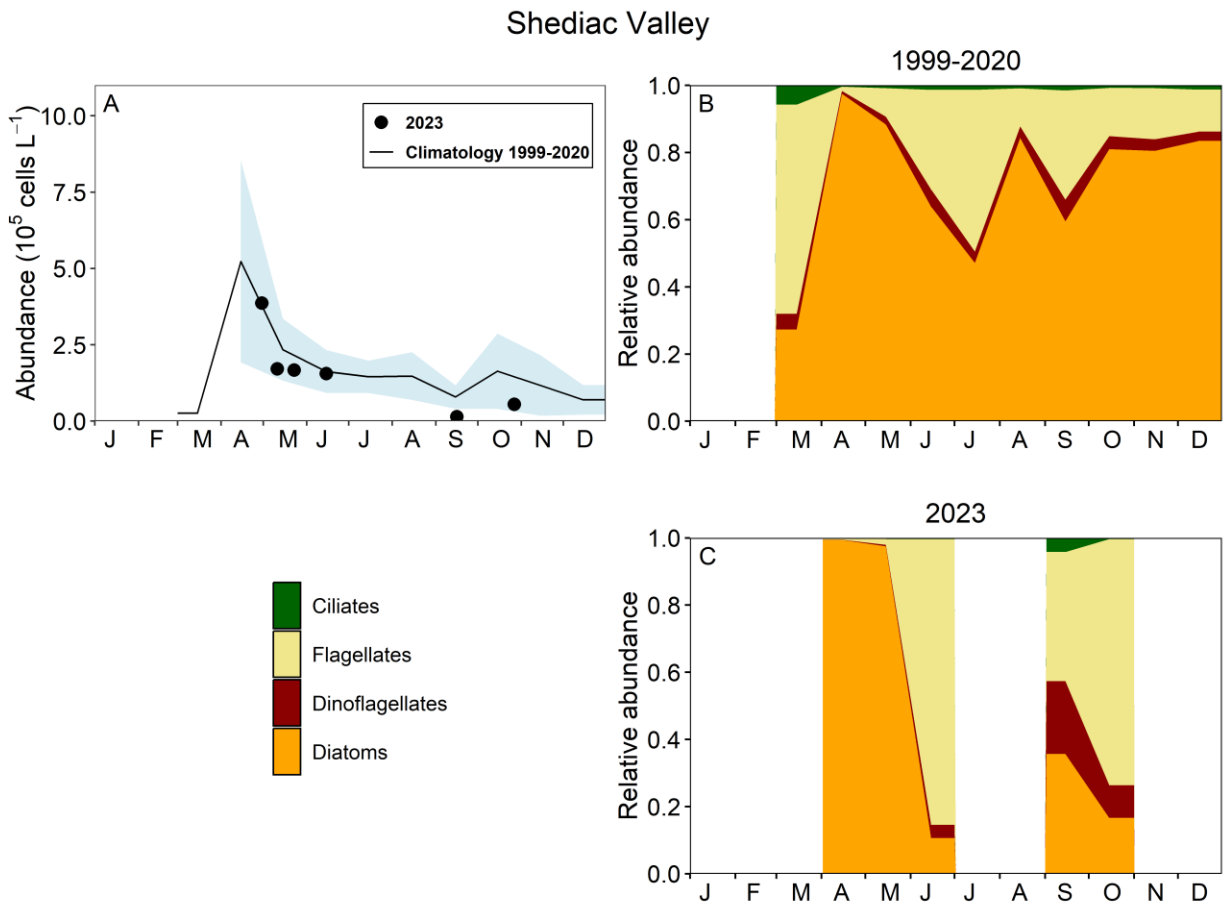

Figure 23. Phytoplankton abundance (A) and community composition at Shediac Valley station for the 1999–2020 climatology (B) and for 2023 (C). Blue shading on panel (A) represents ± 0.5 SD of the monthly mean phytoplankton abundance for the climatology.

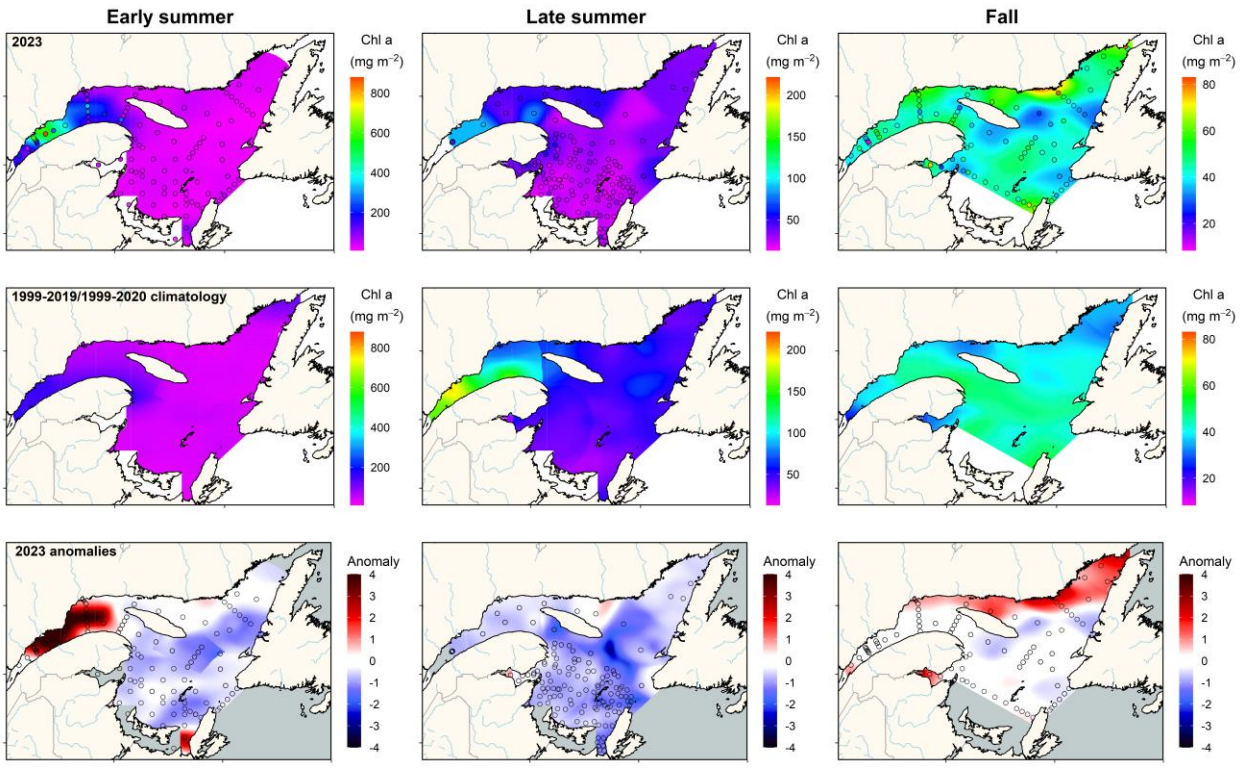

Figure 24. Vertically integrated (0–100 m) chlorophyll *a* inventory (mg m^{-2}) in the Estuary and Gulf of St. Lawrence during early summer (left panels), late summer (middle panels), and fall (right panels) 2023. The climatology (1999–2019 for early summer and 1999–2020 for other seasons; middle panels) and anomalies (lower panels) are shown for each season. Blue colours indicate below-normal levels (negative anomalies), reds are above-normal levels (positive anomalies), and white represents normal levels.

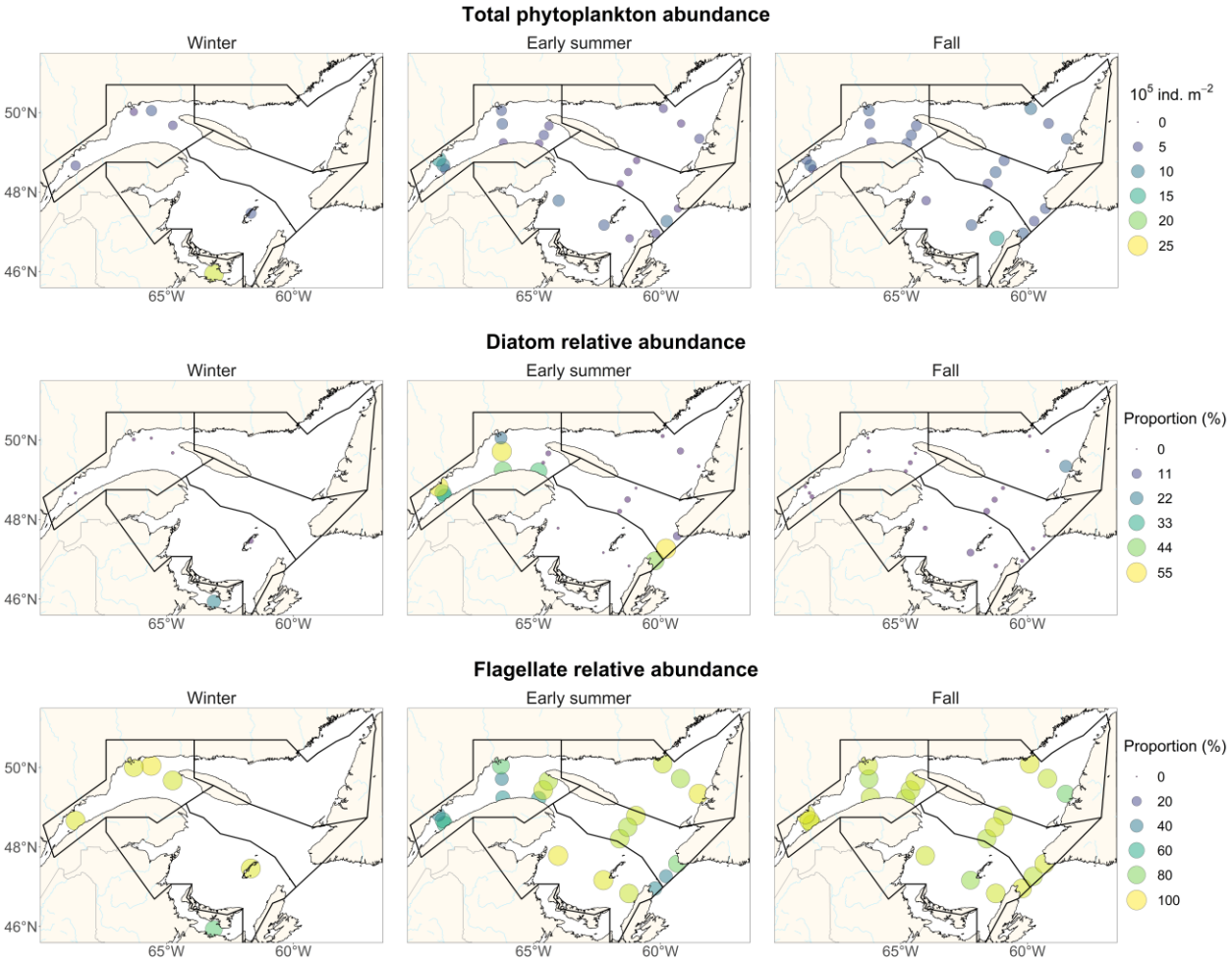

Figure 25. Total phytoplankton abundance (10^5 ind. m^{-2}; top panels) and proportion (%) of diatoms (mid-panels) and flagellates (bottom panels) in the upper 100 m of the Estuary and Gulf of St. Lawrence during winter, early summer and fall 2023.

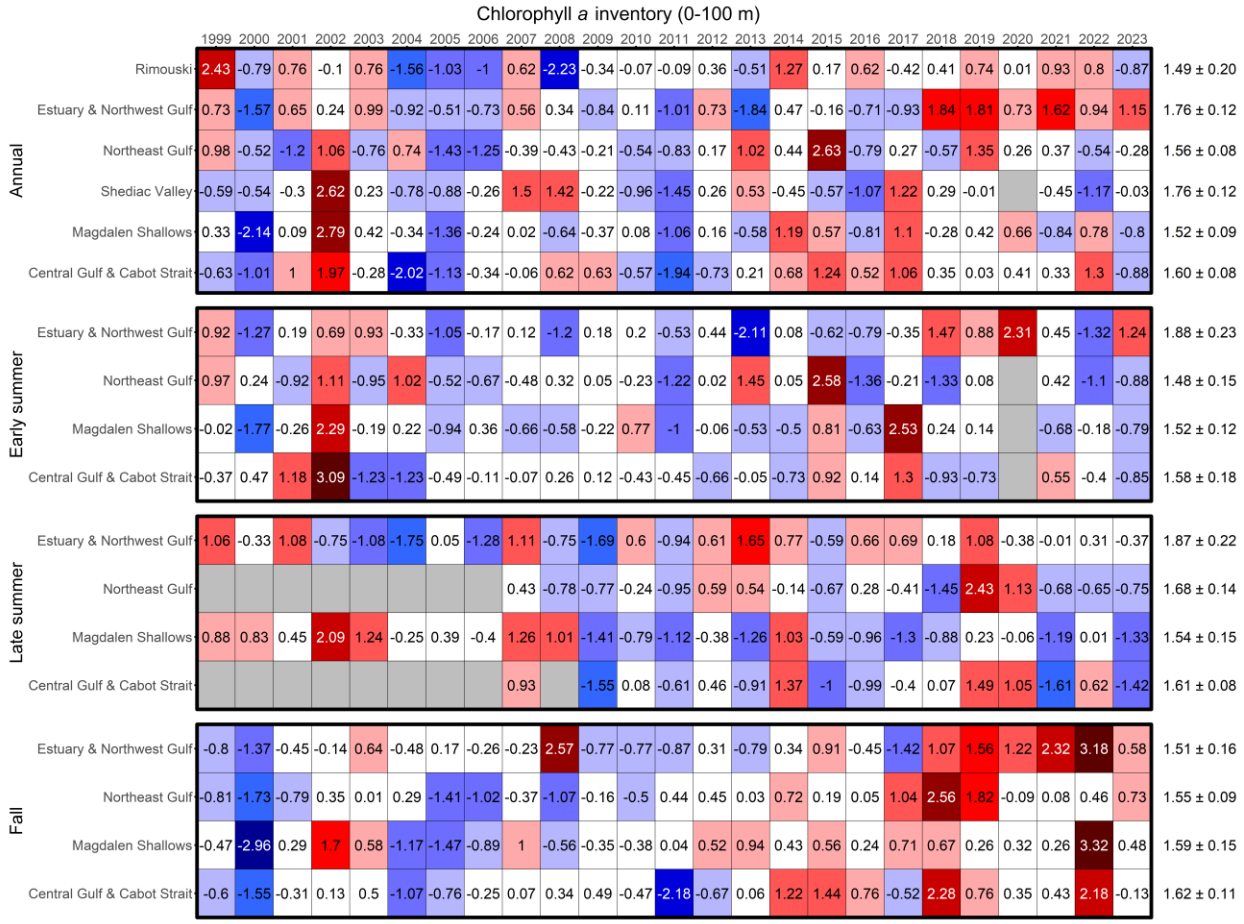

Figure 26. Time series of normalized annual and seasonal anomalies for chlorophyll a inventories (0–100 m) for high-frequency monitoring stations and Gulf regions. The numbers on the right are the 1999–2020 (1999–2019 for early summer) climatological means and standard deviations in units of $\log_{10}(\text{mg m}^{-2})$. Blue colours indicate below-normal levels (negative anomalies), reds are above-normal levels (positive anomalies), and white represents normal levels. Gray cells indicate missing data.

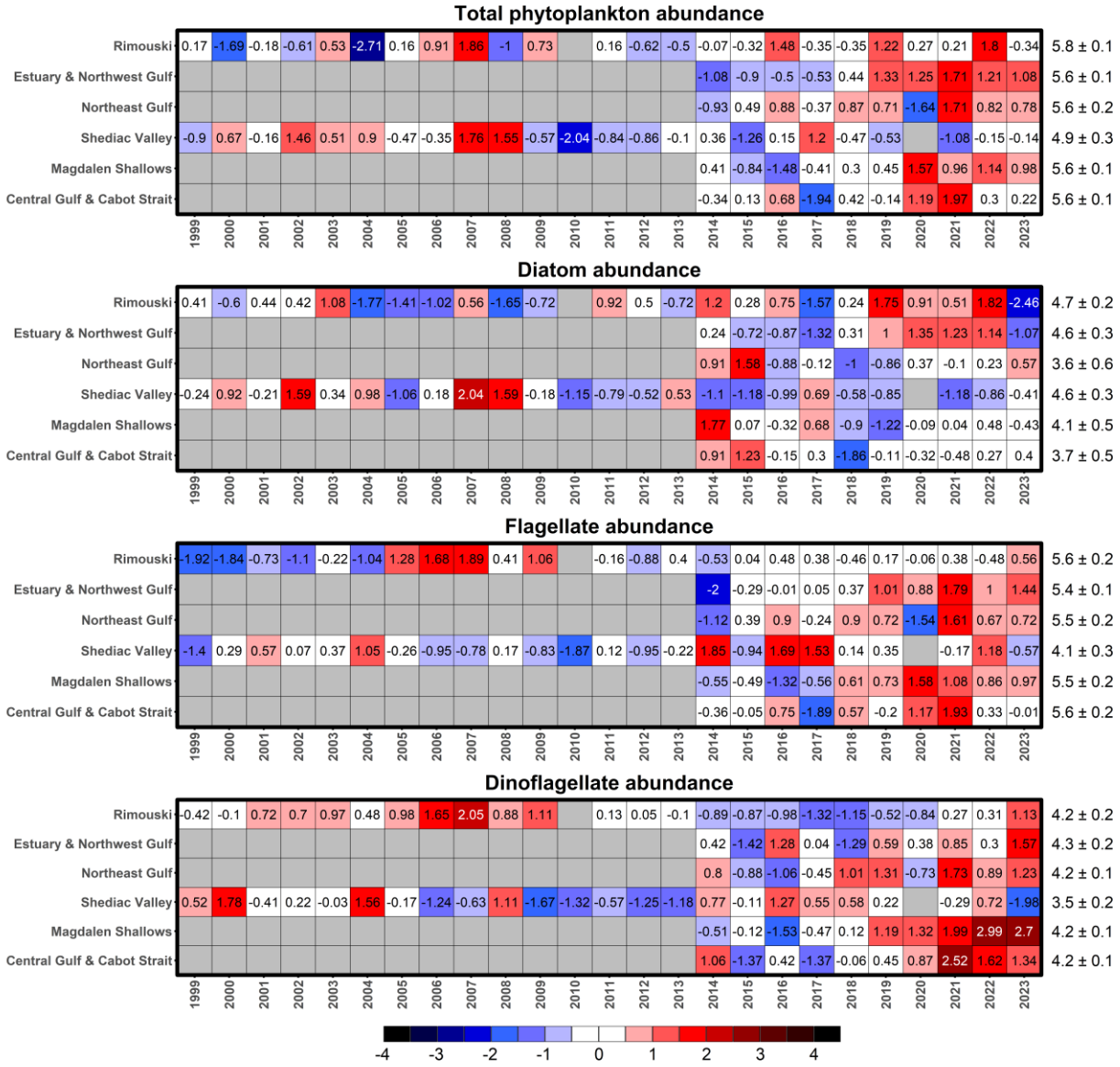

Figure 27. Time series of normalized annual anomalies for total phytoplankton abundance and the abundance of the main phytoplankton taxonomic groups at high-frequency monitoring stations and in Gulf regions. The numbers on the right are the 1999–2020 climatological means and standard deviations in units of $\log_{10}$(cells L^{-1}). Blue colours indicate below-normal levels (negative anomalies), reds are above-normal levels (positive anomalies), and white represents normal levels. Gray cells indicate missing data.

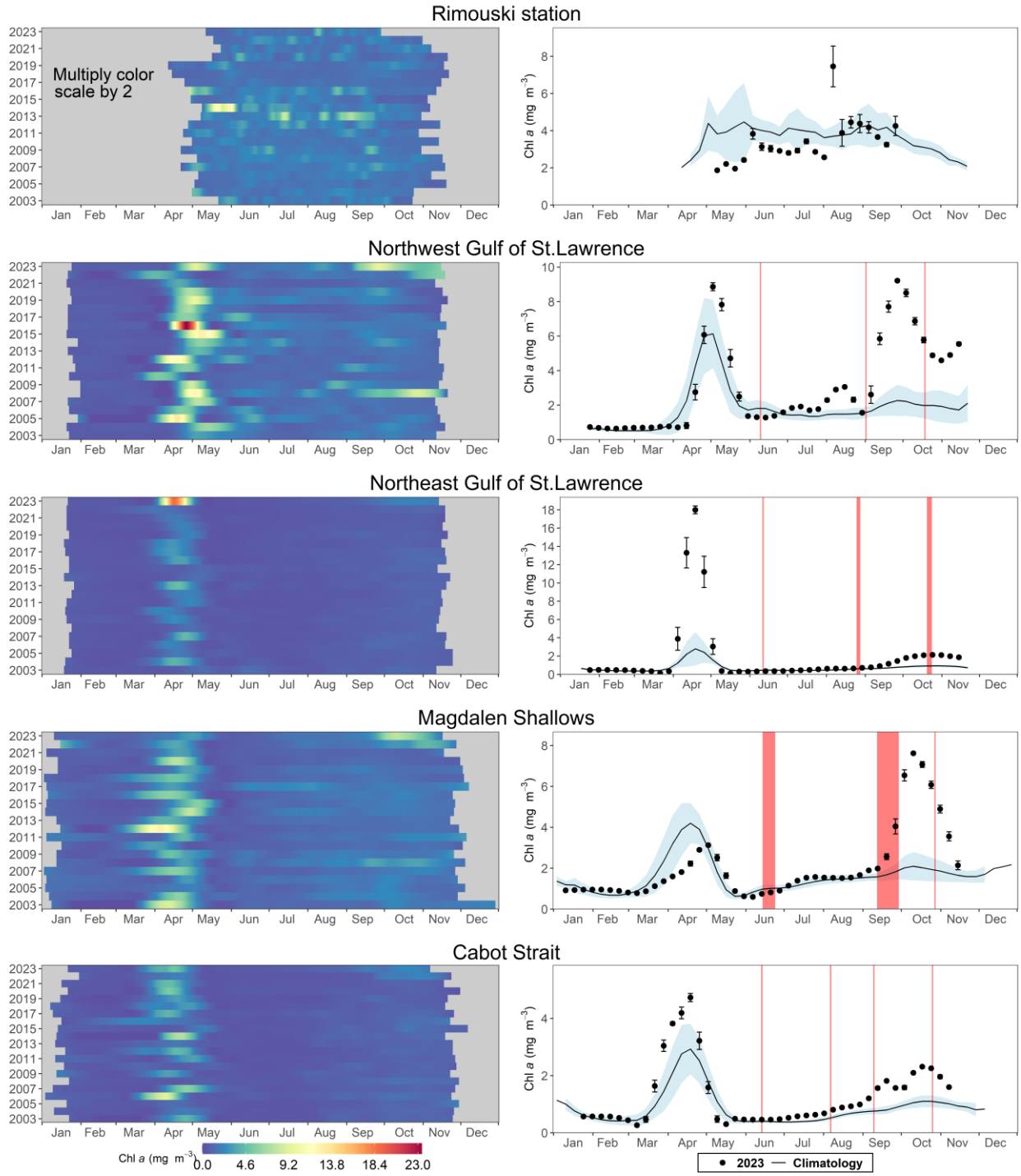

Figure 28. Left panels: LOESS-smoothed time series of daily surface chlorophyll *a* concentrations derived from data recorded by a fluorescence sensor fixed on the oceanographic buoy at Rimouski station (1st row panels) and from MODIS ocean-colour data in the ocean colour polygons (see Fig. 4 for polygon locations). Right panels: comparison of semimonthly mean (± 0.5 SD) of surface chlorophyll *a* estimates in 2023 (black circles) with average (± 0.5 SD) conditions from the 2003–2020 climatology (2002-2020 for Rimouski station; solid line with blue shading) for the same ocean-colour polygons. Red shadings indicate sampling times of the main surveys.

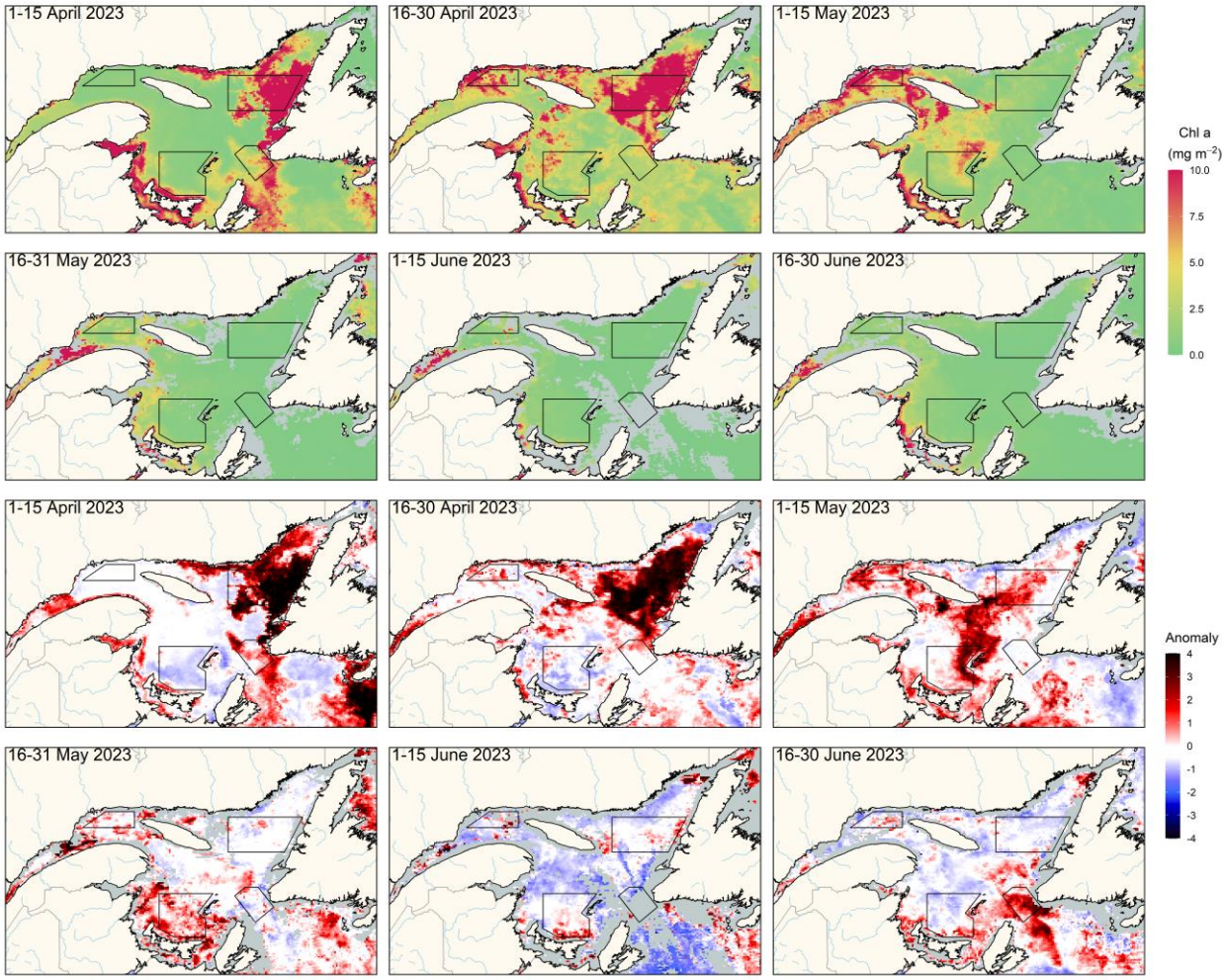

Figure 29. MODIS composite images of surface chlorophyll *a* (upper panels) and chlorophyll *a* normalized anomaly based on the 2003–2020 climatology (lower panels) in the Gulf of St. Lawrence during spring/early summer 2023. Grey colour indicates the absence of data. Blue colours indicate below-normal levels (negative anomalies), reds are above-normal levels (positive anomalies), and white represents normal levels.

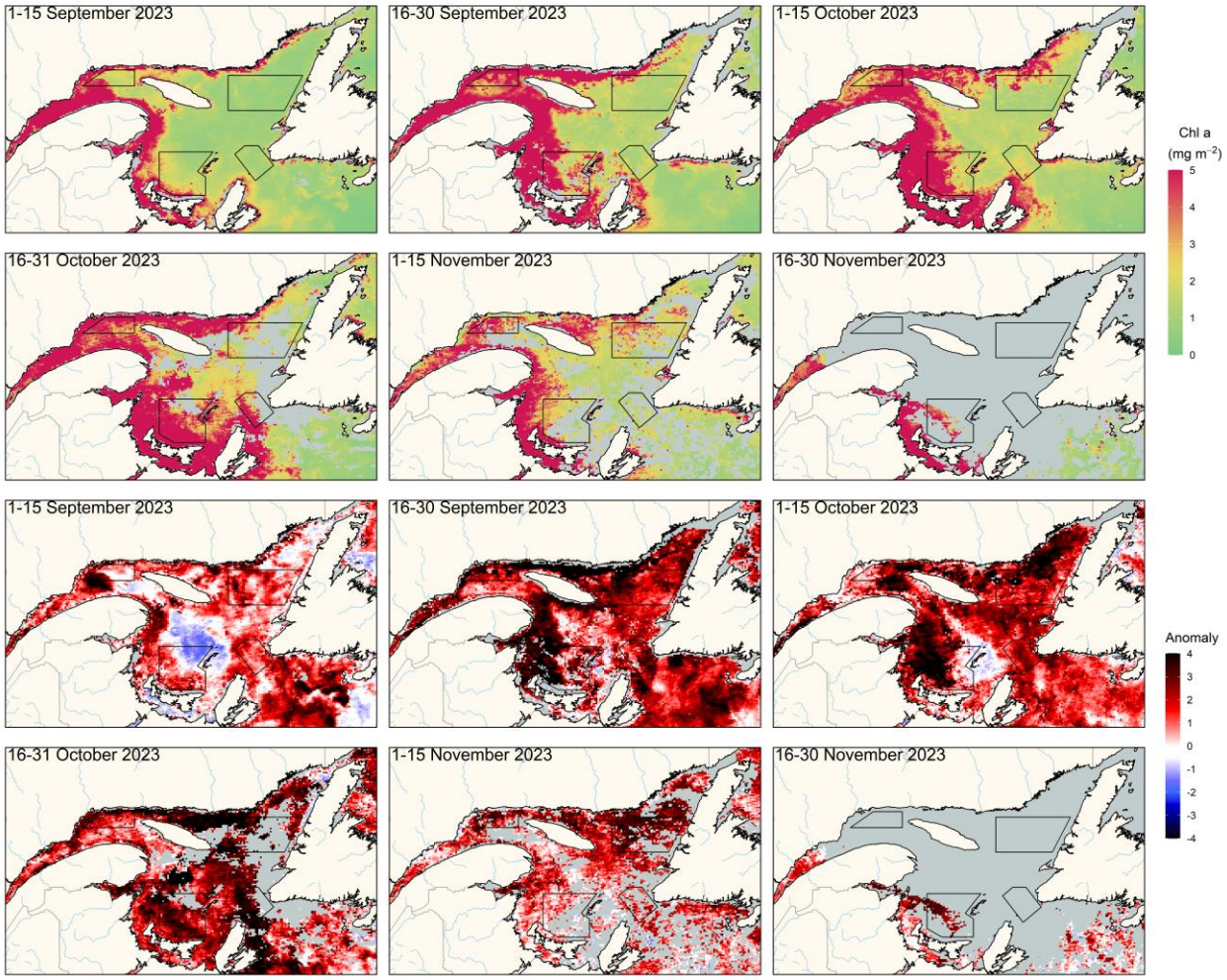

Figure 30. MODIS composite images of surface chlorophyll *a* (upper panels) and chlorophyll *a* normalized anomaly based on the 2003–2020 climatology (lower panels) in the Gulf of St. Lawrence during fall 2023. Grey colour indicates the absence of data. Blue colours indicate below-normal levels (negative anomalies), reds are above-normal levels (positive anomalies), and white represents normal levels.

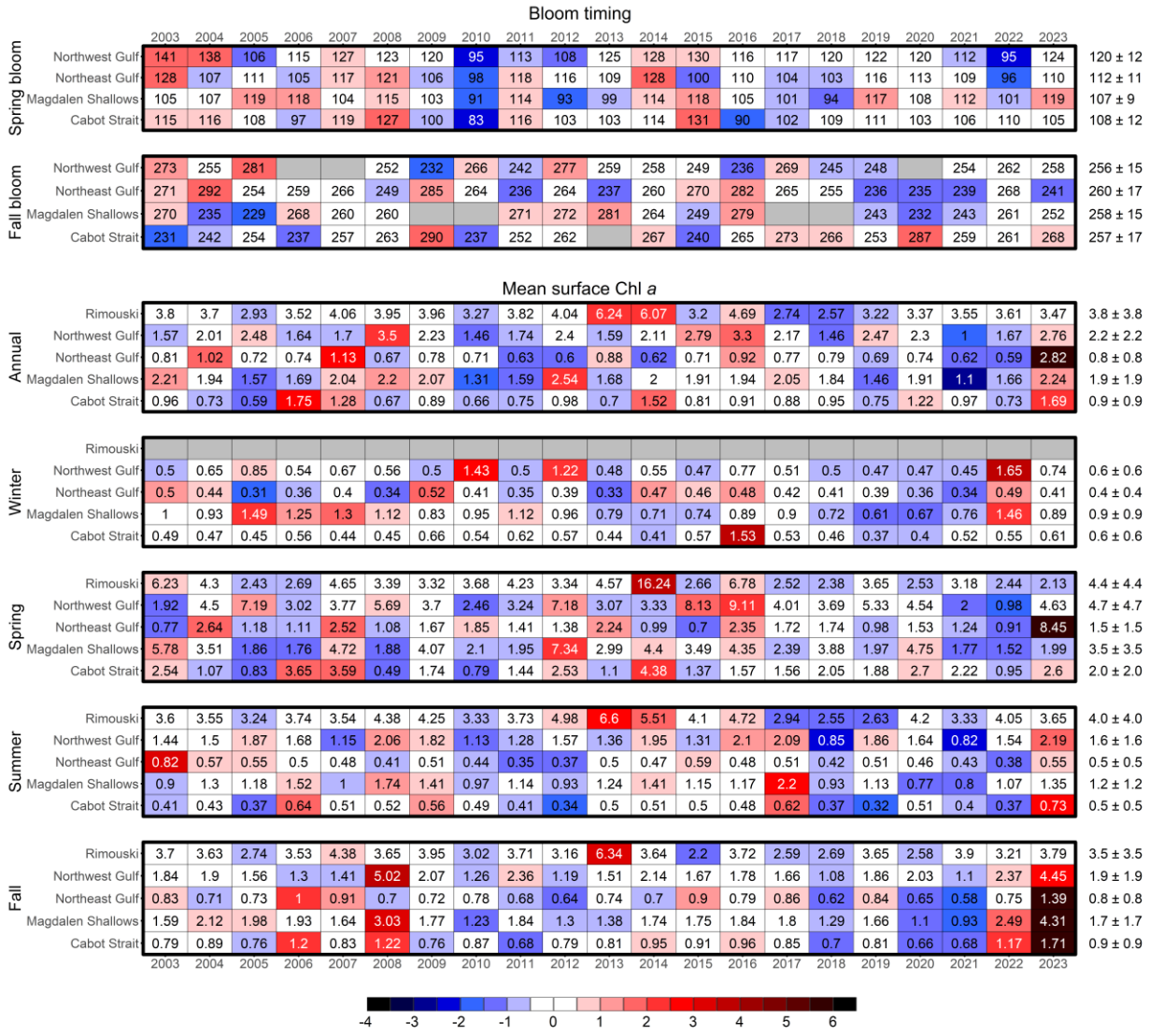

Figure 31. Time series of spring and fall bloom timings (upper section) and annual/seasonal mean surface chlorophyll *a* (mg m^{-3}) estimated from satellite ocean colour data (MODIS: 2003–present) in the Gulf of St. Lawrence ocean-colour polygons (see Figure 4) and from the oceanographic buoy surface sensor at Rimouski station. The bloom timing indices are the spring bloom peak timing (day of the year), and the fall bloom start (day of the year). Variable means and standard deviations for the 2003–2020 climatology are shown to the right of the scorecard. Blue colours indicate below-normal levels (negative anomalies), reds are above-normal levels (positive anomalies), and white represents normal levels.

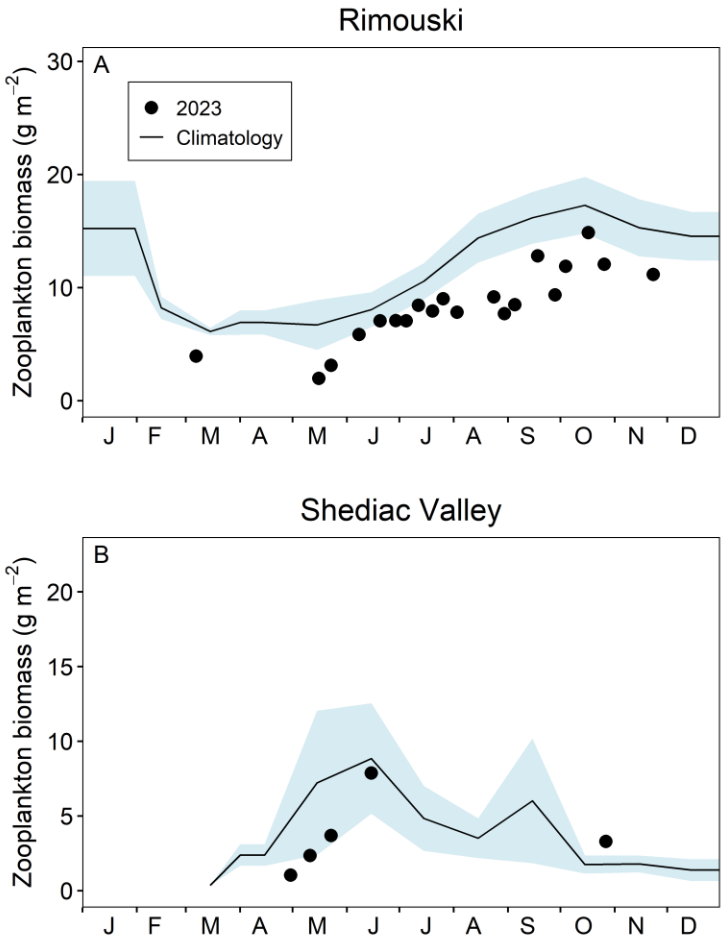

Figure 32. Comparison of total zooplankton biomass (dry weight) in 2023 (circles) with the monthly climatology from (A) Rimouski (2005–2020) and (B) Shediac Valley (1999–2020) stations (black line with blue shading). Blue shading represents ± 0.5 SD of the monthly means.

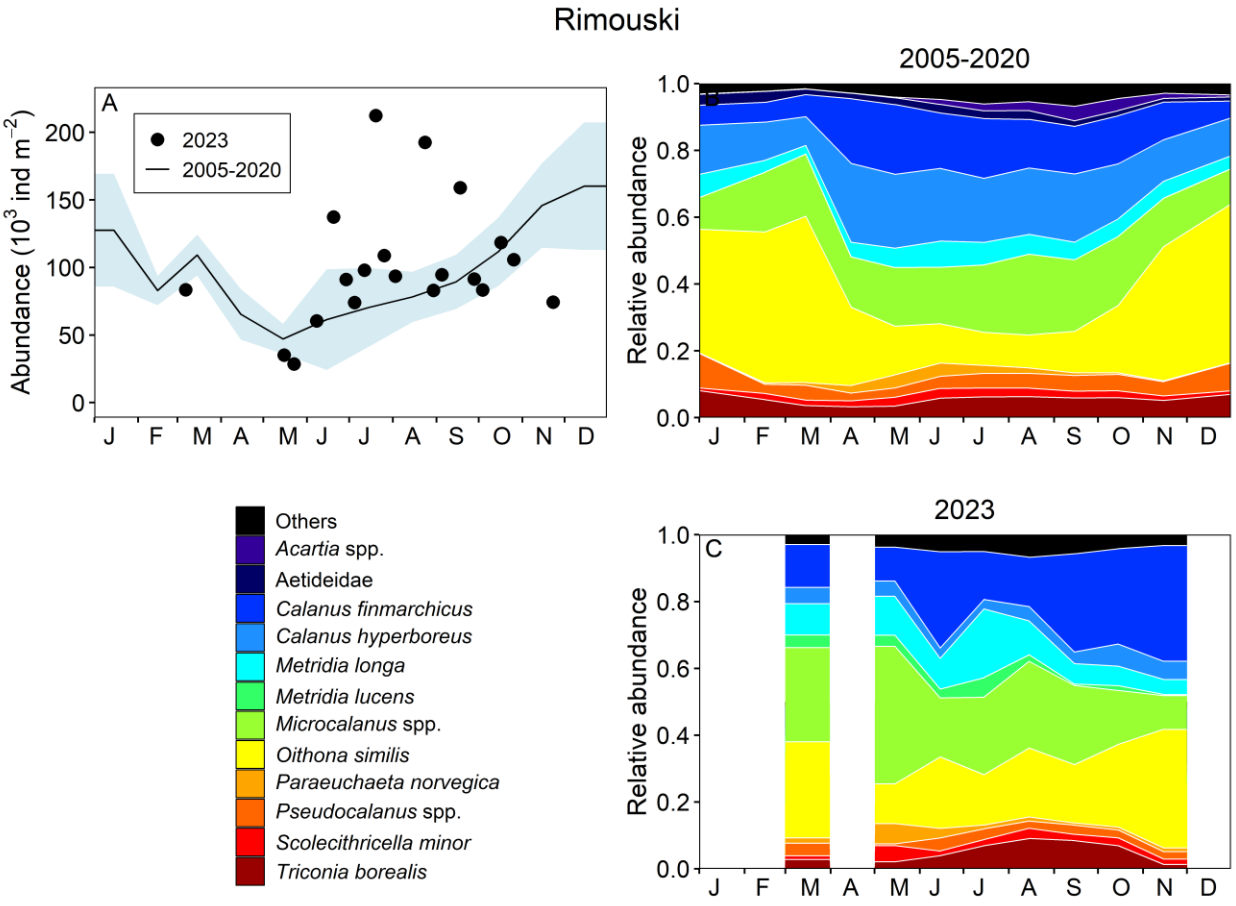

Figure 33. Seasonal variability of dominant copepods at Rimouski station. Climatology of copepod copepodite abundance (10^3 ind. m^{-2}; black line with blue shading indicating ± 0.5 SD) and in 2023 (circles) (A); climatology of the relative abundance of the identified copepod taxa representing 95% of total copepod abundance during the 2005–2020 period (B) and in 2023 (C).

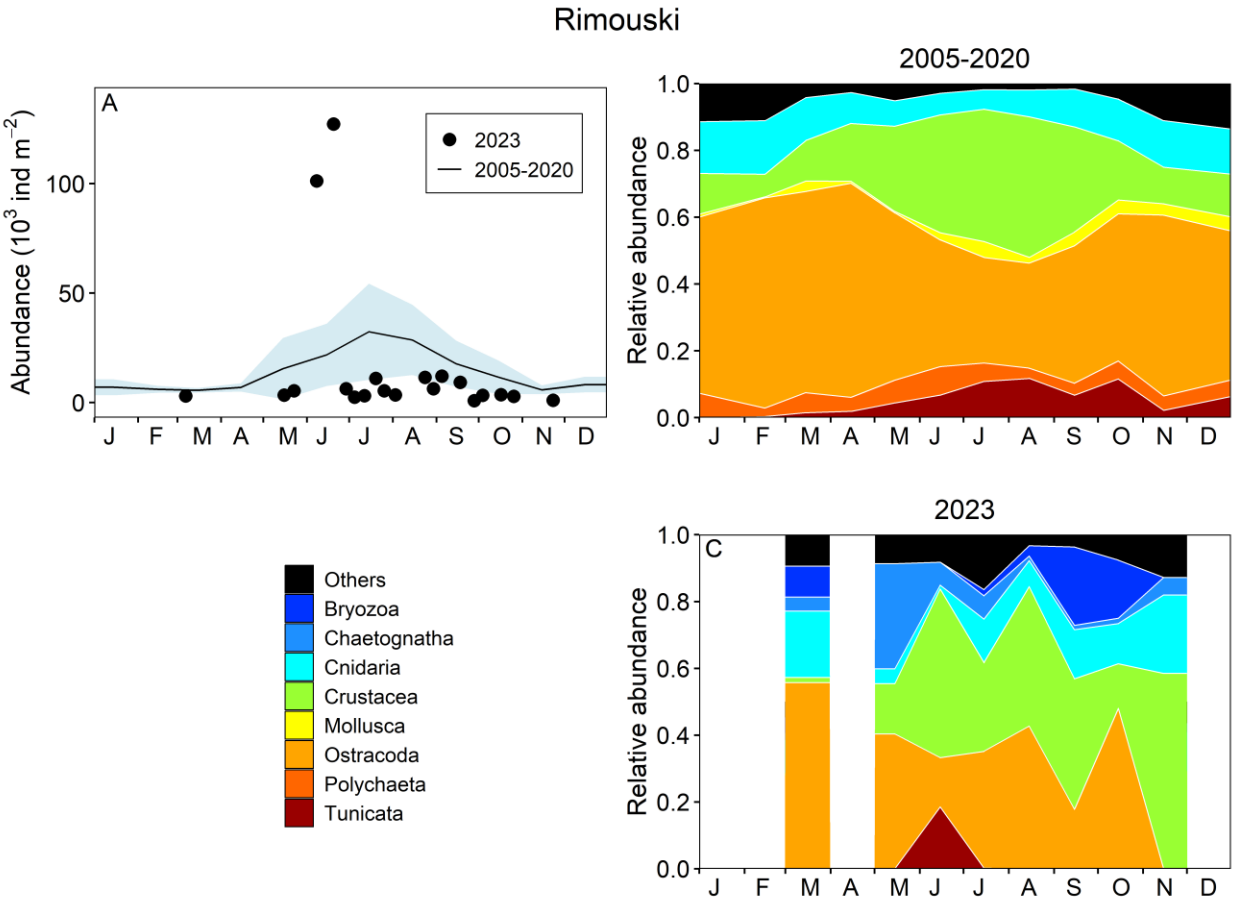

Figure 34. Seasonal variability of dominant non-copepod taxa at Rimouski station. Climatology of non-copepod abundance (10^3 ind. m^{-2}; black line with blue shading indicating ± 0.5 SD) and in 2023 (circles) (A); climatology of the relative abundance of the identified non-copepod taxa representing 95% of total non-copepod abundance during the 2005–2020 period (B) and in 2023 (C).

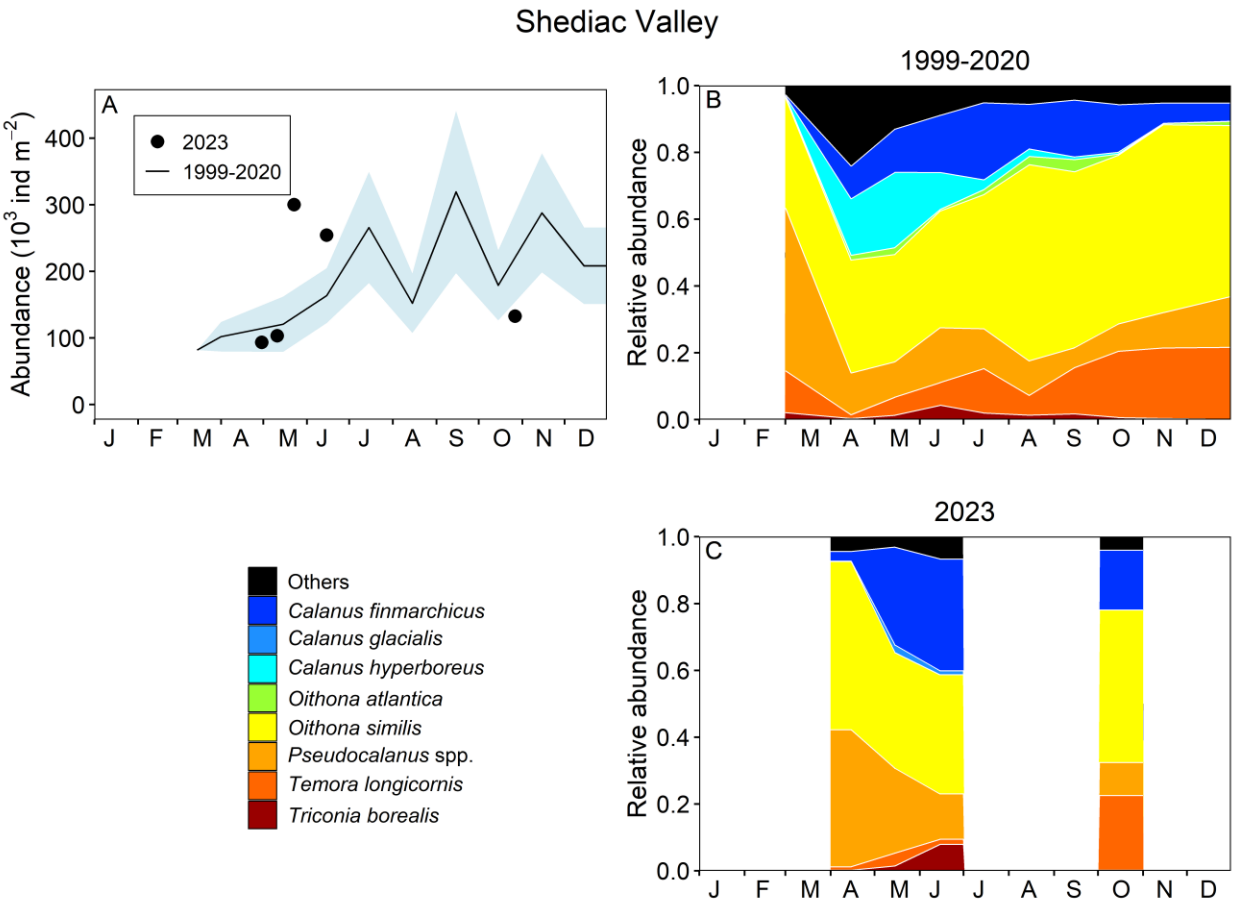

Figure 35. Seasonal variability of dominant copepods at Shediac Valley station. Climatology of copepod copepodite abundance (10^3 ind. m^{-2}; black line with blue shading indicating ± 0.5 SD) and in 2023 (circles) (A); climatology of the relative abundance of the identified copepod taxa representing 95% of total copepod abundance during the 1999–2020 period (B) and in 2023 (C).

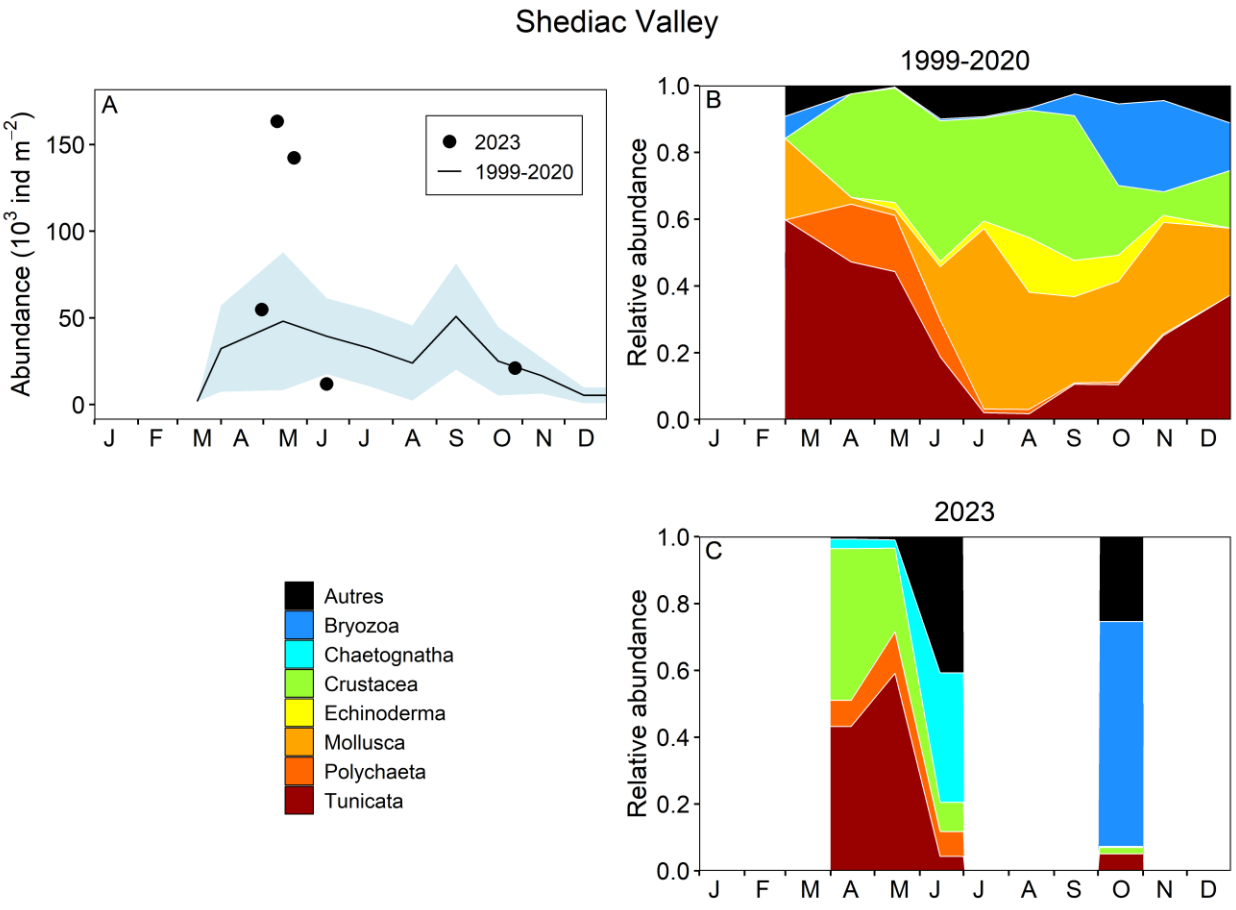

Figure 36. Seasonal variability of dominant non-copepod taxa at Shediac Valley station. Climatology of non-copepod abundance (10^3 ind. m^{-2}; black line with blue shading indicating ± 0.5 SD) and in 2023 (circles) (A); climatology of the relative abundance of the identified non-copepod taxa representing 95% of total non-copepod abundance during the 1999–2020 period (B) and in 2023 (C).

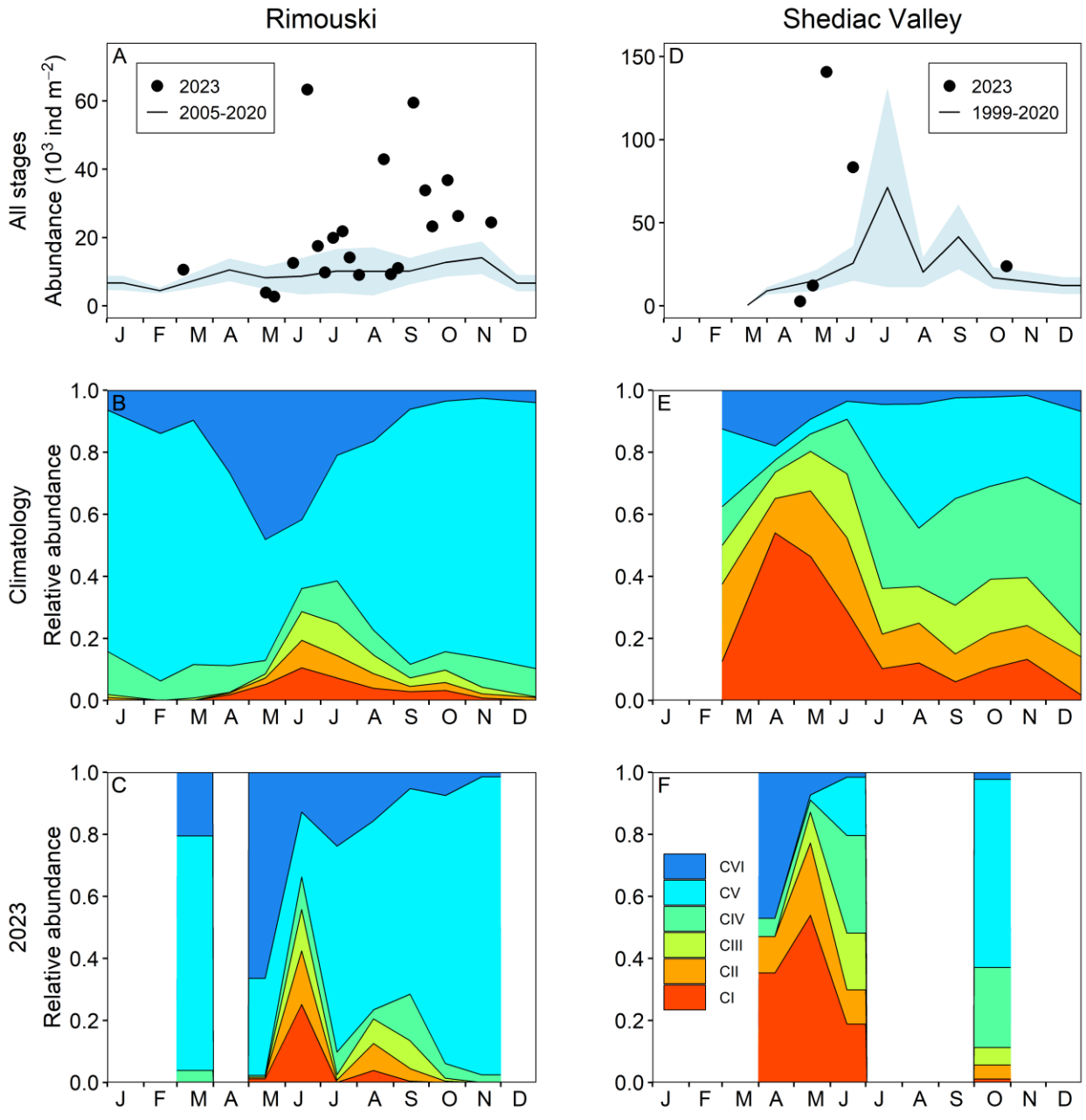

Figure 37. Seasonal variability in *Calanus finmarchicus* copepodite abundance (10^3 ind. m^{-2}) and stage composition at Rimouski (A–C) and Shediac Valley (D–F) stations. Climatology of *C. finmarchicus* abundance (black line with blue shading indicating ± 0.5 SD) with data from 2023 (circles) (A, D). Climatology of individual copepodite stages (B, E) and data for 2023 (C, F).

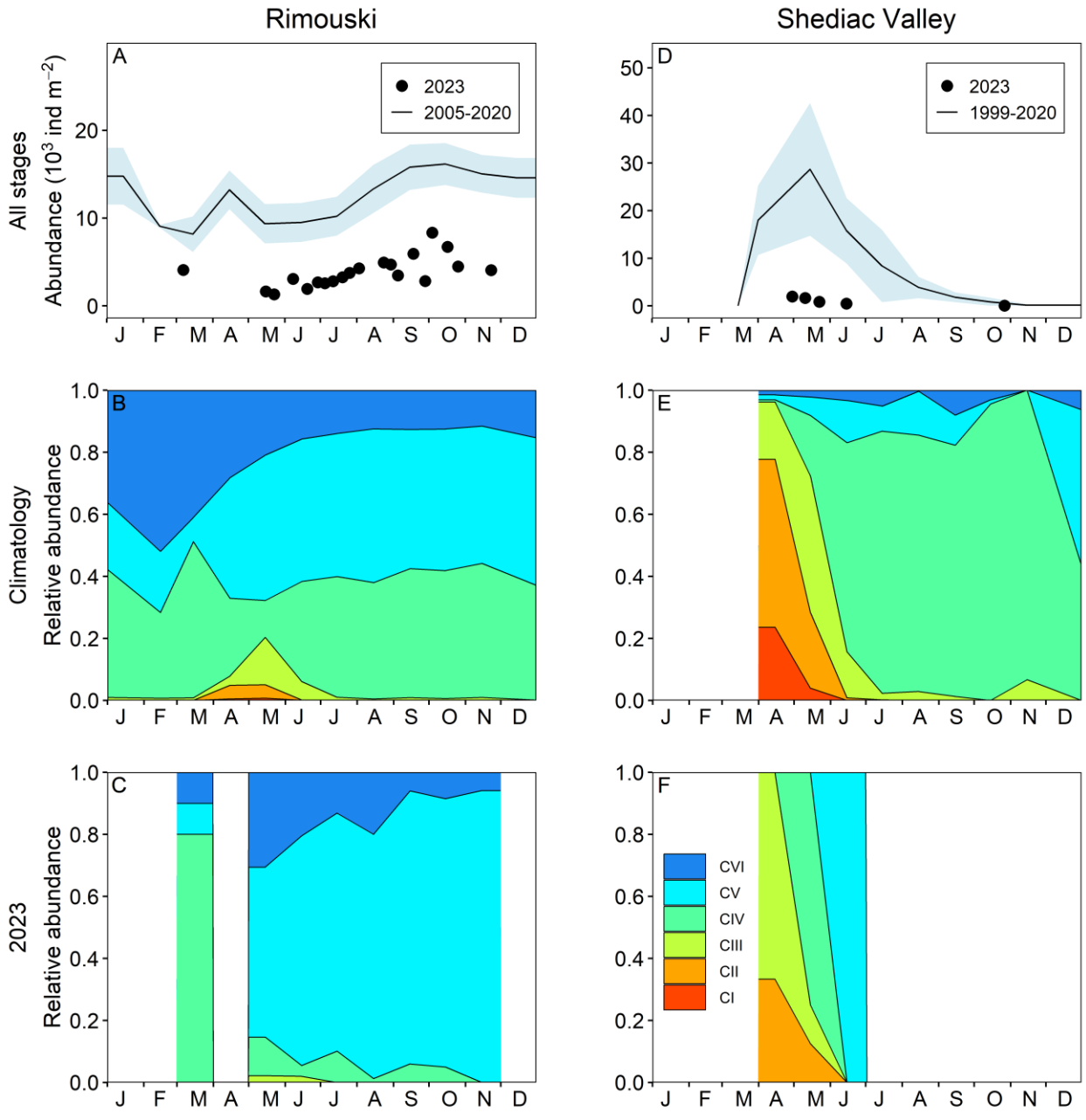

Figure 38. Seasonal variability in *Calanus hyperboreus* copepodite abundance (10^3 ind. m^{-2}) and stage composition at Rimouski (A–C) and Shediac Valley (D–F) stations. Climatology of *C. hyperboreus* abundance (black line with blue shading indicating ± 0.5 SD) with data from 2023 (circles) (A, D). Climatology of individual copepodite stages (B, E) and data for 2023 (C, F).

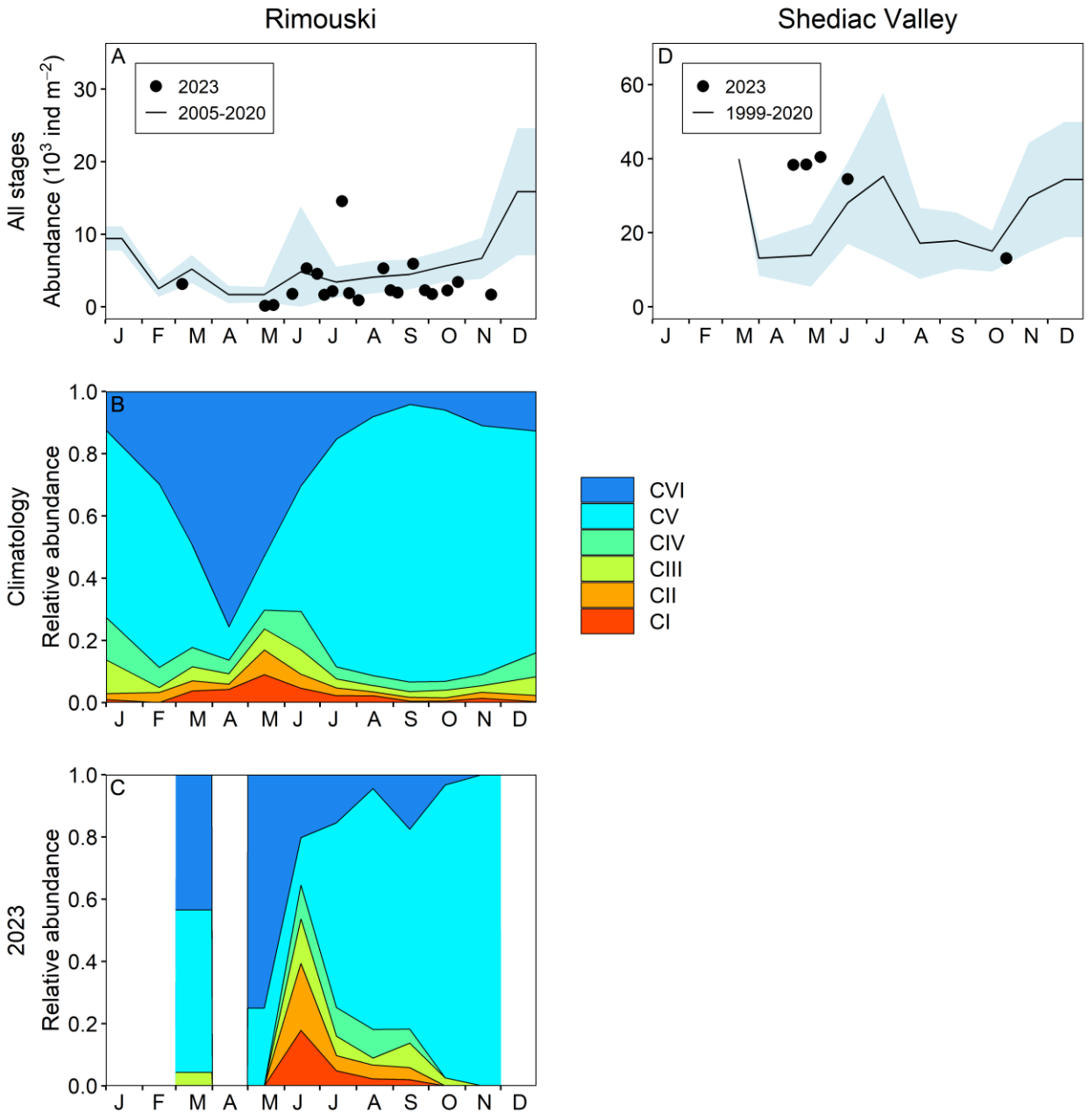

Figure 39. Seasonal variability in *Pseudocalanus* spp. copepodite abundance (10^3 ind. m^{-2}) and stage composition at Rimouski (A–C) and Shediac Valley (D) stations. Climatology of *Pseudocalanus* spp. abundance (black line with blue shading indicating ± 0.5 SD) with data from 2023 (circles) (A). Climatology of individual copepodite stages (B) and data for 2023 (C). Stage information is not available for Shediac Valley.

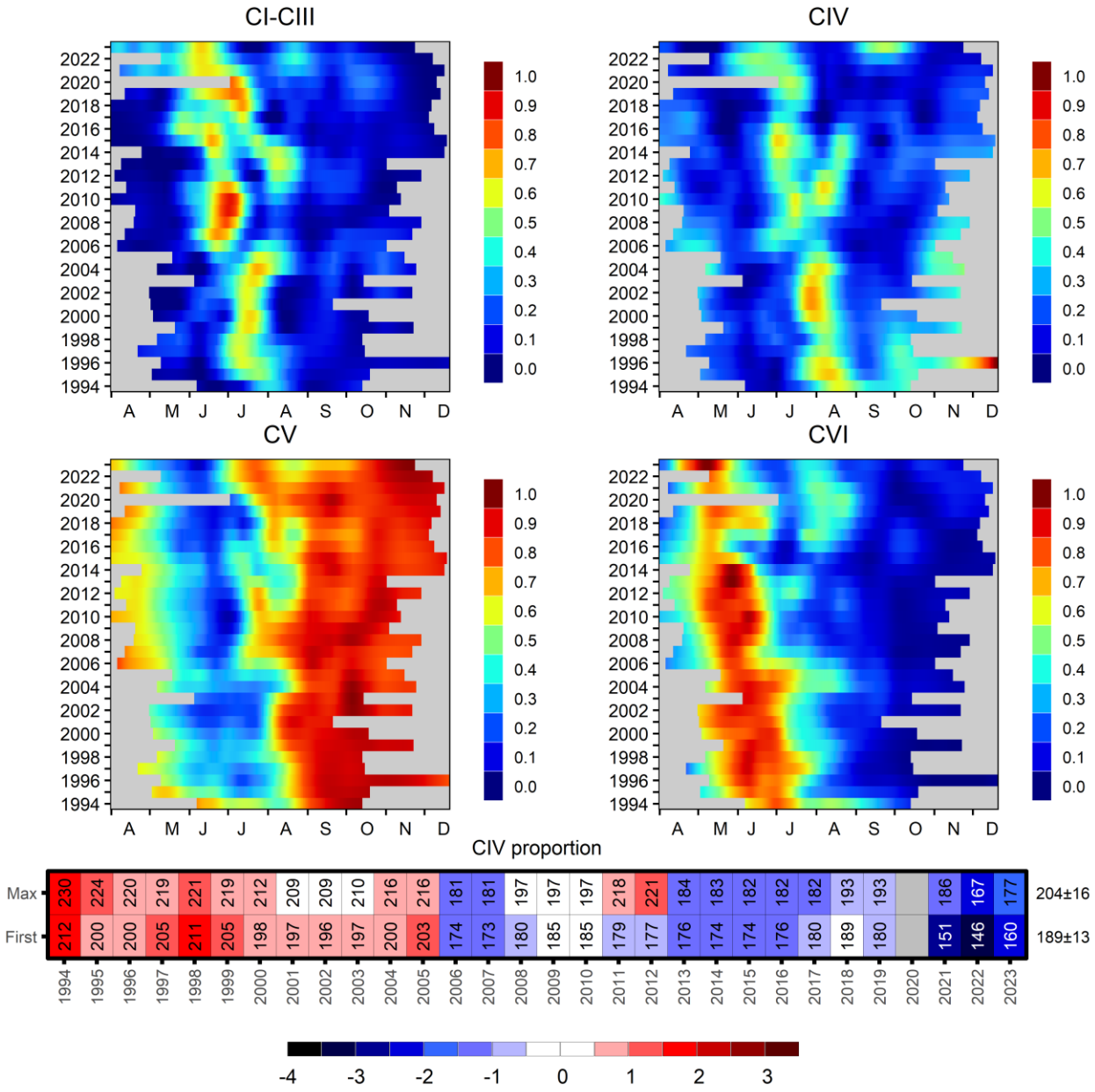

Figure 40. Time series of the seasonal cycle of relative proportion for *Calanus finmarchicus* copepodite stages at Rimouski station. Proportions are normalized by their annual maximum and smoothed using a LOESS regression. Bottom scorecard shows the anomaly time series (climatology 1994–2020) associated with the day of maximum CIV proportion (Max) and the first day when the normalized proportion of CIV copepodite stage was higher than 0.35 (First). Variable means and standard deviations (in units of days) for the 1994–2020 climatology are shown to the right of the scorecard. Blue colours indicate below-normal levels (negative anomalies), reds are above-normal levels (positive anomalies), and white represents normal levels. Gray cells indicate unavailable data.

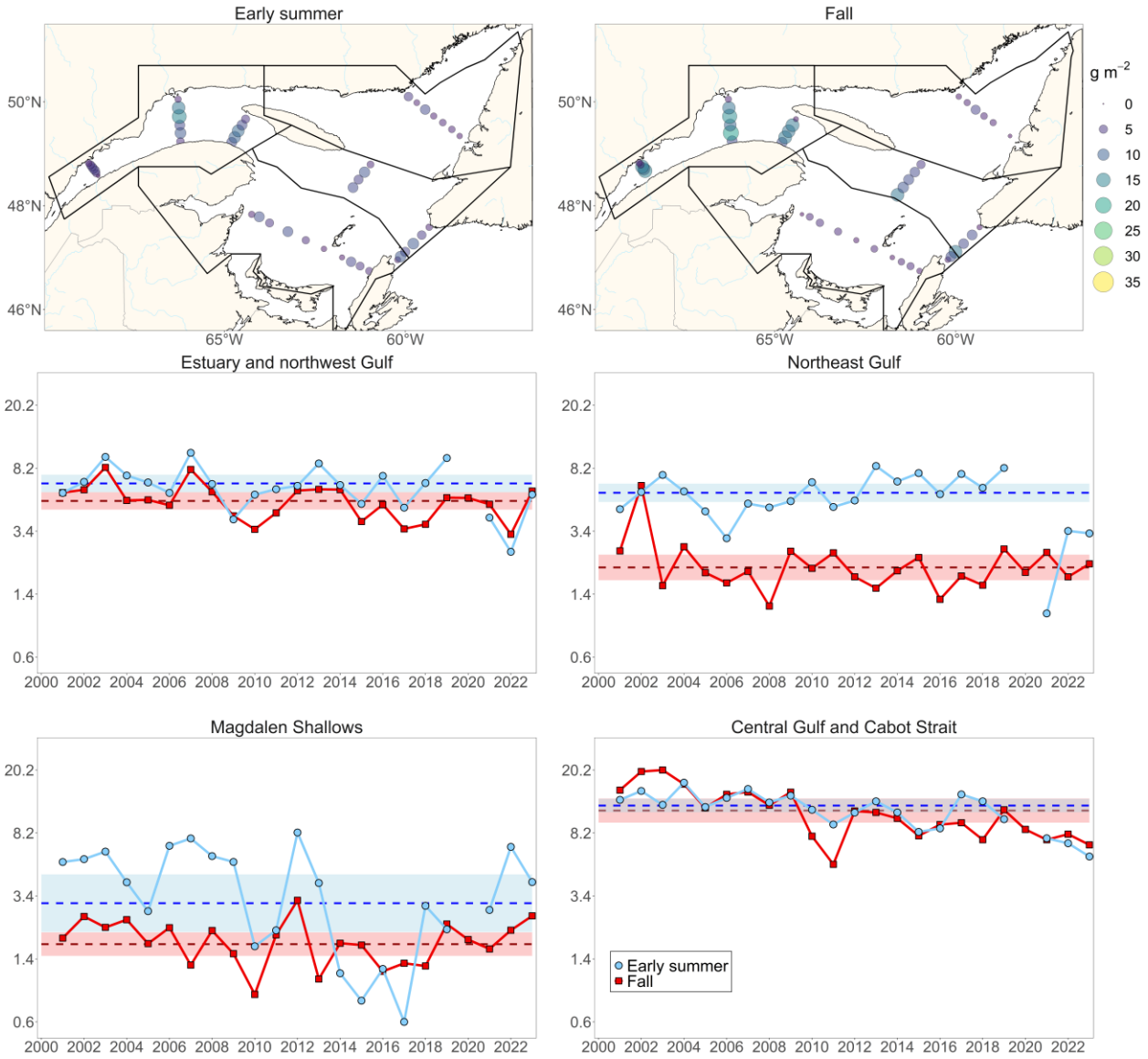

Figure 41. Zooplankton biomass (dry weight; g m^{-2}) spatial distribution during early summer and fall 2023 (upper panels) and regional seasonal time series of mean total zooplankton biomass (g m^{-2}; middle and bottom panels). Dashed blue and red lines represent the climatological (2001–2020) averages (blue and red shaded bands represent ± 0.5 SD) for early summer and fall, respectively.

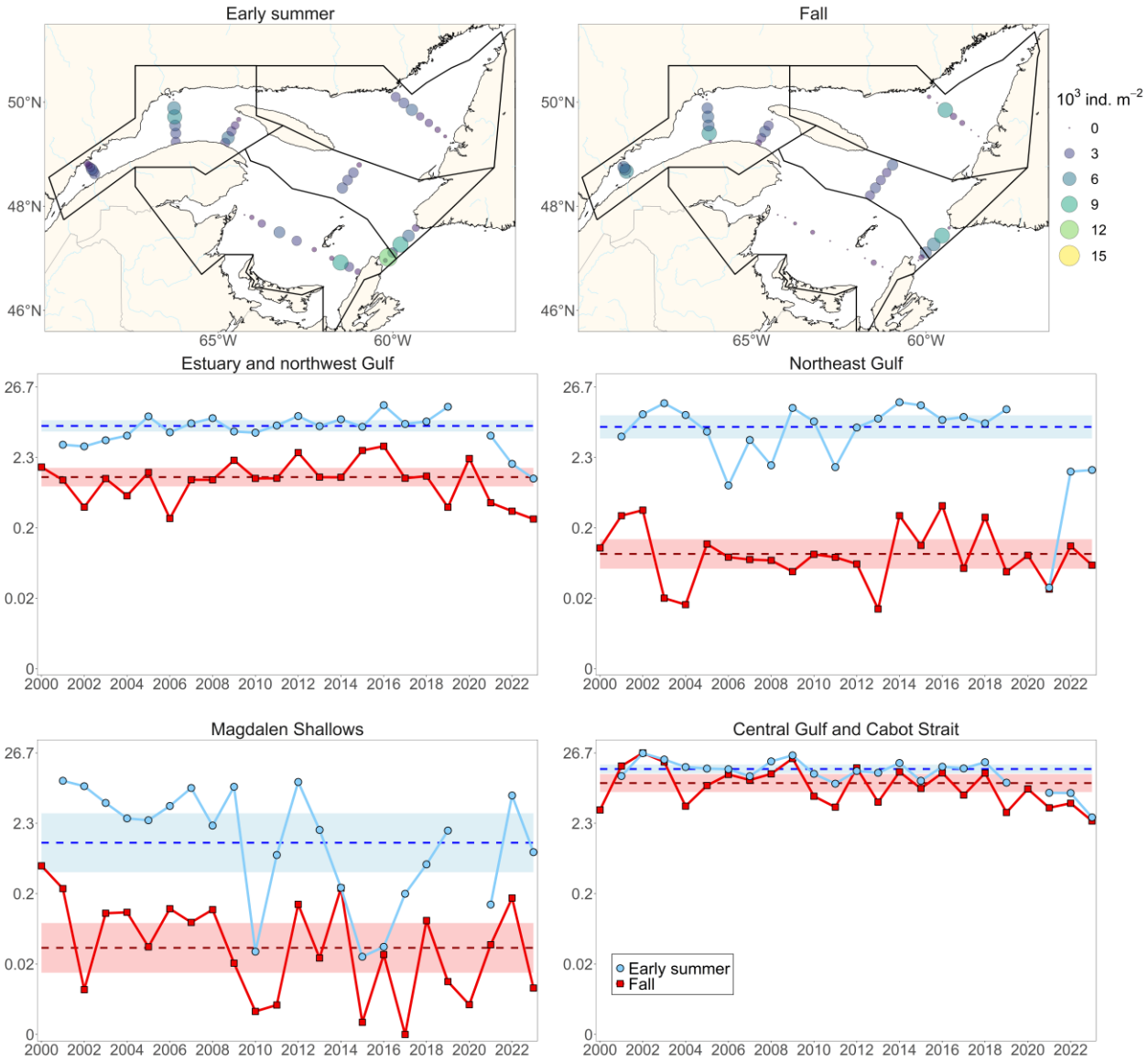

Figure 42. *Calanus hyperboreus* abundance (10^3 ind. m^{-2}) spatial distribution during early summer and fall 2023 (upper panels) and regional seasonal time series of mean total *C. hyperboreus* abundance (10^3 ind. m^{-2}; middle and bottom panels). Dashed blue and red lines represent the climatological (2000–2020) averages (blue and red shaded bands represent ± 0.5 SD) for early summer and fall, respectively.

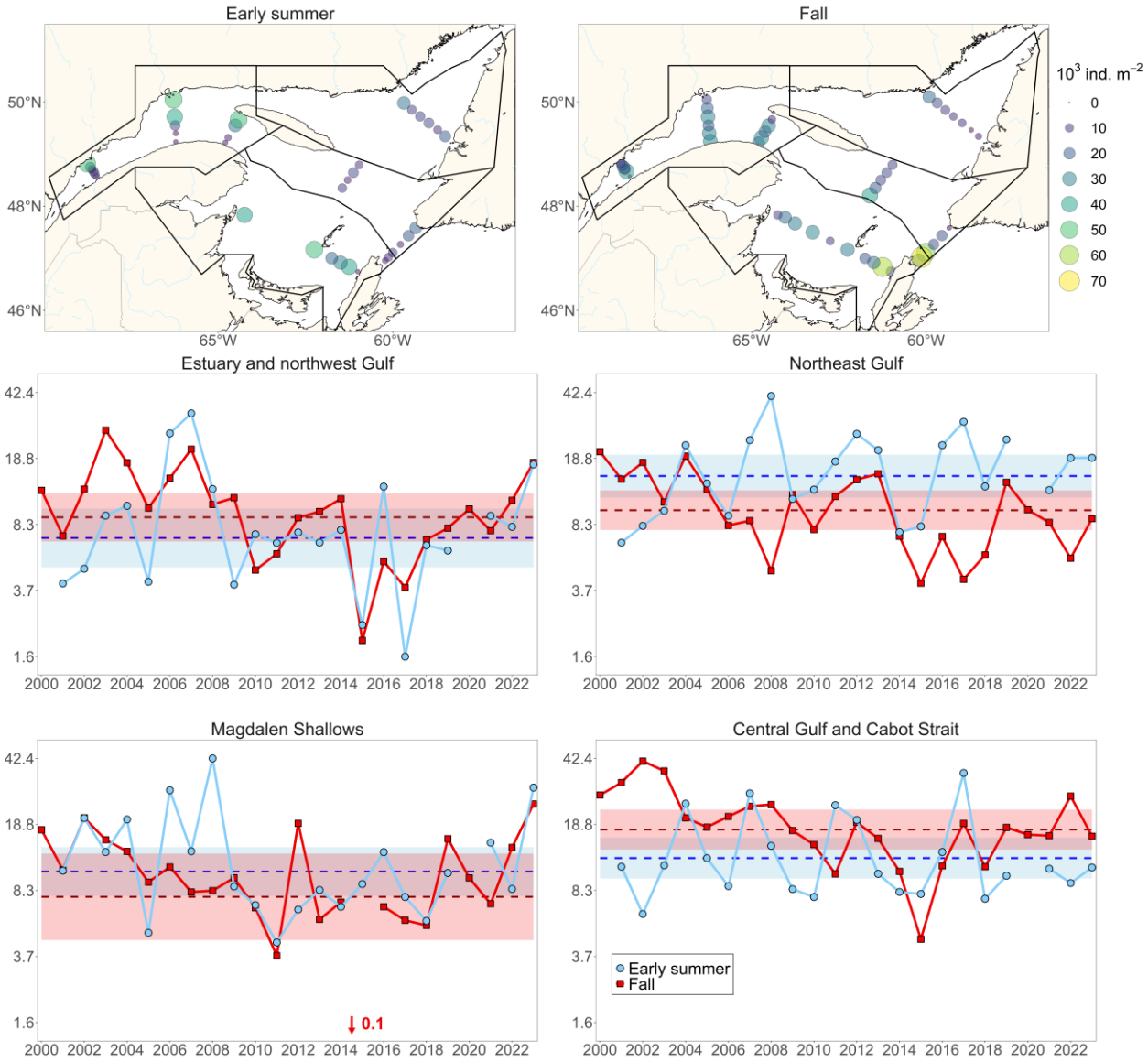

Figure 43. *Calanus finmarchicus* abundance (10^3 ind. m^{-2}) spatial distribution during early summer and fall 2023 (upper panels) and regional seasonal time series of mean total *C. finmarchicus* abundance (10^3 ind. m^{-2}; middle and bottom panels). In the Magdalen Shallows during 2015, the abundance of *C. finmarchicus* (100 ind. m^{-2}) is too low to be shown. Dashed blue and red lines represent the climatological (2000–2020) averages (blue and red shaded areas represent ± 0.5 SD) for early summer and fall, respectively.

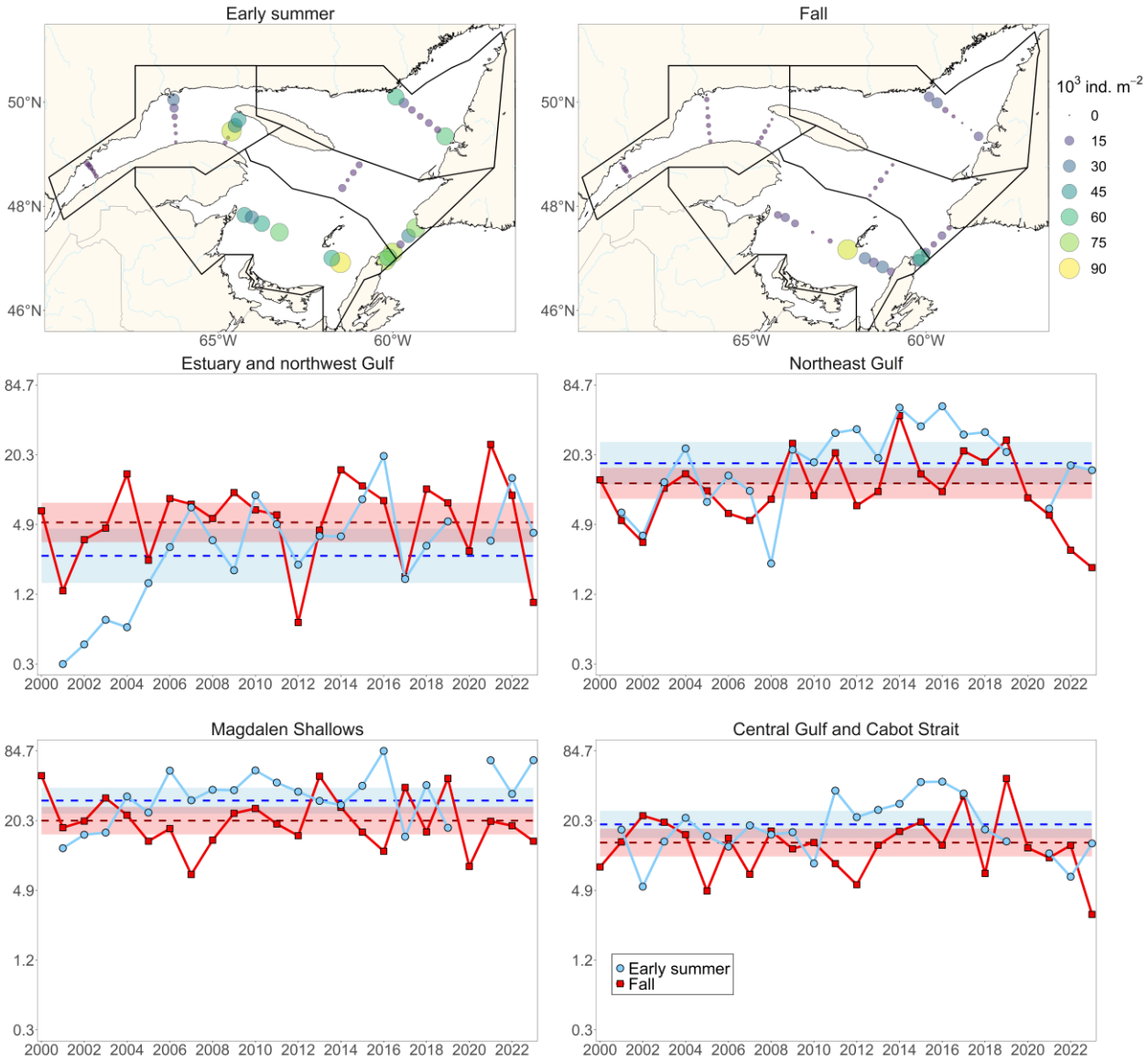

Figure 44. *Pseudocalanus* spp. abundance (10^3 ind. m^{-2}) spatial distribution during early summer and fall 2023 (upper panels) and regional seasonal time series of mean total *Pseudocalanus* spp. abundance (10^3 ind. m^{-2}; middle and bottom panels). Dashed blue and red lines represent the climatological (2000–2020) averages (blue and red shaded areas represent ± 0.5 SD) for early summer and fall, respectively.

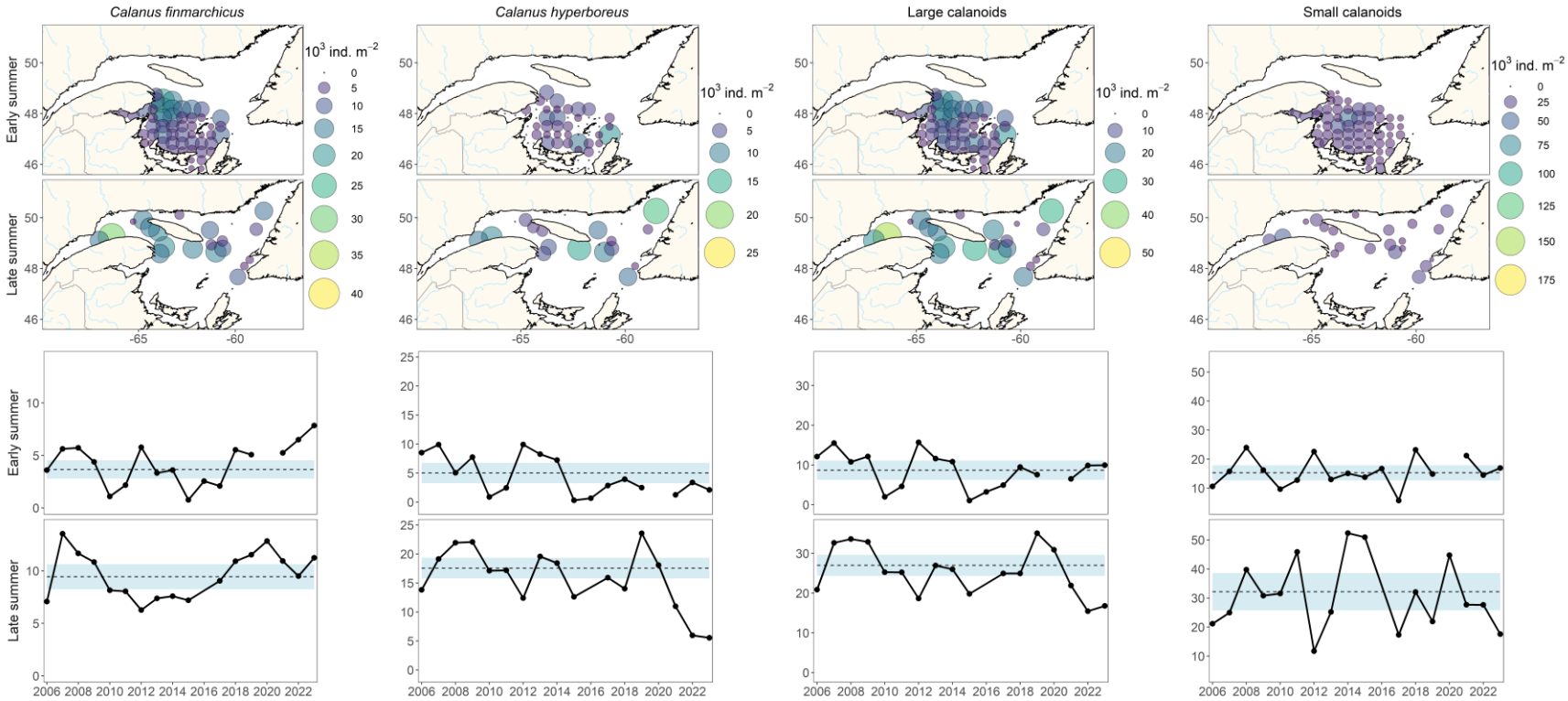

Figure 45. Abundances (10^3 ind. m^{-2}) of main taxa identified through automated numerical zooplankton images analysis (ZooImage) at each sampling station during early summer on the Magdalen Shallows and late summer 2023 in the northern Gulf (upper panels). The annual time series of mean total abundances are also shown for these taxa (10^3 ind. m^{-2}; bottom panels). Dashed lines represent the climatology (2006–2020) averages (blue shading represents ± 0.5 SD). The abundances of *C. finmarchicus* and *C. hyperboreus* include copepodite stages CIV – CVI only. ZooImage does not distinguish between *C. finmarchicus* and *C. glacialis*, thus both species are included in the *C. finmarchicus* index. Large calanoid abundances correspond to the sum of these *C. finmarchicus* and *C. hyperboreus* indices; and small calanoid abundances correspond to the sum of the following taxa: *Temora* spp., *Eurytemora* spp., *Pseudocalanus* spp., *Microcalanus* spp. and *Scolecithricella* spp.

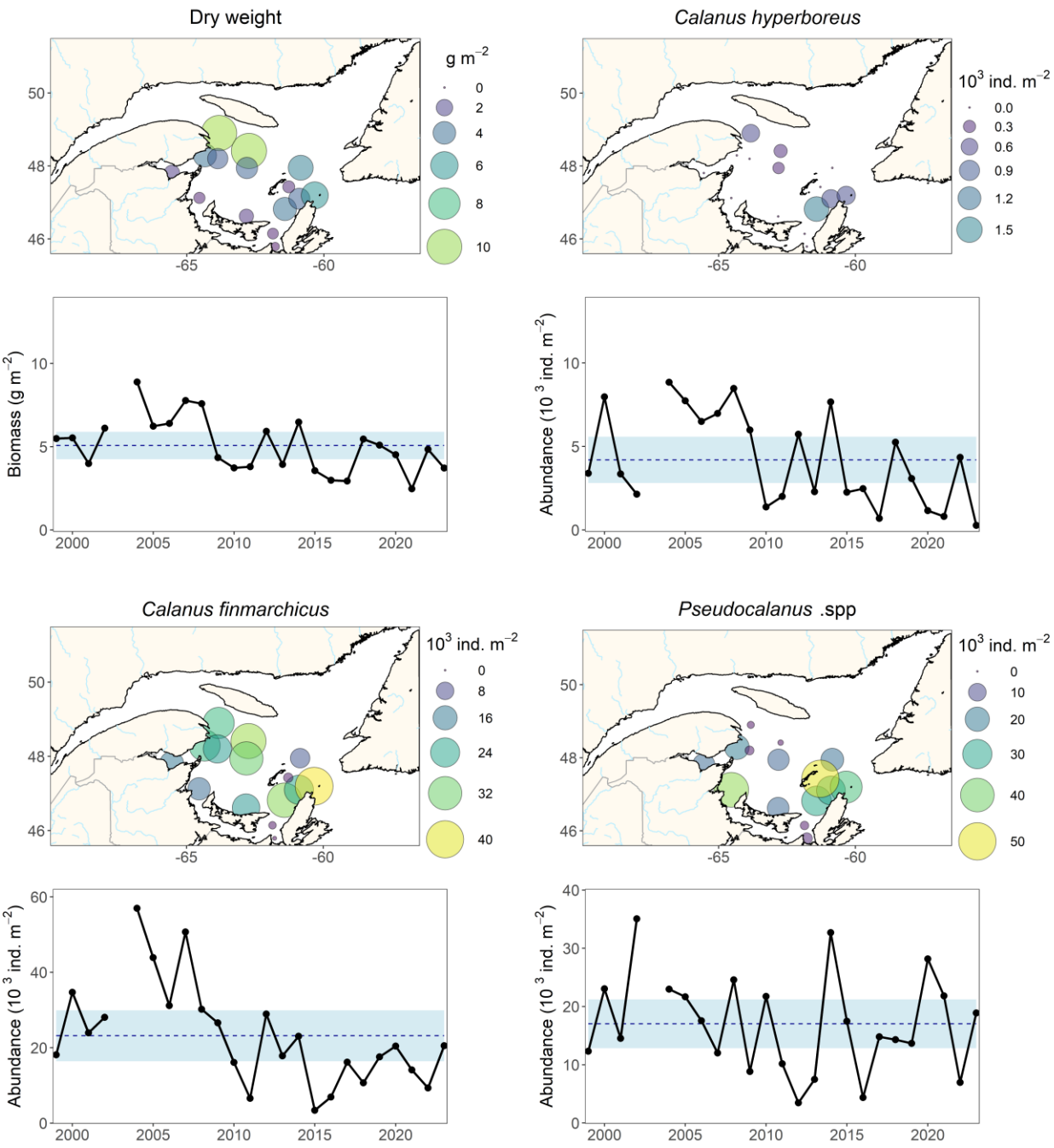

Figure 46. Biomass (g m^{-2}) and abundances (10^3 ind. m^{-2}) of main zooplankton taxa at each sampling station during late summer multidisciplinary survey on the Magdalen Shallows in September 2023. The seasonal time series of mean biomass (g m^{-2}) and total abundances for these taxa are also shown (10^3 ind. m^{-2}; bottom panels). Dashed lines represent the climatology (2000–2020) averages (blue shading represents ± 0.5 SD).

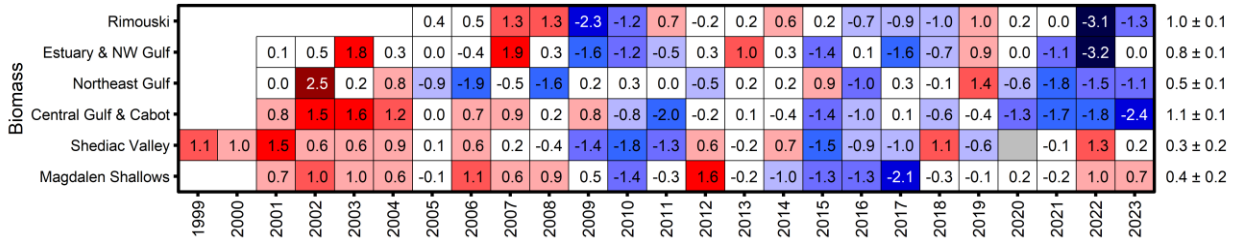

Figure 47. Time series of normalized annual anomalies of zooplankton biomass (dry weight) for the high-frequency monitoring stations and the regions of the Gulf of St. Lawrence. The numbers on the right are the 2001–2020 (2005–2020 for Rimouski; 1999–2020 for Shediac Valley) climatological means and standard deviations in units of $\log_{10}(g\ m^{-2})$. Blue colours indicate below-normal levels (negative anomalies), reds are above-normal levels (positive anomalies), and white represents normal levels.Gray cells indicate unavailable data.

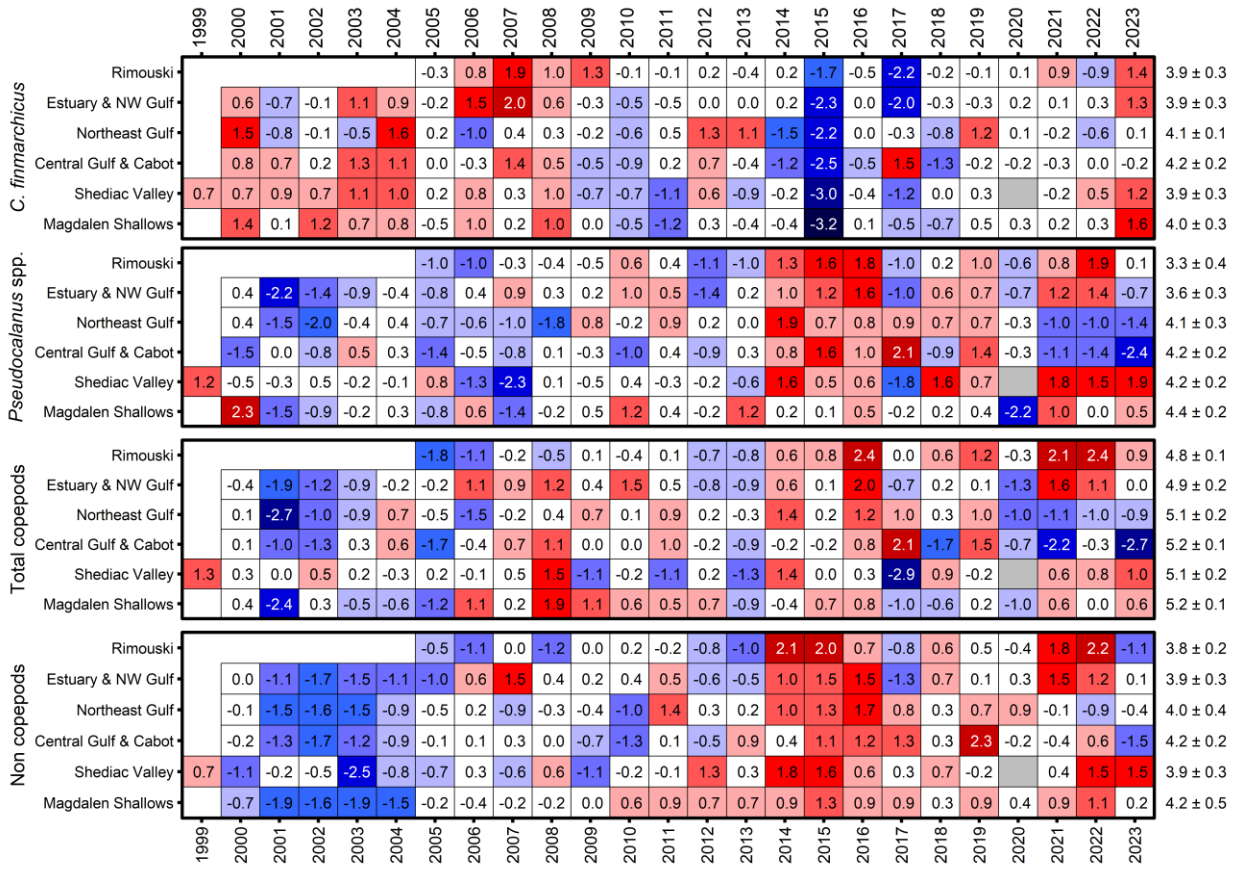

Figure 48. Time series of normalized annual anomalies for the abundance of four zooplankton categories for the high-frequency monitoring stations and regions of the Gulf of St. Lawrence. The numbers on the right are the 2000–2020 (2005–2020 for Rimouski; 1999–2020 for Shediac Valley) climatological means and standard deviations in units of $\log_{10}(ind.\ m^{-2})$. Blue colours indicate below-normal levels (negative anomalies), reds are above-normal levels (positive anomalies), and white represents normal levels.Gray cells indicate unavailable data. GSL: Gulf of St. Lawrence.

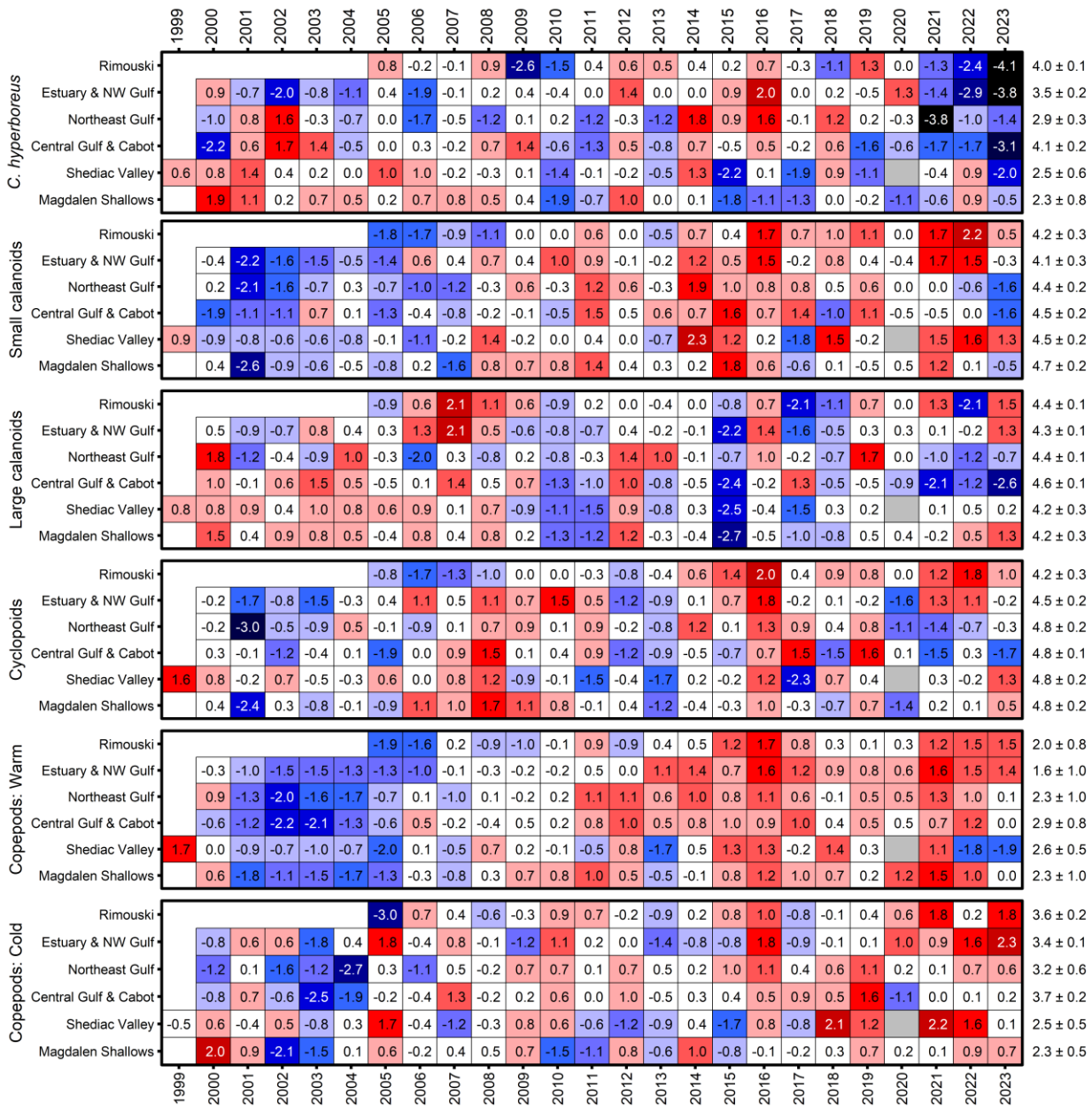

Figure 49. Time series of normalized annual anomalies for the abundance of six categories of zooplankton assemblages for the high-frequency monitoring stations and the regions of the Gulf of St. Lawrence. The numbers on the right are the 2000–2020 (2005–2020 for Rimouski; 1999–2020 for Shediac Valley) climatological means and standard deviations in units of $\log_{10}$(ind. m^{-2}). Blue colours indicate below-normal levels (negative anomalies), reds are above-normal levels (positive anomalies), and white represents normal levels. Gray cells indicate unavailable data. A detailed list of species included in each large copepod index is presented in Appendix 1.

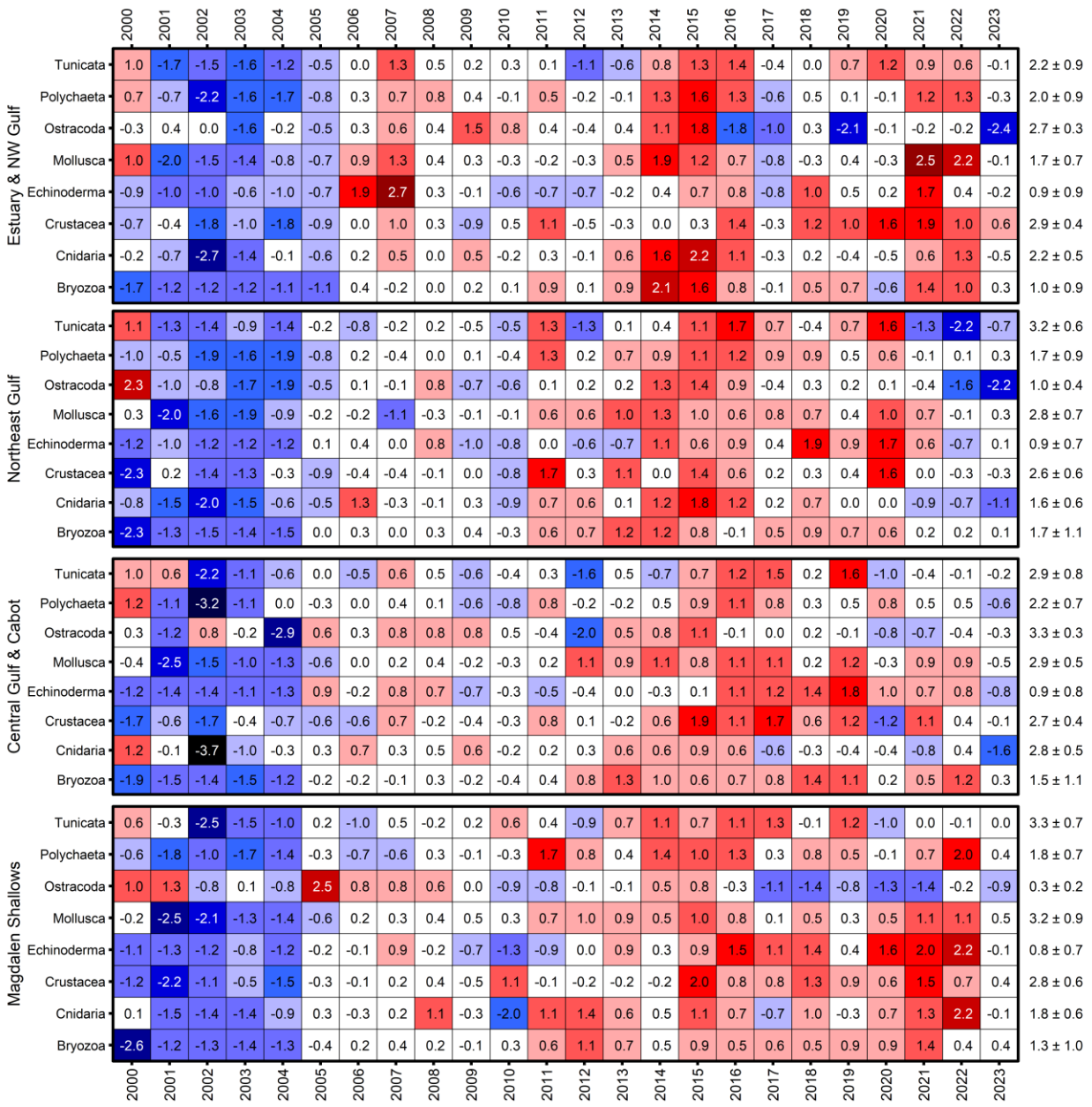

Figure 50. Time series of normalized annual anomalies for the abundance of main non-copepod zooplankton taxa for the regions of the Gulf of St. Lawrence. The numbers on the right are the 2000–2020 climatological means and standard deviations in units of $\log_{10}$(ind. m^{-2}). Blue colours indicate below-normal levels (negative anomalies), reds are above-normal levels (positive anomalies), and white represents normal levels.

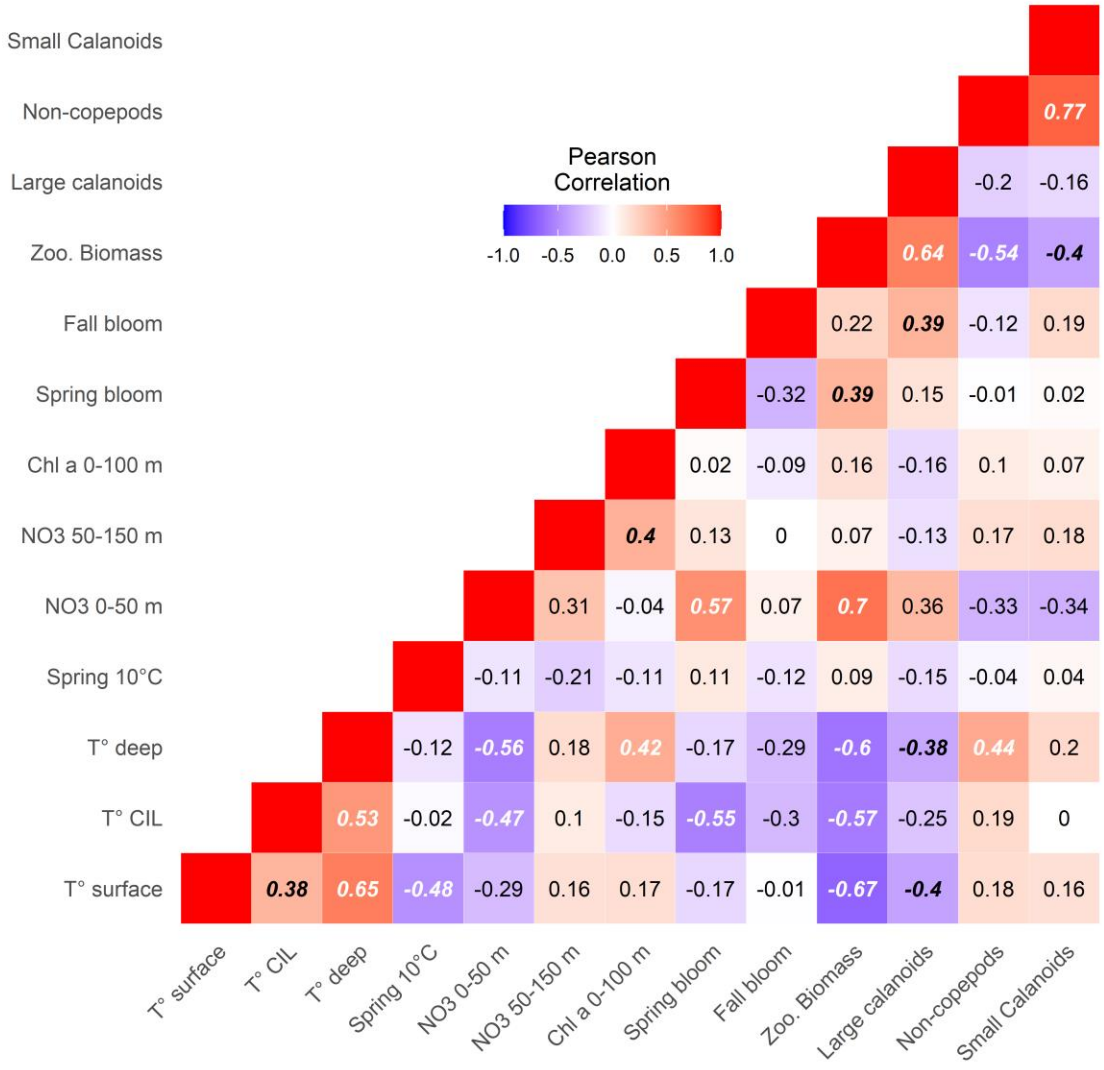

Figure 51. Correlation matrix of weighted averaged anomalies for key Gulf indices. Blue colours indicate negative correlations and reds are positive correlations. Significant correlations are indicated in black bold italic ($p < 0.1$) or in white bold-italic ($p < 0.05$). CIL: cold intermediate layer. Spring 10°C is an index of spring timing based on the date at which average Gulf temperature at the surface warms to 10°C. Spring and fall blooms refer to their timing.

APPENDICES

Appendix 1 : List of taxa associated with each copepod index.

Small calanoids	*Acartia* spp.
	Aetideidae
	Centropages spp.
	Clausocalanus spp.
	Eurytemora spp.
	Microcalanus spp.
	Nannocalanus minor
	Paracalanus parvus
	Pseudocalanus spp.
	Scolecithricella spp.
	Spinocalanus spp.
	Temora spp.
	Tortanus spp.
Large calanoids	*Anomalocera* spp.
	Calanus finmarchicus
	Calanus glacialis
	Calanus hyperboreus
	Euchaeta spp.
	Metridia spp.
	Paraeuchaeta
	Pleuromamma borealis
	Pleuromamma robusta
Warm copepods	*Centropages* spp.
	Clausocalanus spp.
	Metridia lucens
	Nannocalanus minor
	Paracalanus spp.
	Pleuromamma borealis
	Pleuromamma robusta
Cyclopoids	*Oithona* spp.
	Oncaea spp.
	Triconia borealis
	Triconia conifer
	Triconia similis
Cold copepods	*Metridia longa*
	Calanus glacialis

Appendix 2 : Spring and fall bloom fits for 2023 in all Gulf ocean colour polygons using the Phytofit application v1.0.0 (Clay et al. 2021) with the parameters listed below. These bloom fits are used to define spring (peak; plots 1-4) and fall (start; plots 5-8) timing of the bloom, as well as to define season boundaries. The "flagged fit" warning in the Magdalen Shallows spring model time series refers to the fact that the ratio of the amplitude of the Gaussian curve (Amplitudefit) to the real peak value (Amplitudereal) exceeds 1.25. The Northwest Gulf of St. Lawrence fit is similarly flagged, with the added warning that the ratio of the area under the Gaussian curve (Magnitudefit) to the area under the real data points (Magnitudereal) exceeds 1.15. These flags exist in the PhytoFit app to aid the user in detecting bad fits.

1.

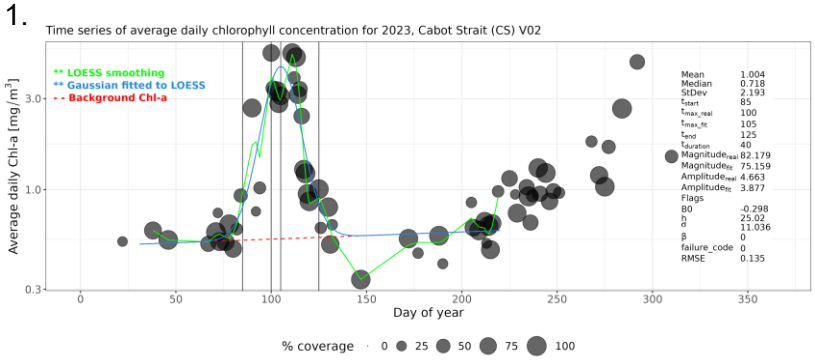

2.

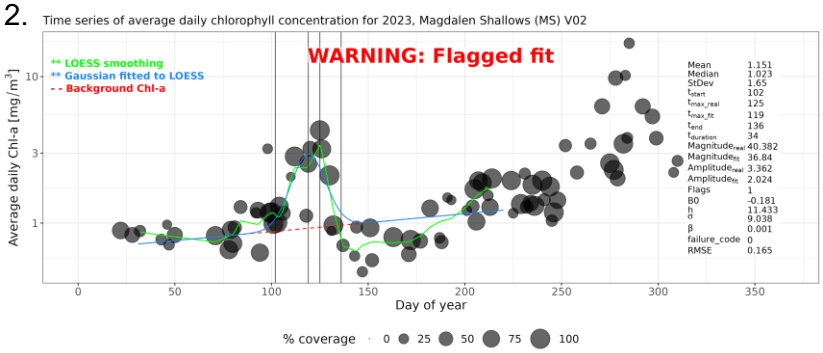

3.

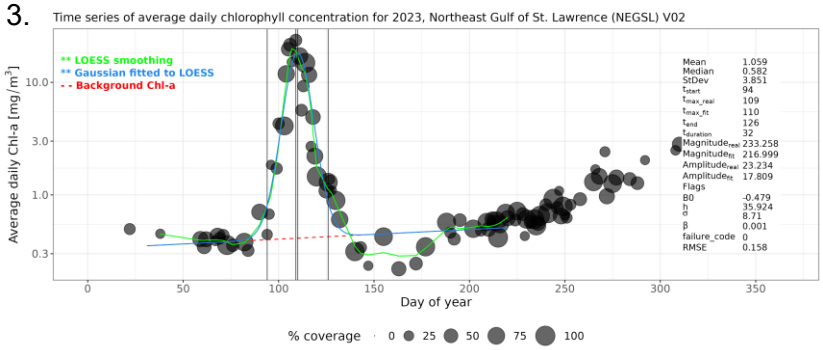

4. Time series of average daily chlorophyll concentration for 2023, Northwest Gulf of St. Lawrence (NWGSL) V02

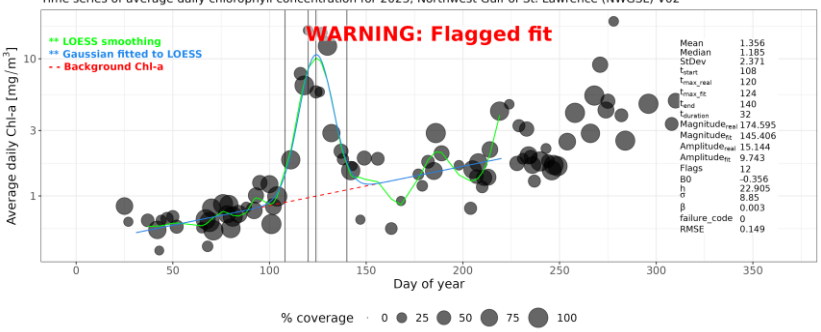

5. Time series of average daily chlorophyll concentration for 2023, Cabot Strait (CS) V02

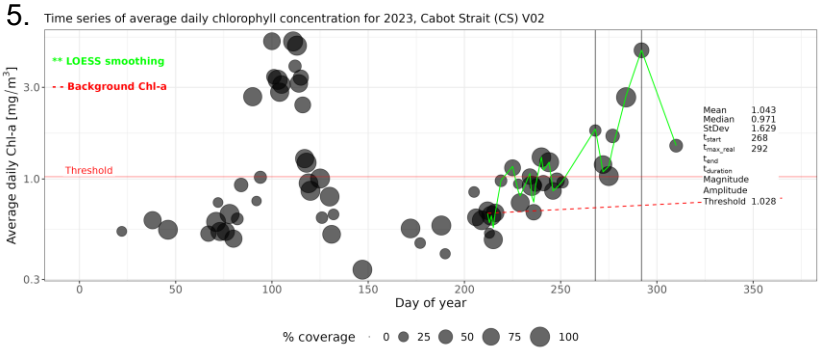

6. Time series of average daily chlorophyll concentration for 2023, Magdalen Shallows (MS) V02

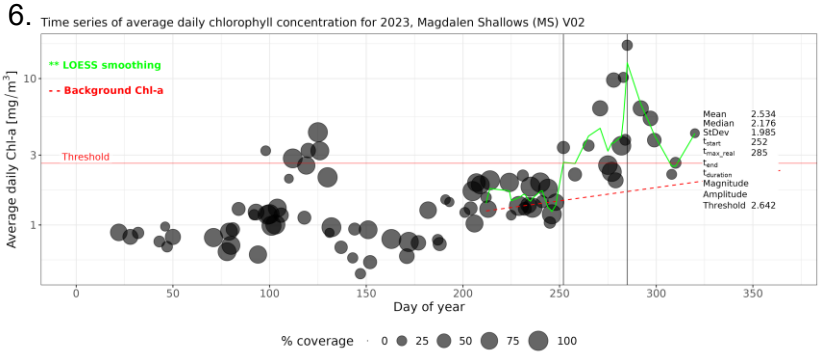

7. Time series of average daily chlorophyll concentration for 2023, Northeast Gulf of St. Lawrence (NEGSL) V02

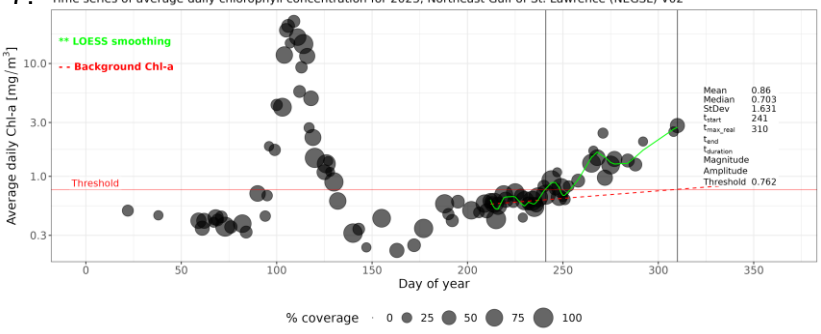

8. 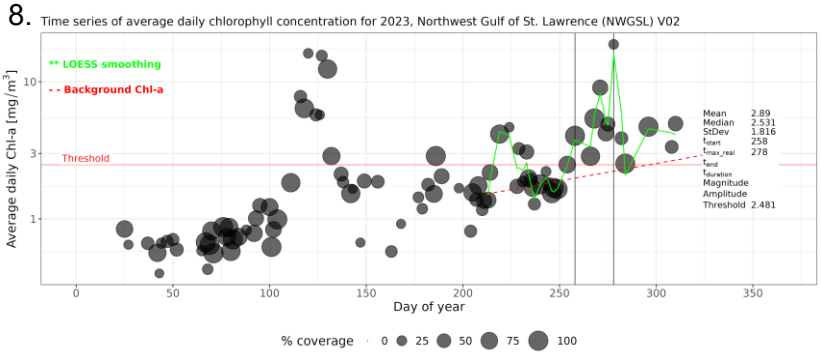

Parameters	Spring	Fall
Settings_region	Gulf of Saint Lawrence 4km	Gulf of Saint Lawrence 4km
Settings_sat_alg	modisaquar2022.0_chleof	modisaquar2022.0_chleof
Settings_concentration_type	full	full
Settings_interval	daily	daily
Settings_log_chla	TRUE	TRUE
Settings_percent	20	20
Settings_outlier	sd3	sd3
Settings_dailystat	average	average
Settings_pixrange1	-	-
Settings_pixrange2	-	-
Settings_fitmethod	gauss	thresh
Settings_bloomShape	symmetric	asymmetric
Settings_smoothMethod	loess	loess
Settings_loessSpan	0.2	0.2
Settings_t_range	31,22	212, 365
Settings_ti_limits	58, 150	212, 265
Settings_tm_limits	91,181	213, 364
Settings_ti_threshold_type	percent_thresh	-
Settings_ti_threshold_percent	20	-
Settings_threshcoef	-	1.05
Settings_tm	TRUE	-
Settings_beta	TRUE	-
Settings_use_weights	TRUE	FALSE
Settings_rm_bkrnd	TRUE	TRUE
Settings_flag1_lim1	0.75	0.75
Settings_flag1_lim2	1.25	1.25
Settings_flag2_lim1	0.85	0.85
Settings_flag2_lim2	1.15	1.15

Appendix 3 : General linear model results for Rimouski and Shediac Valley stations. Significance of the year and month effects as well as the adjusted R squared of the regression for nutrients and chlorophyll *a* are presented.

Station	Index	Year (*p*)	Month (*p*)	R^2
Rimouski	Chlorophyll *a* (0–100 m)	<0.0001	<0.0001	0.42
	Nitrate (0–50 m)	<0.0001	<0.0001	0.39
	Nitrate (50–150 m)	<0.0001	<0.0001	0.26
	Nitrate (150–320 m)	<0.0001	<0.0001	0.38
Shediac Valley	Chlorophyll *a* (0–100 m)	<0.001	<0.0001	0.31
	Nitrate (0–50 m)	<0.0001	<0.0001	0.37
	Nitrate (50–84 m)	<0.0001	<0.0001	0.4

Appendix 4 : General linear model results for Rimouski and Shediac Valley stations. Significance of the year and month effects as well as the adjusted R squared of the regression for phytoplankton groups are presented.

Station	Index	Year (*p*)	Month (*p*)	R^2
Rimouski	Diatoms	<0.0001	<0.0001	0.35
	Dinoflagellates	<0.0001	<0.0001	0.5
	Flagellates	<0.0001	<0.0001	0.35
	Ciliates	<0.0001	<0.0001	0.34
	Total	<0.0001	<0.0001	0.25
	Diatoms/Dinoflagellates	<0.0001	0.001	0.1
	Diatoms/Flagellates	<0.0001	0.01	0.13
Shediac Valley	Diatoms	<0.0001	<0.001	0.33
	Dinoflagellates	<0.0001	0.01	0.3
	Flagellates	<0.0001	<0.0001	0.4
	Ciliates	0.06	0.6	0.07
	Total	<0.0001	<0.0001	0.33
	Diatoms/Dinoflagellates	<0.001	0.001	0.24
	Diatoms/Flagellates	0.04	<0.0001	0.24

Appendix 5: General linear model results for Gulf regions. Significance of the year, season, and station effects as well as the adjusted R squared of the regression for nutrients or chlorophyll a are presented. Btm: Bottom.

Region	Index	Year (*p*)	Season (*p*)	Station(*p*)	R^2
Estuary/ Northwest Gulf	Chlorophyll *a* (0–100 m)	<0.0001	<0.0001	<0.0001	0.31
	Nitrate (0–50 m)	<0.0001	<0.0001	<0.0001	0.63
	N:P (0–50 m)	<0.0001	<0.0001	<0.0001	0.64
	Si:N (0–50 m)	<0.0001	<0.0001	<0.0001	0.24
	Nitrate (50–150 m)	<0.0001	<0.0001	<0.0001	0.34
	N:P (50–150 m)	<0.0001	<0.0001	<0.0001	0.3
	Si:N (50–150 m)	<0.0001	<0.0001	<0.0001	0.33
	Nitrate (150-btm)	<0.0001	<0.0001	<0.0001	0.94
	N:P (150-btm)	<0.0001	0.04	<0.0001	0.14
	Si:N (150-btm)	<0.0001	<0.0001	<0.0001	0.72
Northeast Gulf	Chlorophyll *a* (0–100m)	<0.0001	<0.0001	0.2	0.24
	Nitrate (0–50m)	<0.0001	<0.0001	0.04	0.59
	N:P (0–50m)	<0.0001	<0.0001	<0.0001	0.85
	Si:N (0–50m)	0.01	0.03	1	0.01
	Nitrate (50–150m)	<0.0001	<0.0001	<0.0001	0.54
	N:P (50–150m)	<0.0001	<0.0001	<0.0001	0.58
	Si:N (50–150m)	<0.0001	0.4	<0.0001	0.32
	Nitrate (150-btm)	<0.0001	<0.0001	<0.0001	0.92
	N:P (150-btm)	<0.0001	<0.0001	<0.0001	0.6
	Si:N (150-btm)	<0.0001	<0.0001	<0.0001	0.59
Central Gulf/Cabot Strait	Chlorophyll *a* (0–100m)	<0.0001	<0.0001	0.1	0.16
	Nitrate (0–50m)	<0.0001	<0.0001	<0.0001	0.7
	N:P (0–50m)	<0.0001	<0.0001	<0.0001	0.79
	Si:N (0–50m)	<0.0001	0.01	0.08	0.17
	Nitrate (50–150m)	<0.0001	<0.0001	<0.0001	0.46
	N:P (50–150m)	<0.0001	<0.0001	<0.0001	0.47
	Si:N (50–150m)	<0.0001	<0.0001	<0.0001	0.44
	Nitrate (150-btm)	<0.0001	<0.0001	<0.0001	0.92
	N:P (150-btm)	<0.0001	<0.0001	<0.0001	0.49
	Si:N (150-btm)	<0.0001	0.06	<0.0001	0.32
Magdalen Shallows	Chlorophyll *a* (0–100m)	<0.0001	<0.0001	<0.0001	0.24
	Nitrate (0–50m)	<0.0001	<0.0001	<0.0001	0.42
	N:P (0–50m)	<0.0001	<0.0001	<0.0001	0.64
	Si:N (0–50m)	<0.0001	<0.0001	<0.0001	0.17
	Nitrate (50–150m)	0.03	<0.0001	<0.0001	0.51
	N:P (50–150m)	<0.0001	<0.0001	<0.0001	0.49
	Si:N (50–150m)	<0.0001	0.09	<0.0001	0.32

Appendix 6: General linear model results for Rimouski and Shediac Valley stations. Significance of the year and month effects as well as the adjusted R squared of the regression for each zooplankton index are presented.

Station	Index	Year (*p*)	Month (*p*)	R^2
Rimouski	*Calanus finmarchicus*	<0.0001	<0.0001	0.51
	Pseudocalanus spp.	<0.0001	<0.0001	0.56
	Total copepods	<0.0001	<0.0001	0.58
	Non-copepods	<0.0001	<0.0001	0.45
	Calanus hyperboreus	<0.0001	<0.0001	0.51
	Small calanoids	<0.0001	<0.0001	0.69
	Large calanoids	<0.0001	<0.0001	0.34
	Cyclopoids	<0.0001	<0.0001	0.59
	Copepods: Warm	<0.0001	0.7	0.52
	Copepods: Cold	<0.0001	<0.0001	0.45
	Dry weight	<0.0001	<0.0001	0.69
	Bryozoa	<0.0001	<0.0001	0.23
	Cnidaria	<0.0001	<0.0001	0.62
	Crustacea	<0.0001	<0.0001	0.49
	Echinoderma	<0.0001	<0.01	0.23
	Mollusca	<0.0001	<0.0001	0.37
	Polychaeta	<0.0001	<0.0001	0.44
	Tunicata	<0.0001	<0.0001	0.47
	Ostracoda	<0.0001	0.2	0.29
Shediac Valley	*Calanus finmarchicus*	<0.0001	<0.0001	0.31
	Pseudocalanus spp.	0.04	0.2	0.08
	Total copepods	0.2	<0.0001	0.16
	Non-copepods	<0.001	<0.01	0.2
	Calanus hyperboreus	<0.0001	<0.0001	0.68
	Small calanoids	<0.01	<0.001	0.19
	Large calanoids	<0.0001	<0.0001	0.35
	Cyclopoids	0.2	<0.0001	0.22
	Copepods: Warm	0.04	0.2	0.08
	Copepods: Cold	0.02	<0.0001	0.31
	Dry weight	<0.0001	<0.0001	0.36
	Bryozoa	0.001	<0.0001	0.43
	Cnidaria	<0.0001	<0.001	0.4
	Crustacea	<0.01	<0.0001	0.33
	Echinoderma	0.05	<0.0001	0.18
	Mollusca	<0.001	<0.0001	0.32
	Polychaeta	<0.0001	<0.0001	0.49
	Tunicata	0.01	<0.0001	0.24
	Ostracoda	0.9	0.6	-0.06

Appendix 7: General linear model results for Gulf regions. Significance of the year, season, and station effects as well as the adjusted R squared of the regression for each zooplankton index are presented.

Region	Index	Year (*p*)	Season (*p*)	Station(*p*)	R^2
Estuary/ Northwest Gulf	*Calanus finmarchicus*	<0.0001	0.001	<0.0001	0.64
	Pseudocalanus spp.	<0.0001	<0.0001	<0.0001	0.52
	Total copepods	<0.0001	<0.0001	<0.0001	0.72
	Non-copepods	<0.0001	<0.0001	<0.0001	0.56
	Calanus hyperboreus	<0.0001	<0.0001	<0.0001	0.61
	Small calanoids	<0.0001	<0.0001	<0.0001	0.64
	Large calanoids	<0.0001	<0.001	<0.0001	0.76
	Cyclopoids	<0.0001	<0.0001	<0.0001	0.69
	Copepods: Warm	<0.0001	0.001	<0.0001	0.56
	Copepods: Cold	<0.0001	0.02	<0.0001	0.66
	Dry weight	<0.0001	0.001	<0.0001	0.79
	Bryozoa	<0.0001	<0.0001	<0.0001	0.45
	Cnidaria	<0.0001	0.01	<0.0001	0.7
	Crustacea	<0.0001	<0.0001	<0.0001	0.55
	Echinoderma	<0.0001	0.01	<0.0001	0.38
	Mollusca	<0.0001	<0.0001	<0.0001	0.51
	Polychaeta	<0.0001	<0.0001	<0.0001	0.58
	Tunicata	<0.0001	<0.0001	<0.0001	0.45
	Ostracoda	<0.0001	0.7	<0.0001	0.7
Northeast Gulf	*Calanus finmarchicus*	<0.001	<0.0001	0.01	0.21
	Pseudocalanus spp.	<0.0001	<0.0001	<0.0001	0.33
	Total copepods	<0.0001	<0.0001	<0.001	0.38
	Non copepods	<0.0001	<0.001	<0.0001	0.45
	Calanus hyperboreus	<0.001	<0.0001	<0.0001	0.59
	Small calanoids	<0.0001	0.9	<0.0001	0.43
	Large calanoids	0.009	<0.0001	<0.0001	0.45
	Cyclopoids	<0.0001	<0.0001	0.01	0.48
	Copepods: Warm	<0.0001	<0.0001	0.002	0.49
	Copepods: Cold	<0.0001	<0.0001	<0.0001	0.44
	Dry weight	<0.0001	<0.0001	<0.0001	0.65
	Bryozoa	<0.0001	<0.0001	0.9	0.62
	Cnidaria	<0.0001	0.6	<0.0001	0.34
	Crustacea	<0.0001	<0.0001	<0.01	0.53
	Echinoderma	<0.0001	0.05	0.05	0.21
	Mollusca	<0.0001	1	<0.001	0.32
	Polychaeta	<0.0001	<0.0001	1	0.53
	Tunicata	<0.0001	<0.0001	<0.0001	0.38
	Ostracoda	0.1	<0.01	<0.0001	0.28

Appendix 7 (continued): General linear model results for Gulf regions. Significance of the year, season, and station effects as well as the adjusted R squared of the regression for each zooplankton index are presented.

Region	Index	Year (*p*)	Season (*p*)	Station(*p*)	R^2
Central Gulf/ Cabot Strait	*Calanus finmarchicus*	<0.0001	<0.0001	<0.001	0.26
	Pseudocalanus spp.	<0.0001	<0.0001	<0.0001	0.32
	Total copepods	<0.0001	<0.0001	<0.001	0.21
	Non-copepods	<0.0001	<0.0001	<0.0001	0.46
	Calanus hyperboreus	<0.0001	<0.0001	<0.0001	0.54
	Small calanoids	<0.0001	0.8	<0.0001	0.32
	Large calanoids	<0.0001	0.9	<0.0001	0.36
	Cyclopoids	<0.0001	<0.0001	0.02	0.23
	Copepods: Warm	<0.0001	<0.0001	<0.0001	0.48
	Copepods: Cold	<0.0001	0.6	0.1	0.11
	Dry weight	<0.0001	0.2	<0.0001	0.64
	Bryozoa	<0.0001	<0.0001	0.4	0.48
	Cnidaria	<0.0001	<0.0001	<0.0001	0.46
	Crustacea	<0.0001	<0.0001	0.08	0.46
	Echinoderma	<0.0001	<0.01	<0.001	0.26
	Mollusca	<0.0001	0.05	<0.01	0.16
	Polychaeta	<0.0001	<0.0001	<0.0001	0.6
	Tunicata	<0.0001	<0.0001	0.005	0.41
	Ostracoda	<0.001	0.2	<0.0001	0.38
Magdalen Shallows	*Calanus finmarchicus*	<0.0001	<0.001	<0.0001	0.33
	Pseudocalanus spp.	<0.0001	<0.0001	0.7	0.13
	Total copepods	<0.0001	<0.0001	<0.0001	0.2
	Non copepods	<0.0001	<0.0001	<0.0001	0.5
	Calanus hyperboreus	<0.0001	<0.0001	<0.0001	0.49
	Small calanoids	<0.0001	0.01	0.004	0.19
	Large calanoids	<0.0001	<0.0001	<0.0001	0.5
	Cyclopoids	<0.0001	<0.0001	<0.0001	0.31
	Copepods: Warm	<0.0001	<0.0001	0.005	0.51
	Copepods: Cold	<0.0001	<0.0001	<0.0001	0.4
	Dry weight	<0.0001	<0.0001	<0.0001	0.42
	Bryozoa	<0.0001	<0.0001	0.4	0.63
	Cnidaria	<0.0001	0.03	<0.0001	0.31
	Crustacea	<0.0001	<0.0001	<0.001	0.43
	Echinoderma	<0.0001	0.02	0.05	0.23
	Mollusca	<0.0001	0.04	<0.0001	0.58
	Polychaeta	<0.0001	<0.0001	0.06	0.66
	Tunicata	<0.0001	<0.0001	<0.001	0.33
	Ostracoda	0.02	0.5	<0.0001	0.27